a Coriolis tutorial, Part 4:

Wind-driven ocean circulation; the Sverdrup relation

James F. Price

Woods Hole Oceanographic Institution,
Woods Hole, Massachusetts, 02543
https://www2.whoi.edu/staff/jprice/ jprice@whoi.edu

Version 7.5 25th Jan, 2021 at 08:28

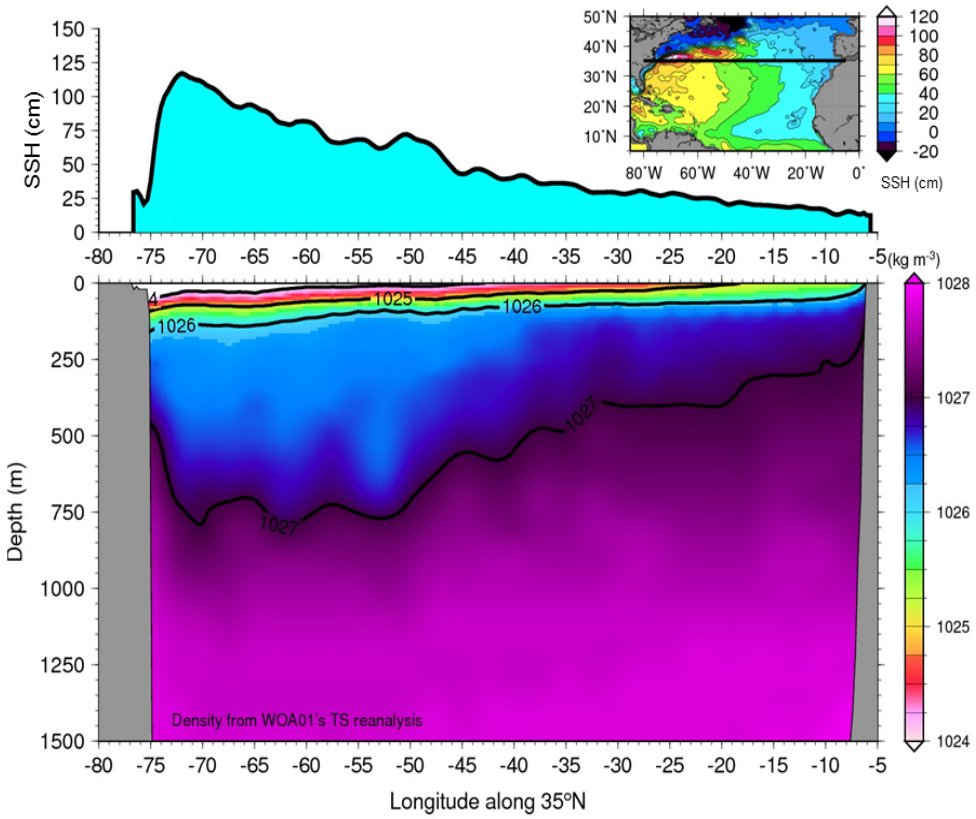

Figure 1: The remarkable east-west asymmetry of upper ocean gyres is evident in this section through the thermocline of the subtropical North Atlantic: **(upper)**, sea surface height (SSH) from satellite altimetry, and **(lower)** potential density from *in situ* observations. Within a narrow western boundary region, longitude -76 to -72, the SSH slope is positive and very large, and the inferred geostrophic current is northward and very fast: the Gulf Stream. Over the rest of the basin, the SSH slope is negative and much, much smaller. The inferred geostrophic flow is southward and correspondingly very slow. This southward flow is consistent with the overlying, negative wind stress curl and the Sverdrup relation, the central topic of this essay.

Abstract. This essay is the fourth of a four part introduction to Earth's rotation and the fluid dynamics of the atmosphere and ocean. The theme is wind-driven ocean circulation, and the motive is to develop insight for several major features of the observed ocean circulation, *viz.* western intensification of upper ocean gyres and the geography of the mean and the seasonal variability.

A key element of this insight is an understanding of the Sverdrup relation between wind stress curl and meridional transport. To that end, shallow water models are solved for the circulation of a model ocean that is started from rest and driven by a specified wind stress field: westerlies at mid-latitudes and easterlies in subpolar and tropical regions. This gives three regions of stress curl, negative over the subtropics, and positive over subpolar and tropical regions. The model used most extensively has just one active layer and makes the reduced gravity approximation. This is essentially the model used in Parts 2 and 3 and is here dubbed 1l-rg. The dynamics of this model are baroclinic only. A second model includes three active layers, including a thick, active abyssal layer and a free sea surface and hence, 3l-fs. This more complete model includes the baroclinic dynamics of the 1l-rg model as well as fast, barotropic dynamics.

Baroclinic response in the 1l-rg solution. The developing baroclinic circulation can be described in terms of four stages. Stage 1 is the direct, local response to the imposed wind stress and includes inertia-gravity oscillations and Ekman transport within the upper, surface layer. The inertial-gravity oscillations die away after a couple of weeks with no evident lasting effect. The Ekman transport remains, and is very consequential for the long term ocean circulation. Ekman transport varies spatially on account of the latitudinal variation of the wind stress and of the Coriolis parameter, f. The resulting divergence of Ekman transport modifies the thickness of the upper layer field and thus the mass field, the pressure field, and hence the circulation. Over the central subtropics, where wind stress curl is negative, the Ekman transport is convergent, which leads to a slowly thickening thermocline (about 30 meters per year in the central subtropics) and a high pressure in the upper ocean. This induces a nearly geostrophic zonal circulation which increases in step with the thickness field. This local response to wind stress curl is called the Stage 2 response, and goes on for about three years until the slow westward, Rossby-wave like propagation ($-\beta R_d^2 = -3$ km day^{-1} in the subtropics) of the zonal thickness gradient balances Ekman convergence and gives a steady state thickness. The steady circulation is then a baroclinic Sverdrup flow, dubbed Stage 3. The transition from Stage 2 to Stage 3 sweeps westward across the basin, just like the westward propagation of a long baroclinic Rossby wave emanating from the eastern boundary. Baroclinic Sverdrup flow thus occurs much sooner in the tropics (months) than in the subpolar region (decades).

The central subtropical gyre reaches steady-state Sverdrup flow in about three years, but the layer thickness continues to increase very slowly and uniformly (spatially) over the next several decades as the subtropical gyre absorbs water expelled from the subpolar region where the wind stress curl is positive and the upper layer becomes dramatically thinner. A basin-wide steady state, Stage 4, arises only after the subpolar gyre has also been swept by a slowly moving long baroclinic Rossby wave. Along the

northern boundary of the 1l-rg model, that requires about 30 years.

The observed, basin-scale horizontal structure of the wind-driven ocean circulation, including western intensification and several of the qualitative differences between tropical, subtropical and subpolar gyres, have a plausible analog in solutions of the baroclinic shallow water model. In particular, the Sverdrup relation plus the observed pattern of wind stress curl provide a concise and convincing explanation of the sense of the circulation over the majority of an ocean basin, e.g., equatorward (southward) meridional flow in the subtropics of the North Atlantic, where the wind stress curl is negative, and the opposite sign in the tropical and subpolar regions. The Sverdrup relation is valid where the dominant terms of the potential vorticity balance are just two: the beta effect acting on a slow meridional flow, and the curl of the wind stress. In practice, this holds in the interior of a basin, where the currents and the friction are both very weak, and well away from zonal or meridional boundaries.

The net transport through any given basin-wide zonal section must vanish in steady state, and the meridional Sverdrup transport in the interior of the basin is balanced in this volumetric sense by a very intense western boundary current (wbc) having a width of order the baroclinic radius of deformation, O(100 km) in the subtropics. The baroclinic transport of a wbc reaches approximate steady state after the ocean interior to the east of the wbc has reached steady baroclinic Sverdrup flow, about five years in the subtropical gyre. The wbc thus follows the interior circulation, despite that it is far more energetic.

The meridional transport must vanish on zonal boundaries, and in the present model the affected zonal boundary regions are fairly wide, up to 1000 km in north-south extent. Within these wide zonal boundary regions, the meridional transport has the sign of the expected Sverdrup transport, but considerably reduced amplitude, going to zero on the boundary.

Experiments with an annually-varying zonal wind stress show that the baroclinic wbc transport responds only weakly to even a large, $\pm 50\%$ annual cycle of the wind stress. In the subtropical gyre, the resulting annual cycle of baroclinic wbc transport is only about $\pm 4\%$ of the mean transport. The annual cycle of wbc transport is even less in the subpolar gyre, and somewhat greater though still not prominent in the tropical gyre. There are some specific regions that do show an appreciable, baroclinic response to an annually varying wind stress, most notably the eastern half of the tropical gyre. There the annual cycle of upper ocean (baroclinic) zonal currents is about $\pm 50\%$ of the mean, or roughly proportional to the wind stress variation. This vigorous seasonal cycle of tropical zonal currents appears to be a mainly local response to the seasonal variation of stress curl, here called Stage 2, but includes a contribution from an annual period, eastern boundary Rossby wave.

A barotropic and then a baroclinic response, 3l-fs. What happens when the same start up experiment is carried out with the three layer, free surface model, 3l-fs? In one key respect the results are strikingly different from that described above — the circulation comes to a nearly steady, *barotropic* Sverdrup flow within just a few weeks, even at subpolar latitudes. The comparatively very short response time of the barotropic circulation is consistent with the very fast zonal propagation of barotropic long Rossby waves,

about -1200 km day^{-1} at 30 N. The basin-scale pattern of the barotropic transport, including the western boundary currents and the zonal boundary regions, is very similar to that of the baroclinic Sverdrup flow found in the 1l-rg model solution described above. This barotropic Sverdrup transport is almost depth-independent (as barotropic usually implies) and thus occurs mainly within the thick, abyssal layer. Consequently the amplitude of upper ocean currents and the SSH anomaly associated with the barotropic response are quite small compared to the observed SSH.

Over the following several years, a baroclinic adjustment occurs in the 3l-fs model solution in just the way it does in the 1l-rg solution. In the central subtropical gyre, a first mode, long baroclinic Rossby wave arrives from the east after about three years. As it passes, the abyssal layer comes to rest, and the Sverdrup transport is thereafter confined to the two upper ocean layers, i.e., it is baroclinic. After about another five years and the passage of a second mode wave, the Sverdrup transport is extinguished in the unforced, lower thermocline layer and thereafter is present only in the uppermost, wind-forced layer. The amplitude of the across-basin SSH anomaly is then fairly realistic, about 1 m across the subtropical gyre. This is mostly the result of a felicitous choice for the initial surface layer thickness, 250 m, rather than a genuine prediction of the near-surface vertical structure of the Sverdrup flow.

More on Fig. 1 The SSH data in the upper panel are the monthly average for September over about twenty years of measurement compiled by the AVISO Project (https://www.aviso.altimetry.fr). The lower panel is the long-term, September average of density along 35^{o}N from the World Ocean Atlas 2001 (http://www.nodc.noaa.gov/OC5/WOA01/pr_woa01.html). Notice that the tilt of the thermocline mirrors the tilt of SSH so that high SSH corresponds to a thick, low density upper layer. The horizontal gradient of density is strongest within the shallowest several hundred meters. The net result of this mass distribution is a comparatively small horizontal gradient of hydrostatic pressure at depths of about 1000 meters and below. This is suggestive of a reduced gravity approximation that will be utilized in many of the numerical experiments to follow. At depths greater than shown here, there are cold, mainly southward flowing currents that constitute the lower limb of the meridional overturning circulation. This figure was kindly provided by Iam-Fei Pun of WHOI.

Contents

1 Earth's rotation and its effects upon large-scale, geophysical flows

This essay is the fourth in a four-part introduction to fluid dynamics on a rotating Earth. These essays were written for students who have some background in classical fluid dynamics, and who are beginning a study of geophysical fluid dynamics (GFD).

Earth's rotation gives rise to some of the most distinctive, important and subtle phenomena of GFD. The first three of essays introduced the Coriolis force in Part 1, geostrophic adjustment in Part 2, and westward propagation in Part 3. These topics are about equally relevant for students of atmospheric and oceanographic science. The present essay continues this introduction to rotation effects, but now with an oceanic theme — wind-driven ocean circulation.

1.1 Two observed properties of the upper ocean circulation

The goal of this essay is to develop some insight for two important, Observed properties of the upper ocean circulation that are evident in Figs. (1) and (2): quasi-steady, horizontally rotating gyres that fill the subpolar and subtropical basins, and zonally elongated, seasonally-varying SSH features that span the tropics (Fig. 2).

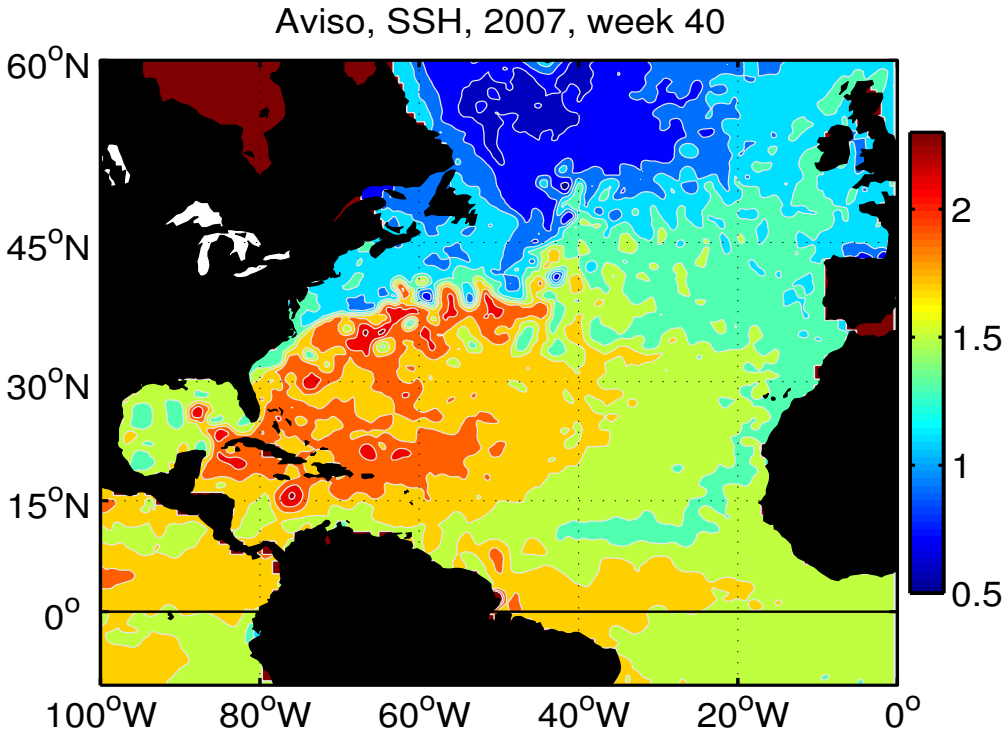

Figure 2: A snapshot of sea surface height (SSH) over the North Atlantic (repeats Fig. 1 of Part 3). The color scale at right is in meters. The largest SSH variability occurs primarily on two spatial scales — basin scale gyres (thousands of kilometers), a clockwise rotating high in the subtropics and a counter clockwise rotating low in the subpolar basin — and mesoscale eddies (several hundred kilometers) that are both highs and lows. The subtropical and subpolar gyres are clearly present in both instantaneous and time-averaged views, while mesoscale eddies are significantly time-dependent, including marked westward propagation. An animation of a year of this data is available at www.whoi.edu/jpweb/Aviso-NA2007.flv and a truly superb view of the global sea surface is available on the AVISO homepage: https://www.aviso.altimetry.fr

1.1.1 O1, Space scales: Upper ocean gyres are markedly asymmetric east to west

SSH sampled along 35^o N across the subtropical gyre shows two distinctly different regions of SSH zonal slope, $\partial\eta/\partial x$ (Fig. 1, upper and Fig. 2). Going from the western boundary toward the east, there is a narrow region adjacent to the western boundary of width L_{wb} that is O(100 km) within which the SSH increases eastward to a maximum $\delta\eta \approx 1$ m. The inferred geostrophic current in this western boundary current, the Gulf Stream, is poleward (northward) and comparatively swift, $U_{wb} \approx g\delta\eta/(L_{wb}f)$ is O(1 m sec^{-1}). To the east, there is a broad interior region, essentially all the rest of the basin, width $L_i \approx 7000$ km, over which there is a gradual decrease of η to approx. zero on the eastern boundary. The inferred

geostrophic current in the interior is equatorward (southward) and very slow compared to the the western boundary current, $U_i \approx U_{wb}L_{wb}/L_i$ is O(0.01 m sec^{-1}) when averaged over zonal scales of O(1000 km). This slow southward flow is mainly wind-driven Sverdrup flow, about which much more below.

A similar structure of rapid western boundary current and much slower interior flow is found also in the subpolar gyre, though with the sense of the SSH anomaly and the circulation reversed. From this cursory inspection it is evident that the east-west asymmetry of upper ocean circulation, often called western intensification, is very pronounced, $L_i/L_{wb} \approx U_{wb}/U_i$ is O(100), which is typical of all of the major upper ocean gyres.

1.1.2 O2, Time scales: The subtropical and subpolar gyres are quasi-steady, while tropical circulation shows large amplitude seasonal variation

The subtropical gyre is always present in the sense that every basin-wide snapshot of SSH (as in Fig. 2) and every across-basin hydrographic section (as in Fig. 1 lower) will show an easily recognizable, poleward-flowing Gulf Stream near the western boundary and an equatorward Sverdrup flow over most of the rest of the basin. Said a little differently, the subtropical gyre and its wbc are evident on long-term average and instantaneously. This holds just as well for the subpolar gyre. The systematic, annual variation of the subtropical gyre, often represented by the Gulf Stream transport, is only about 5% of the time-mean.[1] Such a small annual variation is somewhat surprising, given that the wind stress and air-sea heat flux over the North Atlantic exhibit a substantial annual variation, up to $\pm$50% in the northern North Atlantic. This implies that the response time of the gyre-scale circulation of the subtropical and higher latitudes to a time-changing wind stress is considerably longer than a year.[2]

Tropical ocean circulation appears to be markedly different. Tropical SSH is characterized by one or several narrow, zonally elongated ridges and troughs. The associated, zonal geostrophic currents have alternate signs, e.g., between about 20 ^{o}N and 10 ^{o}N a westward flowing North Equatorial Current, a little further south an eastward flowing North Equatorial Countercurrent, and still further south, a

[1] Rossby, T, C. Flagg and K. Donohue, 2010, 'On the variability of Gulf Stream transport from seasonal to decadal', *J. Mar. Res., 68,* 503-522.

[2] Mesoscale eddies are ubiquitous, and impose large amplitude, but comparatively short time (periods of several months) and space (several hundred kilometers) scale variations on the gyre-scale SSH and currents, Fig. 2. For example, the SSH slope in the interior, if measured on scales of O(100 km), will be dominated by mesoscale eddy variability. Thus the instantaneous (time and space) meridional geostrophic current in the basin interior is just about as likely to be northward as southward. Similarly, any single estimate of the instantaneous Gulf Stream transport may vary by $\pm$15% around the long term mean due to superimposed, apparently random mesoscale eddy variability.[1]

westward flowing South Equatorial Current that crosses the equator.[3] The amplitude of these tropical currents is comparable to that found in the subtropical and subpolar gyres, but the SSH amplitude evident in Fig. (1) is considerably less, a straightforward consequence of geostrophy.

In marked contrast to the quasi-steady subtropical and subpolar gyres noted above, some of these tropical circulation features exhibit systematic, large amplitude seasonality; the North Equatorial Counter Current is strongest in summer and disappears in winter, while the South Equatorial Current fluctuates annually by about $\pm 50\%$ (To see this important annual variability, you will need to follow the links to animations noted in the caption of Fig. 2, and see also the references in footnote 3).

1.2 The Sverdrup relation

The premise (and the promise) of this essay is that insight for the observations O1 and O2 will follow from an understanding of the Sverdrup relation,[4]

$$\boxed{M^y_{Sv} \;=\; \frac{1}{\rho_o \beta} \nabla \times \tau} \tag{1}$$

[3]The connection of these zonal currents with a western boundary current is not clear from observations. There does appear to be a northward-flowing western boundary current in Fig. 2 that crosses the equator and continues northwestward along the coast of South America. This North Brazil Current is thought to be the shallow side of the the global-scale, overturning circulation that imports warm South Atlantic water into the North Atlantic basin and returns cold water at great depth. The meandering North Brazil Current frequently sheds large (several hundred kilometer diameter) eddies that transport a significant part of the warm water flow. The presence of the strong and highly variable North Brazil Current makes it difficult to discern a relationship between the western boundary current and the mainly zonal currents to the east. A concise discussion of equatorial ocean circulation including the annual variability of winds and currents is by Philander, S. G., 2001, 'Atlantic ocean equatorial currents', Academic Press, doi:10.1006/rwos.2001.0361. An excellent depiction of surface currents generally is provided by http://oceancurrents.rsmas.miami.edu/atlantic/north-brazil.html

[4]Sverdrup's pioneering paper that introduced the equivalent of Eqn. (29) is unfortunately not easily read or appreciated, but nevertheless: Sverdrup, H. U., 1947, 'Wind-driven currents in a baroclinic ocean, with application to the eastern Pacific', *Proc. Natl. Acad. Sci. U. S. A.*, **33**, 318-326, which is available online at http://www.pnas.org/content/33/11/318 The first model of a western-intensified wind-driven gyre was by Stommel, H., 1948, and the time-dependent, gyre spin-up problem was discussed by Stommel, H., 1957, 'A survey of ocean current theory', *Deep Sea Res.*, **4**, 149-184. Be sure to see also Stommel's masterpiece, 'The Gulf Stream', 1966, Univ. of California Press. Time-dependence was treated in greater detail by Anderson, D. L. T. and Gill A. E., 1975, 'Spin-up of a stratified ocean with applications to upwelling', *Deep-Sea Research* **22**. These classic research papers are highly readable and may be found at http://www.aos.princeton.edu/WWWPUBLIC/gkv/history/oceanic.html The GFD texts noted in Part 1 each have very good discussion of the Sverdrup interior. Ch. 1 of Pedlosky, J.,1998, 'Ocean Circulation Theory', and Ch. 10 of Marshall, J. and R. A. Plumb, 2008, 'Atmosphere, Ocean and Climate Dynamics', and Ch. 14 of Vallis, G., 2006, 'Atmospheric and Oceanic Fluid Dynamics', are all highly recommended.

which is one of the true bedrocks of ocean circulation theory. The righthand side of (29) is the curl of the wind stress, $\tau(x,y)$, a vector field that is here presumed to be known from observations (Fig. 3). The left hand side is the meridional (north-south) volume transport per unit width that we seek. Meridional transport from a depth $z=-d$ to the the sea surface $z=0$ is

$$M^y_{-d} \;=\; \int_{-d}^{0} v(z)dz. \tag{2}$$

Two important aspects of the Sverdrup relation are that it involves the meridional (north-south) component of the velocity only, and, the appropriate depth, d, of the transport integral, (2), and the depth-dependence of $v(z)$ are not given by the theory.

We will tend to emphasize the limitations of the Sverdrup relation in much of what follows, but there is no doubt of its utility and elegance — given only the Sverdrup relation and the curl of the wind stress, we can predict meridional transport that is in accord with some of the major features of the upper ocean circulation. Notably, the meridional transport expected from a negative stress curl (clockwise rotating wind stress as occurs over the subtropics of the North Atlantic, Fig. 3) will be southward and accompanied by a high of SSH, as indeed does occurs as confirmed by inspection of Figs. 1 and 2. A counterclockwise wind field and thus positive stress curl is expected to produce northward meridional flow, and again, this does occur (cf. Figs. 3 and 2).

Modern observational methods and analyses have made it possible to make detailed, quantitative tests of the Sverdrup relation over almost the full, global ocean.[5] In a nutshell, these studies concur that the Sverdrup relation is reasonably accurate (to within about 25%) over most of the interior of the North Atlantic and North Pacific subtropical gyres, provided that winds and currents are averaged over multi year periods and over horizontal scales of O(500 km) or greater. The Sverdrup relation is not valid near western boundary currents (wbc), which is no surprise, nor is it valid in the eastward extension of the subtropical wbc (Gulf Stream) into the subpolar basin (North Atlantic Current). The subpolar gyres of the North Pacific and North Atlantic have the expected sense of the circulation (counterclockwise), as noted above, but there is a rather poor correlation between the magnitude of the Sverdrup transport and the observed meridional transport. The difference is especially marked in the northerly half of the North Pacific subpolar gyre, which should be the more appropriate case, but where the observed meridional transport is considerably less than the expected Sverdrup transport.

[5]Three excellent, observation-based studies of the Sverdrup relation are by Gray, A. R. and Riser, S. C., 2014, 'A global analysis of Sverdrup balance using absolute geostrophic velocities from Argo', *J. Phys. Oceanogr.*, 1213-1229, doi: 10.1175/JPO-D-12-0206.1, and by Wunsch, C., 2011, 'The decadal mean ocean circulation and Sverdrup balance', *J. Mar. Res.*, **69**, 417-434. online at dspace.mit.edu/openaccess-disseminate/1721.1/74048 and by Thomas, M. D. et al., 2014, 'Spatial and temporal scales of Sverdrup balance', *J. Phys. Oceanogr.*, **44**, 2644-2660. doi: 10.1175/JPO-D-13-0192.1

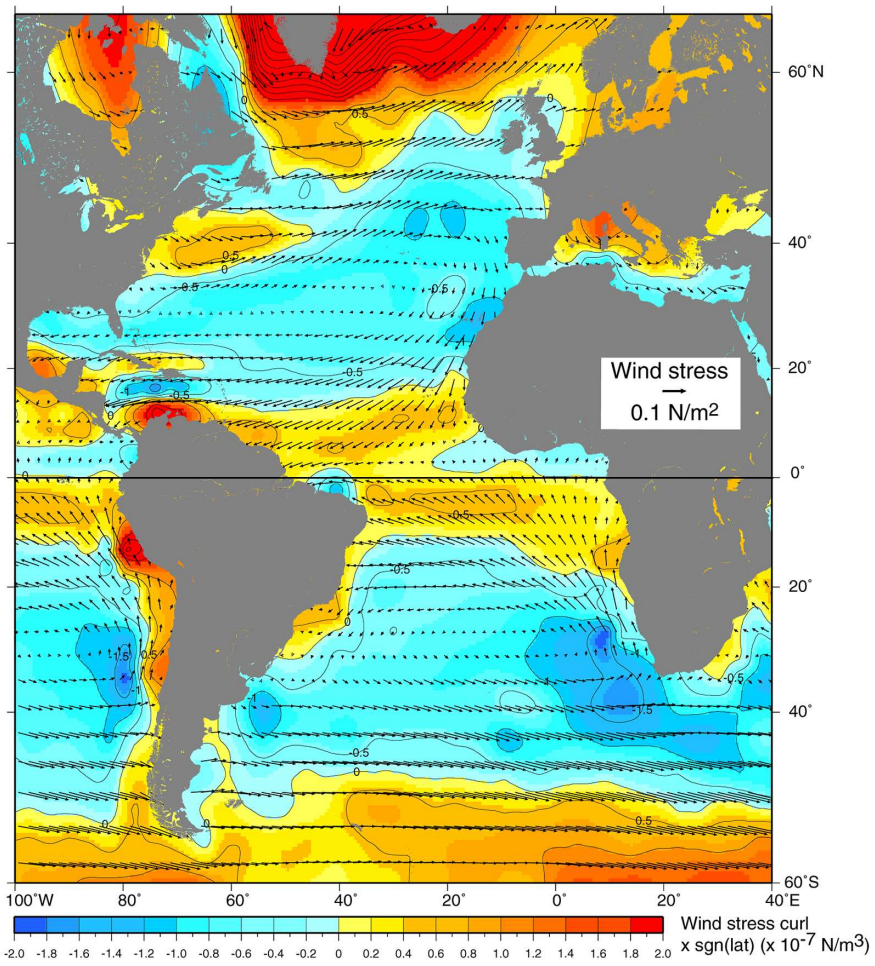

Figure 3: The vector field is the climatological mean wind stress (scale at center right), the color contours are proportional to the curl of the wind stress (scale at the bottom). These data were computed from a reanalysis of observed wind compiled by the National Center for Environmental Prediction. Over both the North Atlantic and South Atlantic basins the broad pattern includes westerly winds from roughly 35^o to 50^o, and easterly winds in tropical regions, latitude less than 20^o, and also in subpolar regions, latitude greater than roughly 55^o. The stress curl is thus negative over the subtropics and positive over the equatorial and subpolar regions. This beautiful and informative figure is thanks to L. D. Talley et al., *Descriptive Physical Oceanography,* Elsevier, Fig. S09.3, http://booksite.elsevier.com/DPO/chapterS09.html

It is fair to claim that the Sverdrup relation serves as at least a partial explanation of the major upper ocean gyres. However, it is also fair to say that the Sverdrup relation is abstract to the point of being abstruse, and could itself use an explanation. **First**, note that the Sverdrup relation is local in space; Eqn. (1) says that the Sverdrup transport at a given point depends only upon the stress curl and the β at that point, regardless of the surroundings, e.g., even a nearby landmass. This can not be true of real ocean currents, which are, of course, blocked at a coastline. **Second**, the Sverdrup relation makes no reference to time, and so evidently applies to steady currents and wind stress. This has a practical side, insofar as the ocean and atmosphere are never truly steady. Hence we can only approximate a steady state by time-averaging over a suitably long interval, perhaps years as noted above. There is a conceptual side to this as well, namely, the Sverdrup relation does not imply a mechanism for establishing such a steady state and hence does not provide a causal explanation, i.e., a mechanism, for ocean circulation. The Sverdrup relation is in very, very good company in this regard, e.g., geostrophic momentum balance is of this ilk, which motivated a study of geostrophic adjustment in Part 2. **Third**, the Sverdrup relation makes

no reference to the depth over which this transport should be expected, i.e., whether confined to a thin surface layer or distributed evenly throughout the water column. This is a significant issue if one intends to test the Sverdrup relation against field data, or, to understand how the Sverdrup transport contributes to the heat and salt balances of the global ocean.

1.3 Objectives and plan of this essay

The conclusion from this very brief look at the Sverdrup relation is that there must be important qualifications on the time and the space scales over which Eqn. (29) could possibly be valid. The refined premise of this essay is that when we understand these limitations, we will at the same time gain considerable insight for O1 and O2. The objectives of this essay are then to:

i) Learn how the Sverdrup relation arises when the circulation of a model ocean is started from rest, and so gain a sense of the time scales and mechanisms implicit in the time-independent Sverdrup relation (relevant to O2).

ii) Show that the Sverdrup relation holds over most of the interior of a model ocean basin and hence the sign of the wind stress curl determines the sense (clockwise or anti-clockwise) of wind-driven gyres (relevant to O1).

iii) Observe that the Sverdrup relation fails near solid boundaries and is supplanted by western or zonal boundary current dynamics (relevant to O1).

iv) Consider some of the processes that determine the depth of the Sverdrup transport.

These are among the foundational problems of physical oceanography and have been addressed many times over, and from a variety of perspectives. This essay will work towards these objectives by an analysis of solutions from two shallow water (layered) models. The first model is familiar from Parts 2 and 3 — one active layer and pressure anomaly computed from the baroclinic density field assuming a quiescent abyssal ocean. This is dubbed the 1l-rg model, and can be thought of as a 'baroclinic only' model. This 1l-rg model configuration is comparatively simple and economical and is appropriate to the first three objectives of this essay. A second model has three active layers and a free (moving) sea surface and dubbed 3l-fs. This model includes the baroclinic dynamics of the first model, as well as a very fast barotropic response that makes this model somewhat burdensome computationally. This model can help us understand some aspects of depth-dependence, but not all. For both models the shallow water model

equations are extended to include wind forcing and dissipation. These new features are described in Section 2, which may be skipped by readers not interested in the fine details (who should nevertheless take a look at the wind stress fields in Figs. 4 and 5). The experiments are started from a state of rest and continue until the circulation reaches a basin-wide steady state, requiring about 30 years of model ocean time (a few hours (1l-rg) or a few days (3l-fs) of computer time on a typical personal workstation). The transient baroclinic circulation is described in Section 3 in terms of four overlapping stages, and e.g., Stage 3 begins with the onset of baroclinic Sverdrup flow. The steady circulation varies a great deal over the basin. Over the majority of the basin, the steady potential vorticity balance is that of the Sverdrup relation. However, near the western boundary, the balance includes a significant torque due to drag on an energetic western boundary current, discussed in Section 4. Section 5 considers several experiments with other wind fields including one with an annual cycle, especially relevant to the annual variation of tropical ocean circulation noted in O2 above. Section 6 describes the solutions from the free surface model, 3l-fs. You could say that this second model solution changes everything, or, you could equally well argue that it changes almost nothing. Closing remarks are in Section 7, and links to the shallow water model and a few homework problems are in Section 8. Sections that are mainly a review of earlier material, or that may be skipped over with little loss of continuity toward the main objectives are noted by a trailing asterisk.

1.4 A brief review of the Coriolis force*

The Part 1 essay of this series examined the classical dynamics of moving parcels observed from a steadily rotating coordinate frame.[6] An immediate consequence of Earth's rotation is the Coriolis force,

$$Coriolis\ force\ =\ -2\Omega\times\mathbf{V},$$

where Ω is Earth's rotation vector which has a magnitude 7.292×10^{-5} sec^{-1} and $\mathbf{V}$ is the parcel velocity having (east, north, up) components $(u,\ v,\ w)$. The Coriolis force is, like gravity, an inertial force, that is exactly proportional to the mass of an object (and hence it might be more appropriate to call it the Coriolis acceleration). The Coriolis force deflects all moving objects, without doing work. For most everyday objects and motions, the Coriolis force is small to the point of being negligible. It is, however, of first importance for the horizontal motions of the atmosphere and oceans, i.e., winds and currents, in large part because all of the other possible horizontal forces are also small. The horizontal component of the Coriolis force acting on a horizontal velocity V is

$$-fe_z\times V\ =\ fve_x-fue_y \tag{3}$$

[6]These essays, including the most recent version of this essay, are available online from https://www2.whoi.edu/staff/jprice/

where e_x, e_y and e_z are the usual east, north and up unit vectors, and

$$f \;=\; 2\Omega \sin(lat) \tag{4}$$

is the all-important Coriolis parameter evaluated at a latitude lat. (Homework problem 1, Sec. 8.2.)

Part 2 went on to consider geostrophic balance, the defining property of large scale, low frequency (extra-equatorial) geophysical flows of the atmosphere and ocean. In a geostrophic balance, the horizontal component of the Coriolis force is balanced by a pressure (or geophysical height) gradient,

$$f v_{geo} \;=\; g' \frac{\partial h}{\partial x} \quad \text{and} \quad f u_{geo} \;=\; -\, g' \frac{\partial h}{\partial y} \tag{5}$$

where $g' \partial h / \partial x$ is the hydrostatic pressure gradient in the special case of a reduced gravity, single layer, shallow water model (as in Parts 2 and 3). Geostrophic balance may be understood using an f-plane approximation in which the latitudinal dependence of the Coriolis parameter (4) is, purely for convenience, represented by a constant evaluated at the central latitude of a model domain, lat_o,

$$f-\text{plane approximation}: \quad f_o \;=\; 2\Omega \sin(lat_o) = const., \tag{6}$$

and the coordinates are rectangular. For this to be appropriate to a given flow, the horizontal scale of the motion should be limited to O(100 km). The dynamics of an f-plane model are isotropic, having no favored direction (recall the isotropic dispersion relation of inertia-gravity waves and geostrophic motion of Part 2, Sec. 2.3).

In contrast to the isotropy of the f-plane, observations of the atmosphere and ocean show that large-scale, low frequency, nearly geostrophic phenomena are often markedly anisotropic in one or more properties. Part 3 studied the striking example offered by mid-latitude, mesoscale eddies, which are observed to propagate westward, slowly but relentlessly, at a speed that depends upon latitude: at 30^o N, the propagation speed is about -3 km per day. In an f-plane model, an isolated, geostrophically balanced mesoscale eddy may be exactly stationary in the sense of being unmoving in space and unchanging in time. However, when the northward increase of f is acknowledged, the same eddy will propagate westward much like observed mesoscale eddies. In Part 3 and here, the northward increase of f is represented by the β-plane approximation, a linear expansion of (1) around a central latitude,

$$\beta-\text{plane approximation}: \quad f_1 \;=\; f_o \;+\; \beta(y - y_o), \tag{7}$$

with y the north coordinate and

$$\beta \;=\; (2\Omega / R_e) \cos(lat_o) \tag{8}$$

and a constant. For this study, $lat_o = 30^o$ N and hence $f_o = 7.29 \times 10^{-5}$ sec^{-1}, and $\beta = 1.98 \times 10^{-11}$sec^{-1} m^{-1}. For this linear approximation of $f(y)$ to be appropriate, the horizontal scale of the phenomena of interest should be somewhat limited, a few thousand kilometers, or less than global.

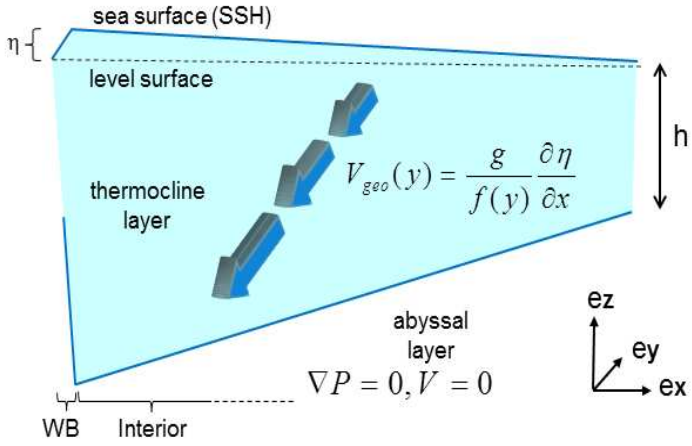

Figure 4: A schematic cross section of the North Atlantic subtropical thermocline, sliced east-west and viewed looking toward the north as in Fig. (1). The upper ocean (thermocline and above) is modeled as a single active layer. The tilt of the thermocline compensates the tilted sea surface so that the horizontal pressure gradient and velocity are vanishingly small in the very thick abyssal layer. The comparatively narrow western boundary region is noted at lower left, and the much wider interior region is all of the rest. The meridional geostrophic current in the interior is equatorward. The three bold arrows are meant to depict the geostrophic current amplitude at three latitudes and increase toward the equator, simply because because f decreases toward the equator. A meridional geostrophic current is thus divergent, $\partial v_{geo}/\partial y > 0$, which is here said to be the beta effect. In this example of equatorward flow, the resulting layer thickness tendency due to the beta effect alone is thus $\partial h/\partial t < 0$, i.e., thinning.

1.5 The beta effect: balanced meridional motion is divergent horizontally

A beta-plane approximation is sufficient to reveal one of the most important consequences of the northward variation of f, that balanced meridional motion is divergent horizontally. To see the significance of this we can examine a vertically integrated continuity equation, or thickness balance, for a single layer (as in a reduced gravity, shallow water model, Part 2),

$$\frac{\partial h}{\partial t} = -(\frac{\partial hu}{\partial x} + \frac{\partial hv}{\partial y}). \tag{9}$$

Now substitute the geostrophic velocity components Eq. (5) and $f(y)$ from (7), to find

$$\boxed{\frac{\partial h_{geo}}{\partial t} = \frac{\beta h}{f} v_{geo}} \tag{10}$$

on the assumption that $\partial^2 p/\partial x \partial y = \partial^2 p/\partial y \partial x$. The subscript geo on the left side is just to emphasize that this is the geostrophic contribution only. This thickness tendency is due to the horizontal divergence

of a balanced meridional velocity in the presence of a northward increase of f, here said to be *the* beta effect.[7] In the example of Fig. (4), a balanced (geostrophic) current is presumed to be southerly, and thus increases in the direction of flow on account of the decrease of f toward the equator. The resulting horizontal divergence $\partial v/\partial y > 0$. Absent some other effect, the layer thickness in this example must then decrease, $\partial h/\partial t < 0$. It is easy to show that if the balanced current is instead poleward, then $\partial v/\partial y < 0$ and the layer will thicken on account of a beta-induced convergence of the horizontal velocity.

Exactly the same thing will happen if there is an applied wind stress and an Ekman current,

$$\boxed{fhu_{Ek} = \frac{1}{\rho_o}\tau_y \quad \text{and} \quad fhv_{Ek} = -\frac{1}{\rho_o}\tau_y} \tag{11}$$

Substituting these into the thickness balance yields

$$\frac{\partial h_{Ek}}{\partial t} = \frac{1}{\rho_o}\left(\frac{1}{f}\frac{\partial \tau_y}{\partial x} - \frac{\partial}{\partial y}(\frac{\tau_x}{f})\right). \tag{12}$$

By expanding the derivative on the rightmost term we can bring out a term that involves beta,

$$\frac{\partial h_{Ek}}{\partial t} = \frac{\beta h}{f}v_{Ek} + \frac{1}{\rho_o f}\left(\frac{\partial \tau_y}{\partial x} - \frac{\partial \tau_x}{\partial y}\right). \tag{13}$$

The wind stress field may (usually will) have some curl, while the pressure gradient field can not.

The geostrophic and Ekman velocities appear in parallel forms here and so it is useful to define their sum to be the balanced velocity,[8]

$$v_{bal} = v_{geo} + v_{Ek} \tag{14}$$

and the sum of (10) and (13) is the corresponding thickness balance,

$$\boxed{\frac{\partial h_{bal}}{\partial t} = \frac{\beta h}{f}v_{bal} + \frac{1}{\rho_o f}\left(\frac{\partial \tau_y}{\partial x} - \frac{\partial \tau_x}{\partial y}\right)} \tag{15}$$

The thickness equation (15) has three modes (notable two term balances). The first and third terms define a forced, time-dependent balance in which the Ekman convergence associated with wind stress

[7] There does not appear to be a wide consensus on the meaning of the phrase 'beta effect'. Many authors, including the Glossary of the American Meteorological Society, use the term to signify anything that happens on a beta plane that would not have happened on an otherwise similar f-plane. By that usage, the divergence of balanced meridional flow would be *a* beta effect.

[8] This use of 'balanced' is evidently not conventional. A balanced velocity is usually meant to indicate a steady, vortical flow in which geostrophy is modified by centrifugal force.

curl thickens or thins the surface layer locally. This is a very important process insofar as it changes the mass and thus the pressure field, but discussion will be deferred to Sec. 3.1.2. The first and second terms define a time-dependent, free (unforced) balance that describes westward propagation, and the second and third terms define a forced, steady flow which is the Sverdrup balance, albeit in a one layer model.

1.5.1 Westward propagation of free motions

The mechanism of westward propagation may be understood as the second mode noted above, the balance between time-dependence and the beta effect. To see this, rewrite the beta term using the geostrophic velocity, to find a first order wave/advection equation (Sec. 8.2, Problem 3),

$$\frac{\partial h_{geo}}{\partial t} \;=\; \beta R_d^2 \frac{\partial h}{\partial x}, \tag{16}$$

where

$$R_d \;=\; \frac{\sqrt{g'h}}{f} \;=\; \frac{C}{f}$$

is the radius of deformation. C is the gravity wave speed; in the subtropics, $C \approx 3$ m sec^{-1}, and at 30^o N, $R_d \approx 40$ km. Eqn. (19) is appropriate for free motions, e.g., elementary waves $h(x,t) \;\propto\; sin(kx - \omega t)$, and so may be characterized by a dispersion relation that connects the wavenumber, $k = 2\pi/\lambda$, and the frequency, ω,

$$\omega \;=\; -k\beta R_d^2. \tag{17}$$

This is the long wave limit of baroclinic Rossby waves (Part 3, Sec. 2.3). In this limit, phase and group speeds are equal to the long Rossby wave speed,

$$\boxed{C_{longRo} \;=\; \frac{\omega}{k} \;=\; \frac{\partial \omega}{\partial k} \;=\; -\beta R_d^2 \;\leq\; 0.} \tag{18}$$

C_{longRo} is independent of k and ω, and so this propagation is nondispersive and westward. Eqn. (16) is thus a first order wave/advection equation,

$$\boxed{\frac{\partial h_{geo}}{\partial t} \;=\; -C_{longRo}\frac{\partial h}{\partial x}} \tag{19}$$

C_{longRo} varies quite a lot with f, but at a fixed site, C_{longRo} is equivalent to a constant, westward advection velocity. Using values from 30^o N, $C_{longRo} \;\approx -3$ km day^{-1}, which is consistent with the observed propagation of mesoscale eddies discussed in Part 3.

What is most important is that all free (unforced) large scale ($\lambda >> R_d$), low frequency ($\omega << f$) phenomena will propagate westward, regardless of planform. If there are indeed no small horizontal scales involved (and so no dispersion), then the planform will be conserved and will appear to be shifted steadily westward, as if by advection, at the constant rate, C_{longRo}. It seems appropriate to call such westward propagating phenomena 'Rossby waves', even if the planform may look nothing like an elementary wave.[9] As we will see in Sec. 3.1.3, an appreciation for this generalized Rossby wave propagation is a key concept needed to understand the response of an ocean circulation to a transient wind. (For a little more on this see Homework problem 3, Sec. 8.2.)

1.5.2 Steady, forced meridional motion is Sverdrup flow

The third mode of (15) is forced, steady motion,

$$\boxed{hv_{bal} \;=\; \frac{1}{\beta\rho_o}\left(\frac{\partial\tau_y}{\partial x} - \frac{\partial\tau_x}{\partial y}\right)} \tag{20}$$

or in a more streamlined notation,

$$M^y_{bal} \;=\; \frac{1}{\rho_o\beta}\nabla\times\tau,$$

which is none other than the Sverdrup relation for this single layer model in which

$$M^y_{bal} \;=\; h(v_{geo} \,+\, v_{Ek}) \;=\; M^y_{geo} \,+\, M^y_{Ek}.$$

This is perhaps the simplest way to envision the mechanism behind the Sverdrup relation: a balance between the beta-induced divergence of a balanced meridional current (geostrophic plus Ekman) and the wind stress curl component of Ekman transport divergence. To say it a little differently, if there is a steady state in the presence of a wind stress curl, then a beta effect acting upon a meridional transport will be implied. The sense and the magnitude of this meridional transport is given by the Sverdrup relation. In this single layer model, the Sverdrup transport is, by default, present entirely within the single active layer, which is also the Ekman layer. Surprisingly, this is also a plausible outcome in a much more capable model that we will come to in Sec. 6, though not necessarily what we see in the ocean.

[9] Much of the pioneering research on the topics discussed in this essay appeared in a series of classic papers by Carl G. Rossby and colleagues published in the late 1930s. A collection of Rossby's highly readable papers is available online at http://www.aos.princeton.edu/WWWPUBLIC/gkv/history/general.html

There is another way to see the Sverdrup relation that combines the previous two descriptions of modes. We have pointed out that every large scale zonal gradient of thickness should have a tendency to propagate westward. Mesoscale eddies conform to this notion — why not same for the basin-scale meridional gradient that we see in Fig. 1? If the gyre was a free motion, it certainly would propagate westward, and the result at a given site would be a thinning of the upper ocean layer as given by Eqn. (19). However, the basin scale flow i.e., the gyre, is subject also to wind stress curl, which will tend to thicken the upper ocean layer, Eqn. (11). If these two tendencies just offset one another, then combining Eqns. (11) and (17) we get that

$$0 = \frac{\partial h_{geo}}{\partial t} + \frac{\partial h_{Ek}}{\partial t} = \beta R_d^2 \frac{\partial h}{\partial x} - \frac{1}{\rho_o}\left(\frac{1}{f}\frac{\partial \tau_y}{\partial x} - \frac{\partial}{\partial y}(\frac{\tau_x}{f})\right). \tag{21}$$

This can be rearranged a little to find

$$\boxed{M^y_{geo} = \frac{1}{\rho_o \beta}\nabla \times \frac{\tau}{f}} \tag{22}$$

the geostrophic form of the Sverdrup relation. Notice that here the curl operates on wind stress divided by f. This is a form that is often used to test the Sverdrup relation against field observations.

1.6 Remarks on depth dependence*

It is helpful to consider briefly what amounts to the complement of a single-layered model, a three-dimensional system that is presumed to be quasi-steady, linear and inviscid and that admits depth-dependence. The three dimensional velocity components of this system are u, v, and w, and e.g., u is $u(x, y, z)$ (note that this holds for the present section only). The three dimensional density, continuity and momentum equations of this system are

$$\left[\frac{\partial \rho}{\partial t}\right] = -w\frac{\partial \rho}{\partial z} + \left[A\frac{\partial^2 \rho}{\partial z^2}\right] \tag{23}$$

$$0 = \frac{\partial u}{\partial x} + \frac{\partial v}{\partial y} + \frac{\partial w}{\partial z}, \tag{24}$$

$$0 = -fv - \frac{1}{\rho_o}\frac{\partial p}{\partial x} + \frac{1}{\rho_o}\frac{\partial \tau^x}{\partial z}, \tag{25}$$

$$0 = fu - \frac{1}{\rho_o}\frac{\partial p}{\partial y} + \frac{1}{\rho_o}\frac{\partial \tau^y}{\partial z}, \tag{26}$$

$$0 = \frac{\partial p}{\partial z} + g\rho. \tag{27}$$

The Coriolis parameter f is $f(y)$ via the β-plane approximation, Eqn. (7), which is crucially important in what follows. There are two steady forces recognized here, the horizontal gradient of the hydrostatic pressure, p,

$$p(x,y,z) = \int_{-z}^{\eta(x,y)} g\,\rho(x,y,z)\,dz,$$

which, like the velocity components, is regarded as an unknown. A second important force is the vertical gradient of a turbulent momentum flux,

$$\tau^x(x,y,z) = \rho_o < u'(x,y,z,t)w'(x,y,z,t) >$$

where the brackets $< \quad >$ indicate a time average over tens of minutes. The small scale, three-dimensional motions u', w' that propagate a turbulent momentum flux are outside the scope of a large scale circulation model. We will, however, presume to know the surface value, $\tau_o = \tau(x,y,z=0)$, which may be estimated from observations of wind over the oceans, i.e., τ_o is said to be the wind stress (Fig. 3). And we also know something about the vertical scale over which the stress is divergent, discussed below.

Given that the momentum balances are steady and linear, we can rewrite the force terms on the right hand side of (25) and (27) in terms of geostrophic and Ekman velocity components, say for the meridional component,

$$v_{geo} = \frac{1}{\rho_o f}\frac{\partial p}{\partial x} \quad \text{and} \quad v_{Ek} = -\frac{1}{\rho_o f}\frac{\partial \tau^x}{\partial z}$$

with no loss of generality, and define the sum to be the balanced velocity,

$$v_{bal} = v_{geo} + v_{Ek},$$

just as before. The meridional transports associated with these velocities are

$$M^y_{bal} = M^y_{geo} + M^y_{Ek} \tag{28}$$

where

$$M^y_{geo} \;=\; \int_{-d_{geo}}^{0} v_{geo}\, dz \quad \text{and} \quad M^y_{Ek} \;=\; \int_{-d_{Ek}}^{0} v_{Ek}\, dz \;=\; -\frac{1}{\rho_o}\frac{\tau^x_o}{f}. \tag{29}$$

The lower limit of depth in these transport integrals is significant. The geostrophic velocity of the major, upper ocean gyres is appreciable to at least the depth of the lower main thermocline, d_{geo} is O(1000 m), and geostrophic currents associated with the global-scale overturning circulation extend over the full depth water column, noted in the discussion of Fig. (1). The Ekman velocity will be significant within an upper ocean surface layer that is mixed by the turbulent stress imposed at the surface by the wind. In density-stratified regions, such as the subtropical gyre, this Ekman layer may be as deep as the top of the seasonal thermocline, d_{Ek} is O(100 m), and hence almost always much less than d_{geo}. This important effect of stratification is something we will come back to when it is time to consider what is missing from a shallow water model (Secs. 4.3.2 and 6.3).

1.6.1 Vorticity balance

Assuming that the wind stress on the sea surface is given, then the Ekman transport is also known. The geostrophic transport remains completely unconstrained, however, and so we can not go any further with momentum balance and continuity alone. To find out what we can learn about this system, it is very helpful to form the vorticity balance: take the partial x derivative of (27) and subtract the y derivative of (25); then eliminate the horizontal divergence $\partial u/\partial x + \partial v/\partial y$ using the continuity equation (24). This eliminates the unknown pressure and yields the steady, linear vorticity balance,

$$\beta v_{bal} \;=\; f\frac{\partial w}{\partial z} \;+\; \frac{1}{\rho_o}\frac{\partial}{\partial z}\left(\frac{\partial \tau^y}{\partial x} \;-\; \frac{\partial \tau^x}{\partial y}\right), \tag{30}$$

that holds at all z where (25) - (24) are valid. The detailed depth-dependence of w and of the wind stress-induced momentum flux are not knowable within this system alone, but we can claim to know some relevant boundary values; depth-integrate (30) from some depth $z = -d$ up to the sea surface where the wind stress is presumed known, τ_o , and the vertical velocity must vanish, *to wit*, the depth integral of (30) is

$$\beta \int_{-d}^{0} v_{bal} dz \;=\; -fw(-d) \;+\; \frac{1}{\rho_o}\left(\frac{\partial \tau^y}{\partial x} \;-\; \frac{\partial \tau^x}{\partial y}\right)\Big|_{-d}^{0}. \tag{31}$$

If d is deeper than the depth of the surface layer (Ekman layer), then $\tau(-d) = 0$ and all of the stress is absorbed over the volume of the integral and so

$$\beta \int_{-d}^{0} v_{bal} dz \;=\; -fw(-d) \;+\; \frac{1}{\rho_o}\left(\frac{\partial \tau^y_o}{\partial x} \;-\; \frac{\partial \tau^x_o}{\partial y}\right). \tag{32}$$

We can rewrite this using symbols already introduced,

$$\boxed{\beta M^y_{-d} \;=\; -fw(-d) \;+\; \frac{1}{\rho_o}\nabla\times\boldsymbol{\tau}_{\mathbf{o}}} \tag{33}$$

(and run out of space for subscripts, and so M_{bal} will be understood.) This is very close to the classic Sverdrup relation (1), but includes the vortex stretching effect of the vertical velocity at $z=-d$, $fw(-d)$. With this term included, (33) is as general as Eqns. (25) - (24), and M^y_{-d} of (33) is the balanced meridional transport above $z=-d$ regardless of what the ultimate cause may be, i.e., whether wind-driven locally in the Sverdrup sense or a geostrophic flow associated with the global-scale overturning circulation.

1.6.2 Considering the vertical velocity, w(z)

The depth-integrated vorticity equation (33) is still not closed as there are two unknowns, the transport M^y_{-d} that we seek, and the vortex stretching term, $fw(-d)$, at the base of the control volume. To estimate the transport we have to argue for some form of $w(z)$.

In theories of small scale, three-dimensional motions, e.g., short wind waves on the sea surface, the vertical velocity is treated exactly on par with the horizontal velocity. However, in large scale circulation models, which deal only with low frequency motions, the vertical velocity is treated very differently. The vertical momentum balance is hydrostatic, Eqn. (24), to a very high approximation, and hence $\partial w/\partial t$ is inaccessible, effectively. Instead, $\partial w/\partial z$ is computed diagnostically from the divergence of the horizontal velocity on the basis that the motion is non-divergent in three dimensions. In a somewhat similar way it is not possible to observe the large scale, low frequency vertical velocity in any kind of widely used field measurement as it is simply too small; a very significant vertical velocity is 10 m year^{-1}. A diagnostic computation via the observed horizontal velocity is also problematic given the very small values of horizontal convergence compared with estimation errors. The saving grace in all of this is that we can claim to know the boundary values of the vertical velocity at the sea surface, $w(z=0)=0$, as already noted, and at the sea floor, $w(z=-b)=0$, with b the depth of a presumably flat sea floor.

Estimating $\mathbf{w(d)=0}$ from field data. If the aim is to estimate the equivalent of Sverdrup transport from field data,[5], then an argument can be made for choosing $w(d)=0$ at $d\approx$ -1000 m. The almost flat isopycnal surfaces at approx. 1000 m depth in Fig. (1) suggest that the vertical shear of the meridional geostrophic current is very small around that depth, and hence the current and its beta-induced divergence are likely to be very small as well. This choice $d=-1000$ m passes a plausibility test insofar as the

observed meridional transport above roughly 1000 m has been found to make a semi-quantitative match to the expected Sverdrup transport over most of the subtropical gyre (Sec. 1.2). This important, additional piece of information regarding the depth of Sverdrup transport is empirical, and leaves open whether this depth could be different in other regions or other circumstances.

The model experiments discussed in Secs. 3 and 6 point to other possibilities for $w(z)$ and d that we discuss briefly. The point in this is to show that a very wide range of velocity profiles can be consistent with Sverdrup transport. First, rearrange Eq. (30) to solve for fw, and integrate from the surface downward,

$$fw(z) \;=\; \beta \int_0^z v_{bal} dz \;+\; \frac{1}{\rho_o}\left(\frac{\partial \tau_o^y}{\partial x} \;-\; \frac{\partial \tau_o^x}{\partial y}\right) - \frac{1}{\rho_o}\left(\frac{\partial \tau^y(z)}{\partial x} \;-\; \frac{\partial \tau^x(z)}{\partial y}\right). \tag{34}$$

For this purpose we are going to imagine a thick surface layer and specify that the depth-dependence of $\tau(z)$ is a linear decrease from the surface value to zero at the depth of the surface layer, $z = z_{Ek} = -0.2$. This linear decrease is equivalent to a constant wind stress acceleration within the surface layer. We can assume that the local wind stress is zero, and that the wind stress field has negative curl. This will cause a converging Ekman transport and a downward vertical velocity (the blue line of Fig. (5 left)), often called Ekman pumping, that is zero at the sea surface and has a maximum at the base of the Ekman layer, $z = -0.2$. At depths below the surface layer, there is no additional divergence due to the Ekman transport, and hence the vertical velocity due solely to the wind stress curl is constant down to the sea floor. In order to have w vanish at the sea floor, some additional source of divergence and thus another contribution to the vertical velocity is required, and the beta effect acting upon a balanced meridional current (geostrophic only in this case) is just the thing. Assuming that the vertical velocity due to Ekman pumping is downward (negative) then the countervailing vertical velocity due to the beta effect must be upwards (positive) requiring that $\partial v/\partial y > 0$ and thus a southward flow (Fig. 4). Just how that southward (Sverdrup) flow is distributed in the water column is not obvious. Inspection of field data noted above gives one possibility (and the most important one!) and here are two other extreme possibilities that we will see in model experiments to come. For this purpose we can assume that $f \;=\; \beta = 1$. Just for illustration, assume that the wind stress curl yields a vertical velocity $w(-0.2) = -1$. In order to satisfy the sea floor boundary condition, the beta term integrated down to the sea floor must be = +1.

Barotropic Sverdrup transport, d = b. One possibility is that the balanced current current uniform could be with depth and have an amplitude -1, Fig. (5, upper). In that case $d = b$, and the transport integral over the full water column is given by the Sverdrup relation. While the vertical velocity will necessarily vanish at the sea floor, at most depths above the sea floor w will be non zero. The velocity may be almost exactly geostrophic and the transport very accurately Sverdrupian, and yet the system will not be in a true steady state since the density will still be evolving, albeit slowly, on account of vertical advection, Eqn. (23). This is what we will find at short times (weeks to months) in experiments with a

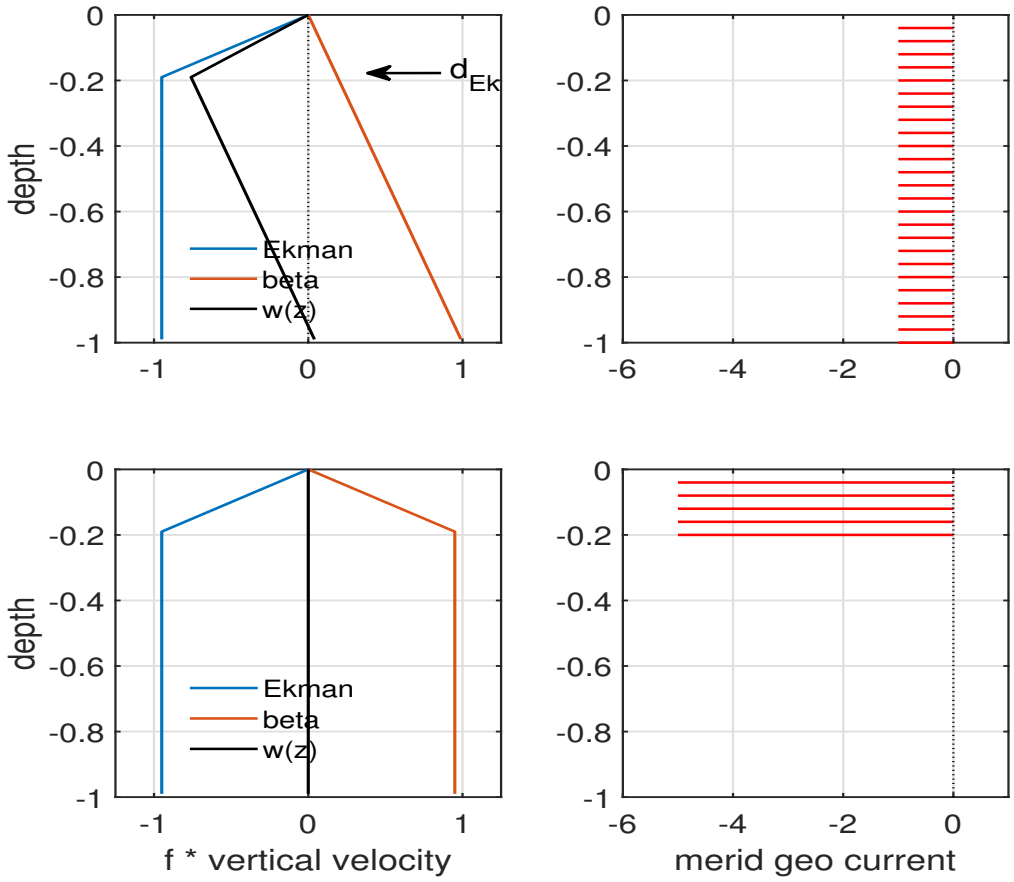

Figure 5: Schematic vertical velocity and gesotrophic velocity profiles that will be encountered in upcoming model experiments. In both cases the depth of the Ekman layer is taken to be $-d_{Ek}$ = -0.2, and the presumed flat sea floor is at $z = -1$. The Ekman transport is presumed to vanish. The vertical velocity associated with wind stress curl is the blue line, which vanishes at the sea surface. In these examples the Ekman-induced vertical velocity is downward, as in the subtropical gyre, and hence the balanced (geostrophic) current must be southward. **(upper)** Barotropic Sverdrup transport. Assuming a geostrophic current that is uniform with depth (sketched at right), the vertical velocity associated with the beta effect is the red line, which we can assume vanishes at the sea surface. The sum of the Ekman and the beta-induced vertical velocity is $w(z)$, the black line, which must vanish at the sea surface and at the sea floor. This determines the amplitude of the geostrophic current, -1 in this case. **(lower)** Baroclinic and surface-trapped Sverdrup transport. In this example, the geostrophic current is confined to the surface layer. In this case, w vanishes throughout the water column, and the geostrophic current has an amplitude of -5.

three layer model that includes an active lower layer and a free sea surface (Section 6). Hence, barotropic Sverdrup transport is quite possible, though it is not what we observe in the long-term average of ocean field data.

Surface-trapped, baroclinic Sverdrup transport, $\mathbf{d} = \mathbf{d_{Ek}}$. Another possibility consistent with the Sverdrup relation is that the balanced current could be confined to the surface layer. In that event, the current must have an amplitude of -5. This configuration yields a vertical velocity that is zero throughout the water column and so literally steady. This surface-trapped Sverdrup regime occurs by default in the single layer model as noted in Sec. 1.5.2, and it also arises in the solution of the three-layer model at very long times (decades after startup, Sec. 6). Interesting though it is, this surface trapped solution is not consistent with the inferred depth scale from field observations, since we expect that d_{Ek} is considerably less than the roughly 1000 m we infer from field data.

2 Shallow water models of wind-driven circulation

The shallow water model introduced in Part 2 can be made into a useful tool for studying some important facets of the wind-driven circulation by 1) defining an appropriate domain and boundary conditions, 2) adding a new term that represents wind forcing, and 3) including a very simple form of dissipation. A straightforward extension to multiple layers is also described.

2.1 Boundary and initial conditions

The ocean domain is taken to be a square basin with sides of length $2L$ centered on 30 ^{o}N. Rotation is treated by a β-plane approximation and the basin size is then chosen so that the southern boundary will correspond to the equator, $f = 0$. Given $\beta(30^o)$, this requires $L = 3600$ km. The resulting basin width, $2L = 7200$ km, is roughly comparable to the average width of the North Atlantic Ocean, but is only about half the width of the mighty Pacific Ocean. The intention is to model a self-contained circulation, and so the boundaries of the model domain are made impermeable by setting the normal component of velocity to zero,

$$\mathbf{V}\cdot\mathbf{n} = 0, \tag{35}$$

598 on all of the boundaries.[10]

599 The initial condition is a state of rest throughout the basin and isopycnals are everywhere flat,

600 $$\mathbf{V}(x,y) = 0 \ \text{ at } \ t = 0, \ \text{ and } \ h(x,y) = constant \ \text{ at } \ t = 0 \ \text{ and for all } \ (x,y). \tag{36}$$

601 The specification of the initial thickness is deferred to Sec. 2.5.

602 2.2 Wind stress and its curl

603 The energy source in these experiments is a wind stress, $\tau(x,y)$, a tangential force per unit area imposed
604 on the sea surface (the subscript $_o$ needed in Sec. 1.3 has been dropped since only the surface value of
605 wind stress will be relevant from here on). The wind stress field has to be specified from outside the
606 model, and here it will be represented by an idealization of the time-mean wind stress that has been
607 computed from observed winds over the oceans, Fig. (3).[11] So far as the Sverdrup relation is concerned,
608 the crucial property of the wind stress field is the curl, $\nabla \times \tau(x,y)$. The shallow water model requires the
609 wind stress itself, and here, just to keep it simple, we will specify the zonal component τ^x only, and
610 assume that τ^x is independent of x, thus

611 $$\tau^x(y) \ = \ \xi \sin(n\pi y/L), \tag{37}$$

612 where the amplitude ξ is a positive constant. For the standard case of Sec. 3, $n = 1$, and the wind stress
613 is eastward over the northern half of the basin, which mimics westerly winds, and westward on the
614 southern half of the basin, i.e., easterlies (Fig. (6). The amplitude is taken to be $\xi = 0.1$ Pa, or about what

[10] The southern and northern boundaries of the real North Atlantic basin are not barriers as the present model domain implies. There is instead a significant poleward flow of warm water from the southern hemisphere into and through the North Atlantic. In the equatorial region this occurs largely within a western boundary current evident in Fig. 2, usually called the North Brazil Current. At the northern boundary, some of this warm inflow continues poleward into the Norwegian-Greenland Sea as the North Atlantic Current (or Drift). The shallow, warm poleward flow is balanced by a deep, cold equatorward flow (deeper than the thermocline layer shown in Fig. 1). The cross-equatorial exchange of warm and cold water is a very important component of the global-scale, meridional overturning circulation. The overturning circulation is not driven directly by basin-scale winds, as are the upper ocean gyres of Fig. 2, and so an overturning circulation does not arise in the present experiment.

[11] A particularly handy reference for such climate data is by Peixoto and Oort, 1992, *Physics of Climate*, American Inst. of Physics, New York, NY. There are now more than a dozen wind stress climatologies that are consistent at the semi-quantitative level needed here (see Townsend, T. L., H. E. Hurlburt and P. J. Hogan, 2000, 'Modeled Sverdrup flow in the North Atlantic from 11 different wind stress climatologies', *Dyn. Atmos. Oceans*, **32**, 373-417.) The differences in detail between the various wind stress climatologies make an easily detectable and in some ways important difference in the computed Sverdrup flow, as does the basin topography.

is estimated for the mean wind stress by the westerlies. In the experiment of Sec. 3, this wind stress field is assumed to be constant in time once it is switched on. (In Sec. 5.1, the amplitude, ξ, will be made to oscillate with an annual cycle, and in Sec. 5.3 the wind stress will be made meridional.)

A very important parameter of (37) is

$$\text{the meridional length scale of the wind field; for n } = 1, \quad L_\tau = L/n\pi \approx 1200 \text{ km}.$$

This is comparable to though a little less than two other important horizontal scales in this problem,

$$\text{the basin scale,} \quad L = 3600 \text{ km, and,}$$

$$\text{the planetary scale on which } f \text{ varies,} \quad R_f \;=\; R_E/2 \approx 3300 \text{ km},$$

where R_E is the radius of the Earth. All of these length scales are much greater than the natural horizontal length scale of the baroclinic ocean,

$$\text{the baroclinic radius of deformation at } 30^o \text{ latitude,} \quad R_d \approx 40 \text{ km}.$$

The wind stress is applied to the surface layer of the model ocean as if it was a body force absorbed evenly throughout the surface layer and hence the acceleration due to wind stress alone is just

$$\frac{D\mathbf{v_1}}{Dt} \;=\; \frac{\tau}{\rho_o h_1}, \tag{38}$$

which is a valid approximation of the full momentum balance for very short times, $t \ll 1/f$, a few hours or less. In a shallow water model, $d_{Ek} = h_1$, and here we have chosen $h \;=\; 250$ m (three layer model), or 500 m (single layer reduced gravity model), in order to have a realistic baroclinic wave speed. In the real, stratified ocean, d_{Ek} is less than this, typically 25 - 100 m. We will consider some of the implications of this as we go along, but for now note that the Ekman current in this model is considerably weaker than in the real ocean, but the Ekman transport and the Sverdrup transport are the same whether the wind stress is absorbed in a comparatively thin surface layer (as actually occurs) or over the entire upper ocean layer that is wind-driven in the Sverdrup sense, as happens in a shallow water model.

The very important curl of the wind stress given by (37) is

$$\nabla\times\tau(x,y) \;=\; -\frac{\partial\tau^x}{\partial y} \;=\; -\frac{n\pi\xi}{L}\cos(\pi y/L), \tag{39}$$

which has an amplitude $\xi/L_\tau \;\simeq\; 0.8\times10^{-7}$ N m^{-3} ($n \;=\; 1$). This is comparable to typical values of stress curl seen in Fig. (3), but less than the maximum values, which are roughly 2×10^{-7} N m^{-3} . The

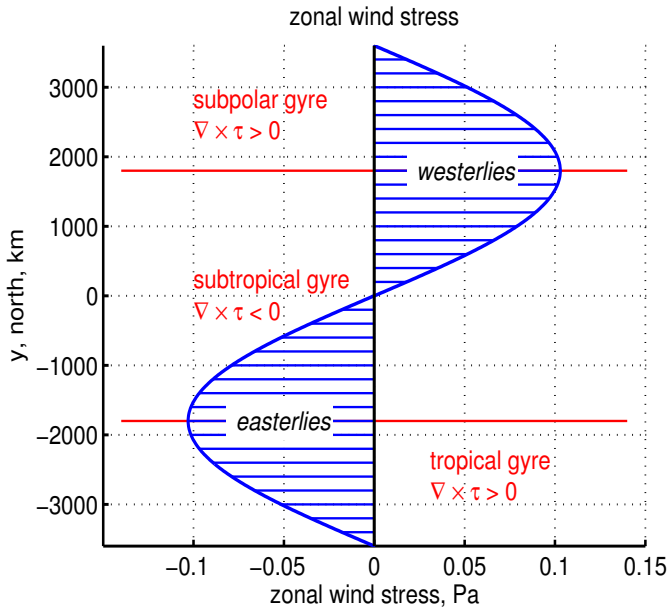

Figure 6: An idealized, zonal wind stress field that is applied to the shallow water model. The horizontal red lines appear in subsequent figures to show the axes of the easterly and westerly wind maxima, and thus the boundaries of the stress curl — negative (clockwise) in the large subtropical region between the westerly and easterly axes, and positive (anti-clockwise) over the smaller tropical and subpolar regions. These red lines correspond closely to the gyre boundaries.

sign of the wind stress curl defines three regions: a central subtropical region where the stress curl is negative (clockwise turning), and tropical and subpolar regions where the curl is positive (anti-clockwise), Fig. (6).

This idealized stress field is least realistic for the tropical region insofar as it omits a secondary maximum of the easterly winds often present near the equator (most pronounced in the Pacific). This gives a narrow region of negative stress curl within a few degrees of the equator that, if included here, would give two smaller tropical gyres vs. one rather large tropical gyre that results from (37). This error in the tropical winds is left in place because the goal is not so much a realistic simulation of the observed ocean circulation — which would require much more than just a better wind field — but rather to investigate how the wind-driven circulation varies with latitude. The idealized stress field Eqn. (37) is appropriate to this goal since the wind stress curl magnitude of (37) is the same over the three regions (tropical, subtropical and subpolar). β is also the same, and hence so too is the Sverdrup transport. The actual transport of the subpolar and tropical gyres is, however, *not* the same as Sverdrup transport because of zonal boundary effects that extend many hundreds of kilometers into the tropical and subpolar gyres (Sec. 4.2.3).

2.3 An expedient parameterization of drag on ocean currents*

With a wind stress included, and if we intend to compute up to a possible steady state, then there has to be some mechanism to dissipate the energy and potential vorticity that are supplied by the wind. The present model follows the classic treatment by Stommel (1948)[4] in choosing a linear drag that is proportional to and anti-parallel to the velocity,

$$drag \;=\; -rh_o\mathbf{V}, \tag{40}$$

sometimes called Stokes drag. This has the dimensions of a stress/density, and the resulting acceleration is $-rh_o\mathbf{V}/h$ (as in the single particle model of Part 1, Section 5, aside from varying layer thickness). The coefficient r is taken to be $r = 1/(15 \text{ days})$, the smallest value of r that will allow the ocean circulation in this system (wind stress included) to reach a near steady state. Given a nominal layer thickness, $h \approx h_o$, the Ekman number at 30 ^{o}N is $E = r/f \approx 0.01$. This E may seem quite small, but nevertheless, the model dynamics are almost certainly more viscous overall than is the real ocean. In Secs. 3 and 4 we will find out how this value of r is related to the natural width of the western boundary current, the radius of deformation.

In some contexts it might be argued that the Stokes drag represented by Eqn. (40) is a crude treatment of bottom drag. However, that is not plausible here since the active layer is not imagined to be in contact with a sea floor. It is probably better to think of the Stokes drag as nothing more than the simplest form of a drag or dissipation process that permits a steady state in this model. Given this *ad hoc* basis for (40), we will have to be careful not to over interpret those aspects of the solution that depend sensitively upon the value or r, most notably the zonal boundary current width of Sec. 4.3.

2.4 Momentum and vorticity balances

With wind stress and drag included, the shallow water continuity (thickness balance) and momentum equations (derived in Part 2) are

$$\frac{Dh}{Dt} \;=\; \frac{\partial h}{\partial t} \;+\; \mathbf{V}\cdot\nabla h \;= -h\nabla\cdot\mathbf{V}, \tag{41}$$

$$\frac{D\mathbf{V}}{Dt} \;=\; \frac{\partial \mathbf{V}}{\partial t} + \mathbf{V}\cdot\nabla\mathbf{V} \;=\; -\nabla P/\rho_o \;-\; f\mathbf{k}\times\mathbf{V} \;+\; \frac{\tau}{\rho_o h} \;-\; \frac{rh_o}{h}\mathbf{V}. \tag{42}$$

The P is hydrostatic pressure anomaly defined in the next subsection. Notice that the thickness balance (41) is adiabatic in the sense that the thickness can change only by way of a divergent thickness flux, and

hence the net (basin integral) thickness is conserved.[12] This is not true for the momentum balance because of the wind stress source term and the Stokes drag dissipation term.

The shallow water potential vorticity is

$$q = \frac{\nabla\times\mathbf{V} + f}{h}, \tag{43}$$

and the q-balance is

$$\frac{Dq}{Dt} = \frac{\partial q}{\partial t} + \mathbf{V}\cdot\nabla q = \frac{1}{\rho_o h}\nabla\times\frac{\tau}{h} - \frac{rh_o}{h}\nabla\times\frac{\mathbf{V}}{h}. \tag{44}$$

Part 3 studied free Rossby waves that could be described via the mechanisms of q conservation, $Dq/Dt = 0$. Rossby wave-like motions are possible also in (44) and are a crucial part of the time-dependent dynamics discussed in Sec. 3.3.

2.5 Models of stratification and pressure

The last piece is to connect the hydrostatic pressure P with the mass field, i.e., the stratification. Two models are used here.

2.5.1 Single layer, reduced gravity model, 1l-rg

The stratification model used most extensively here is exactly the shallow water, single layer, reduced gravity model of Parts 2 and 3, *viz.*, a single active upper ocean layer above a quiescent (infinitely deep) abyssal layer. In that event, the hydrostatic pressure anomaly within the upper ocean layer is just

$$P = g\delta\rho(h - h_o) \tag{45}$$

[12] This adiabatic property is especially convenient for some diagnostics of the time-changing stratification. However, it is also a liability, insofar as the layer thickness given by (41) can vanish under some plausible forcing regimes, especially at high latitudes. Vanishing layer thickness means instant death for a numerical integration. A partial remedy is to start with a fairly thick initial layer, 500 m, as is done here. Better would be the inclusion of a vertical mixing process that kept the upper layer thickness finite at all times, but which is not attempted here.

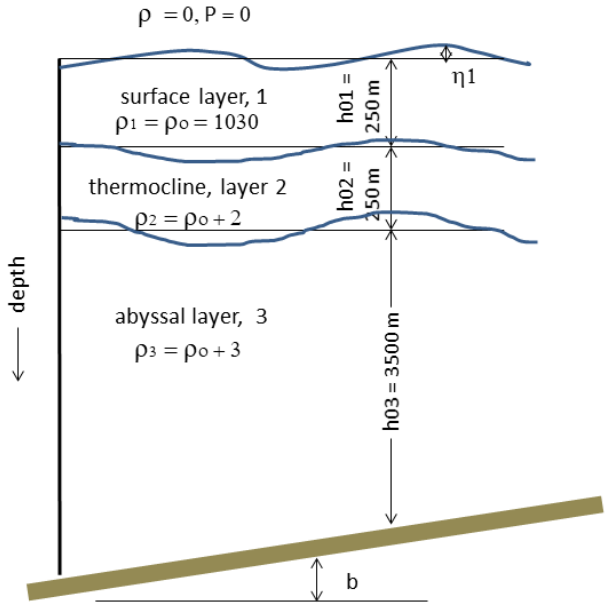

Figure 7: A three layer representation of the density stratification of the open ocean. The density and the thickness of each layer is noted. These thickness and density values are most apropos the subtropical ocean, but are presumed to hold throughout the basin. In this study the bottom depth b is presumed constant, i.e., a flat bottom.

which gives a high pressure (anomaly) where the layer thickness is large. The equivalent SSH, which is useful for comparison to the observed SSH (Figs. 1 and 2) is just

$$\eta_1 = \frac{\delta\rho}{\rho_0}(h - h_o). \tag{46}$$

The initial thickness is chosen to be fairly large, $h_o = 500$ m, and the density difference fairly small, $\delta\rho = 2$ kg m^{-3}. The nominal gravity wave speed is thus $= \sqrt{g\delta\rho h_o/\rho} = 3$ m sec^{-1}, which is a realistic baroclinic gravity wave speed for the subtropics, but a little high for the tropics and subpolar regions of the ocean. The radius of deformation at 30^o is $R_d = 42$ km, and the equatorial radius of deformation is $R_{deq} = \sqrt{C/\beta} = 400$ km.

2.5.2 Three layer, free surface model, 3l-fs

In this somewhat more realistic model, the stratification is represented by two upper ocean layers, and a comparatively thick abyssal layer (Fig. 7). This is still quite truncated, but sufficient to make a few

important points (Sec. 6). The surface layer, h_1, is presumed to absorb all of the wind stress. Layer 2 is the thermocline, which follows the same momentum balance as does layer 1, though with zero wind stress, and layer 3 is the thick abyssal layer, same comment. In general, the thickness of the abyssal layer should include a significant term due to the spatially variable sea floor depth, which for now is taken to be uniform, $b = 0$. This three layer model is a straightforward generalization of the shallow water (layered) model of Parts 2 and 3, sometimes referred to as a stacked shallow water model. The initial thickness and the constant density difference, $\delta\rho$, across the top of these layers is taken to be

h_{0i}, m	ρ_i, kg m^{-3}	$\delta\rho_i$, kg m^{-3}
250	1030	1030
250	1032	2
3500	1033	1

The density and pressure of the overlying atmosphere are presumed to vanish and hence the density contrast across the sea surface, the top of layer 1, is $\delta\rho_1 = \rho_o = 1030$ kg m^{-3}, the nominal density of sea water. The density contrast across the top of layers 2 and 3 is very much less, $\delta\rho_2 = 2$ kg m^{-3} and $\delta\rho_3 = 1$ kg m^{-3}. In that sense, the ocean is very weakly stratified internally. Nevertheless, this internal stratification is of first importance for many oceanic phenomenon. The surface layer thickness is taken to be 250 m to delay the occurrence of $h \to 0$, and so is too large by a factor of about five. Hence the wind-driven surface layer currents in this model are weak compared to observations.

Layer thickness is a conserved quantity, barring vertical mixing (which undoubtedly occurs), meaning that the thickness of a given layer can change only if there is a divergence of volume flux within that layer, i.e.,

$$\frac{\partial h_1}{\partial t} = -\left(\frac{\partial (h_1 u_1)}{\partial x} + \frac{\partial (h_1 v_1)}{\partial y}\right), \tag{47a}$$

$$\frac{\partial h_2}{\partial t} = -\left(\frac{\partial (h_2 u_2)}{\partial x} + \frac{\partial (h_2 v_2)}{\partial y}\right), \tag{47b}$$

$$\frac{\partial h_3}{\partial t} = -\left(\frac{\partial (h_3 u_3)}{\partial x} + \frac{\partial (h_3 v_3)}{\partial y}\right). \tag{47c}$$

The horizontally-varying pressure anomaly is due to the displacement of the density surfaces away from their nominal, resting, flat state. From the bottom up, the interface displacements are

$$\eta_3 = h_3 - h_{o3} - b, \tag{48a}$$

$$\eta_2 = \eta_3 + h_2 - h_{o2}, \tag{48b}$$

$$\eta_1 = \eta_3 + \eta_2 + h_1 - h_{o1}. \tag{48c}$$

The motions of interest have very gentle accelerations compared to g, and so the pressure anomaly that accompanies the displaced density field may be assumed hydrostatic, i.e., due to the weight of the overlying water column. The hydrostatic pressure anomaly within each layer is then, from the surface layer down,

$$P_1 = g\,\rho_o\,\eta_1, \tag{49a}$$

$$P_2 = P_1 + g\,\delta\rho_2\,\eta_2, \tag{49b}$$

$$P_3 = P_2 + g\,\delta\rho_3\,\eta_3. \tag{49c}$$

The height of a given density interface thus depends upon the thickness of the fluid layers below, while the pressure depends upon the displaced density surfaces above. This bottom-up density/thickness relationship and top-down pressure/density relationship is what you would expect physically from hydrostatic pressure.

The description of motions that develop in this system is oftentimes aided by reference to the normal modes of the system. In fact, the normal modes show up fairly distinctly in the solutions that follow. A method for computing the normal modes was discussed in Part 2, Sec. 4.2 (and implemented via the Matlab script twolayer_eig.m available online, Sec 7.1) and so we will go straight to the results, the eigenvectors of velocity and thickness, and the eigenvalues that are the gravity wave (non-rotating) phase speeds of the modes,

Barotropic mode
gravity wave phase speed $C \approx \sqrt{g(h_1+h_2+h_3)} = 200$ m sec^{-1}
radius of deformation at 30^o N, $\mathrm{R}_d = C/f = 2800$ km
long Rossby wave speed at 30^o N, $\beta R_d^2 = 142$ m sec^{-1} = 1230 km day^{-1}.

$$\begin{pmatrix} u & h \\ 1 & 0.07 \\ 1 & 0.07 \\ 1 & 1 \end{pmatrix}$$

Baroclinic mode 1
phase speed $\approx \sqrt{g(\delta\rho_2+\delta\rho_3)(h_1+h_2)/\rho_o} = 2.9$ m sec^{-1}
radius of deformation, 42 km
long Rossby wave speed, 0.033 m sec^{-1} = 2.9 km day^{-1}.

$$\begin{pmatrix} u & h \\ 1 & -0.7 \\ 0.41 & -0.3 \\ -0.1 & 1 \end{pmatrix}$$

Baroclinic mode 2
phase speed $\approx \sqrt{g\ \delta\rho_3\ h_1/\rho_o} = 1.5$ m sec^{-1}
radius of deformation, 22 km
long Rossby wave speed, 0.009 m sec^{-1} = 0.8 km day^{-1}.

$$\begin{pmatrix} u & h \\ 1 & 1 \\ -1 & -1 \\ 0 & 0 \end{pmatrix}$$

The eigenvectors of velocity are normalized so that the surface layer has an amplitude of 1; the thickness

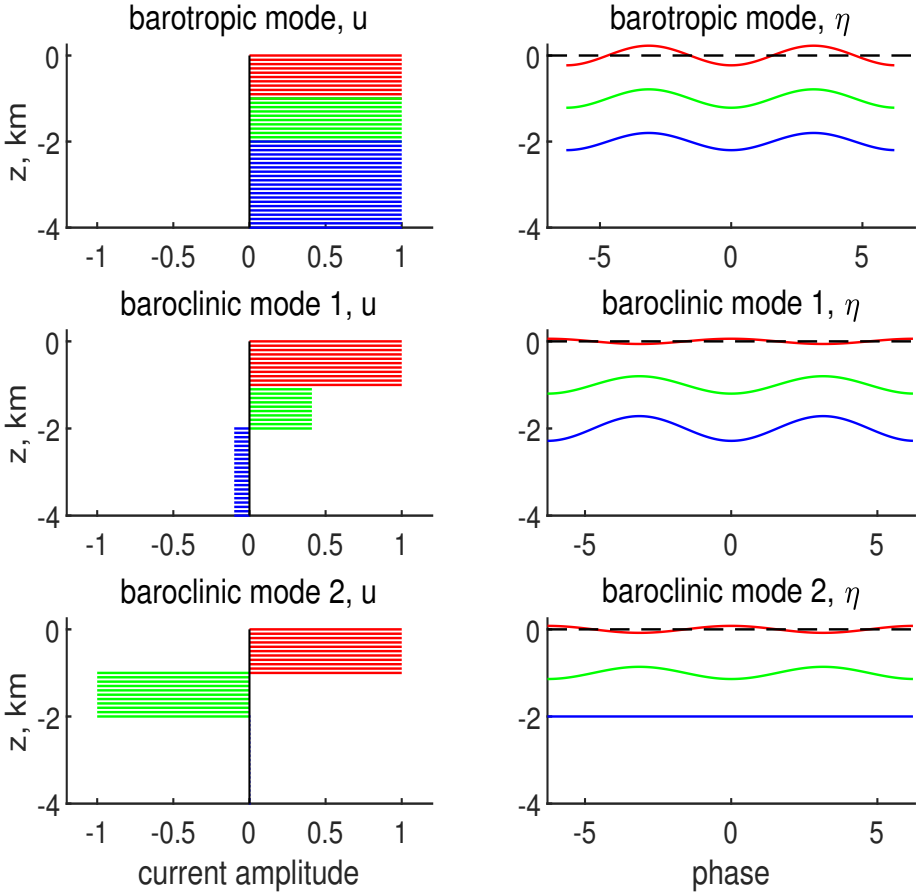

Figure 8: **(left)** Eigenvectors of the velocity from the three layer model. The layer-to-layer relative amplitudes of the velocity eigenvectors are meaningful, but their apparent thickness and thus depth is not to scale in this figure (the upper layer thicknesses have been quadrupled for the purpose of illustration). **(right)** Interface displacement computed from the eigenvectors of thickness by integrating from the bottom up, as in Eqn. (48). The amplitude of the interface displacements is schematic only but the phases are meaningful. For example, in the first baroclinic mode, the surface layer and the thermocline move up and down in phase in a 'sinuous' mode. Baroclinic mode 2 is confined almost entirely to the thermocline and surface layers, and is a 'varicose' mode in which the thickness changes in these layers are of almost equal magnitude and are out of phase.

763 eigenvectors are normalized so that the largest amplitude in any layer is 1, Fig. (8).

764 Compared with the reduced gravity model, the crucial new property of this system is that it supports
765 a barotropic wave having a very, very fast phase speed, 200 m $\sec^{-1} \approx 1700$ km day^{-1}. Thus, a
766 barotropic wave can traverse an entire ocean basin in a few days, vs many months for a baroclinic wave.

The interface displacements of the barotropic mode are in phase with depth, but are largest at the sea surface and decrease linearly to zero at the bottom (not apparent in this figure). The pressure gradient is determined almost entirely by the displacement of the sea surface, and the associated barotropic velocity is essentially uniform with depth. Such a barotropic motion would be the only thing possible in a model having no internal stratification whatever. There are two baroclinic normal modes that, are, by comparison, quite sluggish, having phase speeds approx. 3 m $\sec^{-1}$ and 1.5 m $\sec^{-1}$. The velocity in these baroclinic normal modes is depth-dependent, and has vanishing transport when integrated over the full water column.

These normal modes are orthogonal and span the space, in the sense that any free motions (e.g., any wave) that can occur in the three layer model can be formed as the linear sum of these modes. Since all of the eigenvectors are required to make a complete set, we can't really claim that any one of them is more important than the others. However, the first baroclinic mode does have the most prominent role in the basin-scale adjustment process to an imposed wind, *viz.* the changeover from a (largely) barotropic state that forms very quickly after the wind starts, to a baroclinic, surface intensified state (Sec. 3.3) at much longer times. This is implicit in the choice of parameters of the single layer, reduced gravity model that was intended to mimic the first baroclinic mode of this more complete multi-layered model or of the real ocean.

3 The circulation of the 1l-rg solution develops in four stages

Now, finally, we are ready to integrate and find a solution. First up will be the single layer, reduced gravity model, and then the more complex three layer model (in Sec. 6). It would be more efficient of space on paper if we jumped straight into the more complex model. But for the purposes of an introduction to this material, it seems (to this author) that it is preferrable to start slowly and add complexity later. Be assured that everything that we learn about the 1l-rg solution will be valuable in understanding the more complete results that will follow.

The wind stress is switched on to full amplitude at time = 0 and held constant for about 30 years. This long time is necessary to allow the solution to reach a (nearly) basin-wide steady state, (Fig. 40, bottom panel). The transient circulation develops in four more or less distinct, temporal (but noncontiguous) stages that are characterized by the onset of specific phenomenon.

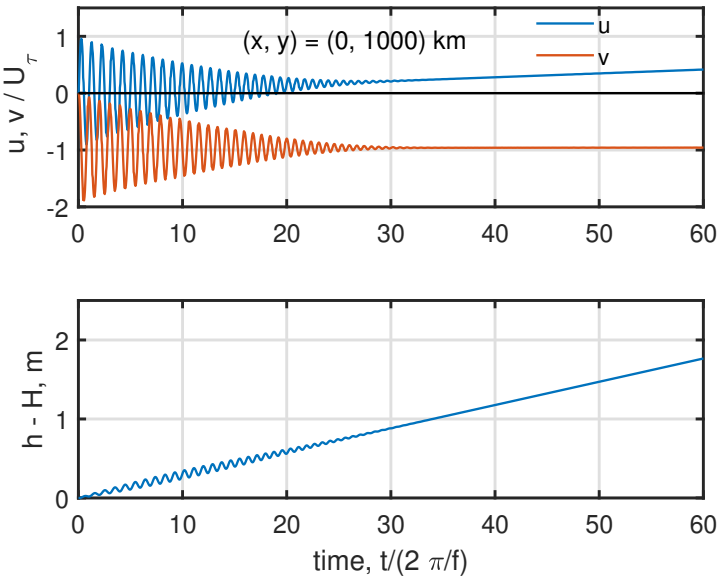

Figure 9: The short time evolution of currents. These data were sampled at 20 min. intervals on the northern side of the subtropical gyre, $(x,y) = (0,1000)$ km. This site was chosen since there is an appreciable wind stress, $\tau^x = 0.08$ N m^{-2}, which is eastward, and also a significant divergence of the Ekman transport. **(upper)** A time series of east and north current components, u and v. These are shown in units of the wind-driven velocity scale, U_τ. The high frequency oscillations are near-inertial motion; the time-mean (steady) v is southward Ekman flow which in these units has the value -1. **(lower)** Layer thickness anomaly, $h - h_o$, which shows a steady increase at about 15 m year^{-1}. This increase in layer thickness is caused by the convergence of Ekman transport, and the slow increase of the east current seen above is the associated zonal geostrophic flow (discussed in Sec 3.2). Notice the very small but dynamically significant oscillations of thickness in the first several weeks. These are evidence that the high frequency oscillations of the current are best described as near-inertial (very long wavelength) gravity wave motions.

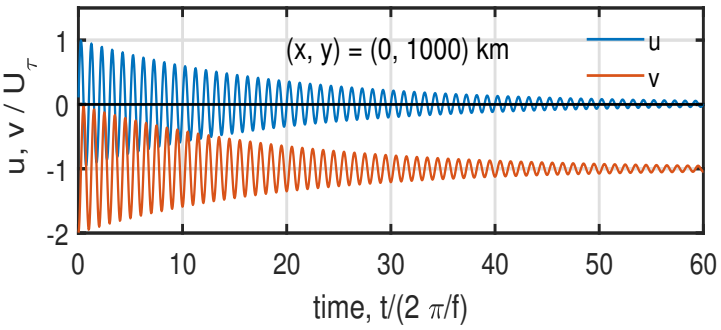

Figure 10: The solution for local, damped wind-driven motion, Eqn. (53) that may be compared to the full model solution, Fig. (9). There is no layer thickness shown here since in this local model there is no velocity divergence, and hence $h = h_o$ and constant.

3.1 Stage 1: Short time, local response to the wind

The dominant motions in the first several weeks after the wind is switched on are inertial motions and Ekman currents (Fig. 9). These are essentially local phenomenon that may be modelled by the linearized

subset of Eqn. (42) in which all the terms involving horizontal spatial derivatives are omitted,

$$\frac{\partial h}{\partial t} = 0, \tag{50}$$

$$\frac{\partial u}{\partial t} = fv - ru + \frac{\tau^x}{\rho_o h}, \tag{51}$$

$$\frac{\partial v}{\partial t} = -fu - rv.$$

You may notice that these equations are exactly the form used to model the motion of a dense parcel released onto a slope (Part 1, Sec. 5), though of course here the external force is a wind stress rather than a buoyancy force. These equations are local in the sense that they apply to what amounts to a single parcel, or since the equations are linear, a single position, and that does not interact in any way with its surroundings, i.e., no pressure gradient and no advection. Very important *non*-local effects will come soon.

Given an initial condition that is a state of rest,

$$u(t=0) = 0 \text{ and } v(t=0) = 0,$$

the solution for the so-called Stage 1 velocity is, in dimesional form,

$$\begin{pmatrix} u \\ v \end{pmatrix} = \frac{\tau^x}{\rho_o f h}\left(\frac{1}{1+(r/f)^2}\right)\begin{pmatrix} r/f + \exp(-rt)(\sin(ft) + (r/f)\cos(ft)) \\ -1 - \exp(-rt)(\cos(ft) - (r/f)\sin(ft)) \end{pmatrix}, \tag{52}$$

In non-dimensional form the same solution is

$$\begin{pmatrix} u \\ v \end{pmatrix}/U_\tau = \left(\frac{1}{1+E^2}\right)\begin{pmatrix} E + \exp(-E\gamma)(\sin(\gamma) + E\cos(\gamma)) \\ -1 - \exp(-E\gamma)(\cos(\gamma) - E\sin(\gamma)) \end{pmatrix}, \tag{53}$$

where

$$\gamma = tf$$

is time scaled by the rotation time, $1/f$,

$$E = r/f \tag{54}$$

is the Ekman number, and finally

$$U_\tau = \frac{\tau^x}{\rho_o f h} \tag{55}$$

is the amplitude scale of the directly wind-driven velocity. Notice that the latter is just the direct, wind-stress induced acceleration Eqn. (38) times the rotation time scale, $1/f$. The velocity of the local model (53) is the sum of a time-dependent inertial oscillation and a time-independent Ekman flow (Fig. 10).

3.1.1 Inertial oscillations*

Inertial oscillations are a clockwise rotation of the velocity at a rate f; at 30^o N, the frequency is the Earth's rotation rate, 7.292×10^{-5} sec^{-1}, and the period is approximately one day.[13] At the site sampled in Figs. (37) and (10) $(x,\ y) = (0, 1000)$ km, equivalent to about 41 ^{o}N, the inertial period is about 17 hours and the wind stress is about $\tau^x = 0.008$ N m $^{-2}$. The amplitude of the inertial oscillation at this site is thus $U_\tau \approx 0.002$ m sec^{-1}, which is unrealistically small because of the excessively thick wind-driven layer, $h = 500$ m. If the amplitude of inertial oscillations played an important part in the low frequency response (they do not), then this would be a serious shortcoming of a single layer shallow water model that was configured to have a reasonable baroclinic wave speed. The inertial oscillation of (53) decay with time as $\exp(-Eft)$, e-folding in 15 days due to Stokes drag. The time during which inertial oscillations are appreciable may be used to define the duration of

$$Stage\ 1: \quad 0 < t < \frac{1}{r}.$$

The inertial oscillations computed by the full shallow water model Fig. (9) differ from the solution of the local model (53) in that the frequency of rotation is a few percent greater than f (hard to see this in the present figure) and the amplitude decay is somewhat faster than is given by the frictional e-folding alone. These two features plus the very small but nevertheless significant oscillation of the layer thickness (Fig. 9, lower) indicate that what to a first approximation look like inertial oscillations are better described in detail as very long wavelength, near-inertial gravity waves. The longer term (several weeks) evolution of the inertia-gravity waves is significantly influenced by the variable f of this shallow water model, which leads to propagation towards the equator.

3.1.2 Ekman currents and transport

Along with the (near) inertial oscillation, the wind-driven current has a time-mean that is consistent with Ekman balance modified very slightly by friction,

$$\begin{pmatrix} u \\ v \end{pmatrix} / U_\tau \approx -\left(\frac{1}{1+E^2}\right)\begin{pmatrix} E \\ -1 \end{pmatrix}. \tag{56}$$

[13] The inertial period is less than a day by the fraction $\approx 1/365$. Can you recall from Part 1 why the inertial period at 30^o N is less than a day, and why that value?

Ignoring the small effects of friction, the amplitude of the Ekman flow is equal to the amplitude of the inertial oscillation, The amplitude of the Ekman current is $\propto U_\tau$, and is unrealistically small, as noted already. The direction is perpendicular and to the right of the wind stress, and so is southward at the site shown in Fig. (37) where the wind stress is eastward. The approximate solution for Ekman flow is indistinguishable from the solution computed by the shallow water model. The Ekman currents are present within hours of the start-up, and persist for the duration of the experiment since the wind stress is held steady.

The Ekman transport is

$$M^y_{Ek} \;=\; hV_{S1} \;=\; -\frac{\tau^x}{\rho_o f} \;=\; -\frac{\xi}{\rho_o f}\sin(\pi y/L), \tag{57}$$

and is independent of the layer thickness. At the site shown in Fig. (37), which is equivalent to about 41 ^{o}N, the Ekman transport is $M^y_{Ek} \approx -1.3$ m^2 sec^{-1}, which is a significant magnitude. To find the consequent *volume* transport, $l^3\,t^{-1}$, this M has to integrated or multiplied over a horizontal distance, say the width of the North Atlantic basin, to find a volume transport (symbol N) at this y (latitude) of about $N_{Ek} \;=\; M_{Ek} * 2L \;=\; -10\times 10^6$ m^{3}sec^{-1}, or 10 Sv southward. This is a significant fraction of the total meridional transport at this latitude. Moreover, Ekman transport will be made up from the shallowest and generally the warmest water in the water column, and so makes a very important contribution to the heat flux carried by the ocean circulation.

It is notable that the amplitude of Ekman transport goes as $1/f$, and so for a given wind stress, the Ekman transport is considerably larger in the tropics than in the subpolar region. The same applies for a given pressure gradient and the amplitude of geostrophic currents, and is a part of the reason that tropical SSH anomalies are comparatively small (Fig. 2).

While Ekman transport is significant in its own right, it has an even more important indirect role in generating the changes in layer thickness that lead to geostrophic and Sverdrup transports, discussed in Sec. 3.2 and forward.

3.1.3 Fast and slow time scales

The wind-forced currents and thickness vary on two quite different time scales, the fast time scale of the (near) inertial motions, and a much slower variation that here looks like a linear trend in the v velocity and in the thickness. When we see a much longer time series of these data, the latter will emerge as a low

frequency Rossby wave-like motion, and/or a part of the developing, steady circulation. Given that our main interest here is the low frequency phenomenon, then it is reasonable to ask whether it is desirable or necessary to also compute the high frequency phenomenon. The shallow water system naturally includes both kinds of motions, but the high frequencies can be suppressed easily enough by ramping up the wind stress over a few weeks (vs. the nominal, impulsive start). The resulting low frequency and steady circulation is the same either way the integration is started. This important result (no memory of the startup scenario) is consistent with the fundamental notion of the quasi-geostrophic system that the important low frequency motions are not far from geostrophic balance. The quasi-geostrophic system makes approximations (constant layer thickness, and a constant, background f, though with β) that are not consistent with some aspects of the shallow water solutions found here.[14]

3.1.4 Latitudinal dependence; is there trouble coming on the equator?

One of the subthemes of this essay is the latitudinal dependence of the ocean response and circulation. With respect to the steady circulation, the natural demarcation of latitude is by gyre, i.e., supolar gyre, subtropical gyre. At this stage there are no gyres, and so to investigate how the response varies with latitude we will just pick two sites, the easterly and westerly wind maxima, roughly 15 ^{o}N and 45 ^{o}N, and consider the zonal, u velocity component only (Fig. 11). The data are shown in two formats; in dimensional form (Fig. 11, left column) and in nondimensional form (right column) in which the speed is normalized with $U_\tau = \tau/(\rho_o f h)$ and time with the local inertial period, IP = $2\pi/f$. The dimensional format doesn't require any explanation (a good thing) but neither does it give anything more than a qualitative hint at parameter dependence, i.e., it is clear that the amplitude of inertial motion and the period of the inertial motion is greater at lower latitude.

Given the non-dimensional format, we can see that the amplitude is ≈ 1 at both sites, evidence that the amplitude varies as U_τ, and thus as $1/f$. Moreover, the period of the oscillation is very close to 1 IP at both sites and thus the period of the high frequency oscillation is $\propto 1/f$. Neither of these results is the least bit surprising given the solution Eqn. (53), but we could have made these inferences even without an explicit solution given the appropriate nondimensional scaling. The latter may be found by dimensional analysis and then verified with numerical experiments, a procedure that is generally far more accessible than is an explicit solution. If the main goal of a modeling study is to explore and expose parameter dependence rather than simulation of an observed case, then the non-dimensional format will have merit. That is certainly a part of our goal here, and so we will use nondimensional format (units) when it adds

[14] Most GFD texts (footnote 4) include a discussion of quasi-geostrophic theory, and a superb online source aimed mainly at meteorologists is http://www.meteor.iastate.edu/classes/mt411/powerpoint/METR4424qgtheory.pdf

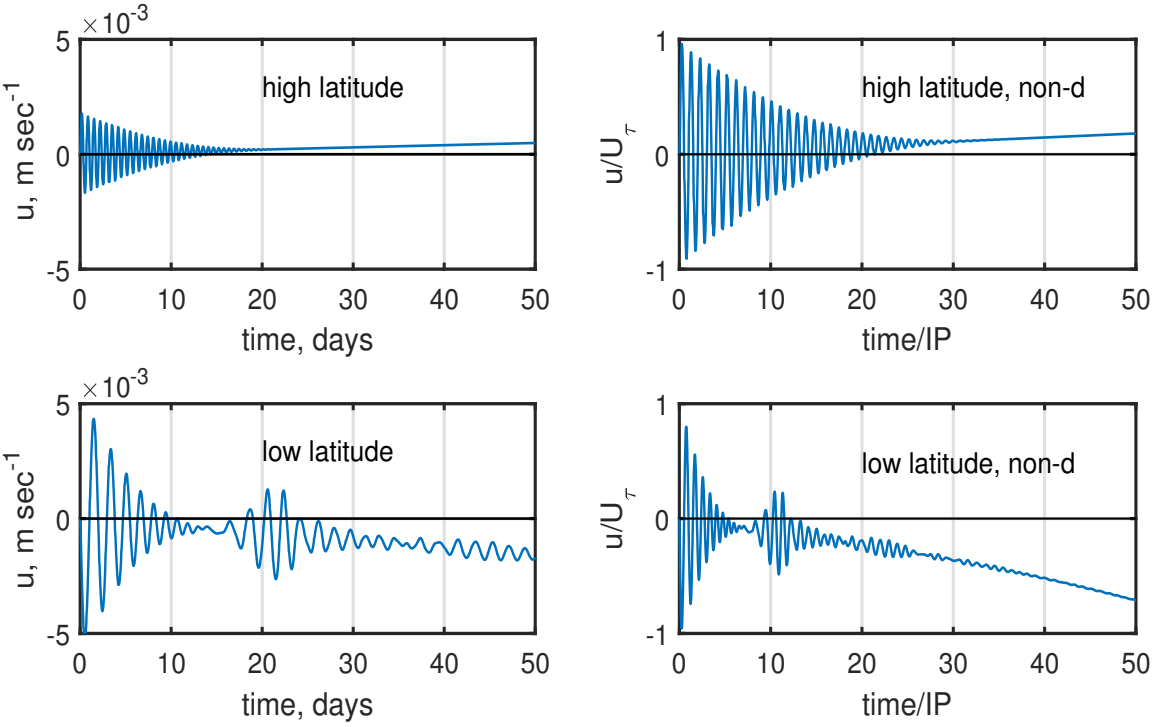

Figure 11: The zonal or u component of velocity sampled at two sites, **(upper row)** a comparatively high latitude site on the axis of the westerly winds, and **(lower row)** a low latitude site, the axis of the easterly winds. The data are plotted in dimensional format **(left column)** and in a non-dimensional format **(right column)**. The former emphasizes the significant differences in the response due to the differing latitude, while the latter makes clear that the sites have two things in common; the amplitude of near-inertial motion goes as U_τ and the period of the oscillation is approximately the local inertial period.

value. Otherwise we will stay with more prosaic dimensional units.

The near-equatorial region is especially noteworthy with respect to latitudinal dependence insofar as $1/f$ is singular, and hence geostrophy and the Ekman relation imply a blowup of equatorial currents. However, rotation, and thus the Coriolis force, is not a dominant process on or very near the equator, as the Ekman and geostrophic relations presume, and happily, no such a blowup occurs in the numerical solution. A somewhat trivial and parochial reason is that the wind stress given by Eqn. (37) has been assumed to vanish on the equator. But even with a significant equatorial stress included, which is more realistic of the real ocean, near-equatorial wind-forced currents are effectively limited by a rapid baroclinic response manifested in (or by) equatorial Kelvin wave propagation (Part 3, Sec. 4), which sets up a basin-wide pressure gradient that opposes the wind stress within a couple of weeks. In other words,

something else happens (Kelvin wave) that was not anticipated by the rotational scaling. In the experiments that we discuss here, the circulation very near the equator is a consequence mainly of the larger scale circulation in the tropical gyre, which is our main interest, and so (unfortunately) we won't have occasion to discuss distinctly equatorial phenomena. We will, however, see this apparent equatorial singularity crop up again.

3.2 Stage 2: Locally wind-forced, zonal geostrophic currents

The so-called Stage 1 response described above was present over the entire basin at once, though with significant differences in detail depending upon latitude. The Stage 2 and Stage 3 responses described next are very different in as much as they are present at the same time, but in different regions of the basin. The boundary between these regions is a Rossby wave front that sweeps westward across the basin, Fig. (40), and taking about 30 years to cover the entire basin. Stage 2 is a local response to wind stress curl (discussed below) that is present to the west and north of the wave front, and Stage 3 is Sverdrup flow, found to the east and south of the wave front, discussed in Sec. 3.3.

3.2.1 Divergent Ekman transport changes the mass field

While Ekman transport is significant in its own right, it has an even more important indirect role by generating changes in layer thickness (mass field) and thus the pressure field. This indirect effect of the wind is apparent within only a few days as a slowly developing change in layer thickness (Fig. 37, lower). The sense and the magnitude of the change is predicted well by the thickness tendency due to the divergence of Ekman transport alone (no geostrophic flows, yet) (Eqn. 13),

$$\frac{\partial h_{Ek}}{\partial t} \;=\; -\nabla\cdot(h\mathbf{V_{Ek}}) \;=\; -\frac{1}{\rho_o}\nabla\times(\frac{\tau}{f}),$$

and in the special case considered here that τ is $\tau^x(y)$ only, then

$$\frac{\partial h_{Ek}}{\partial t} \;=\; \frac{1}{\rho_o}\frac{\partial}{\partial y}\left(\frac{\tau^x}{f}\right) \;=\; \frac{1}{\rho_o f}\left(\frac{\partial \tau^x}{\partial y} \;-\; \frac{\beta}{f}\tau^x\right), \tag{58}$$

which varies with y only. This has terms proportional to the wind stress curl and to β times the meridional component of the Ekman transport. Both are important, with the beta-divergence term especially important at lower latitudes (Fig. 13).

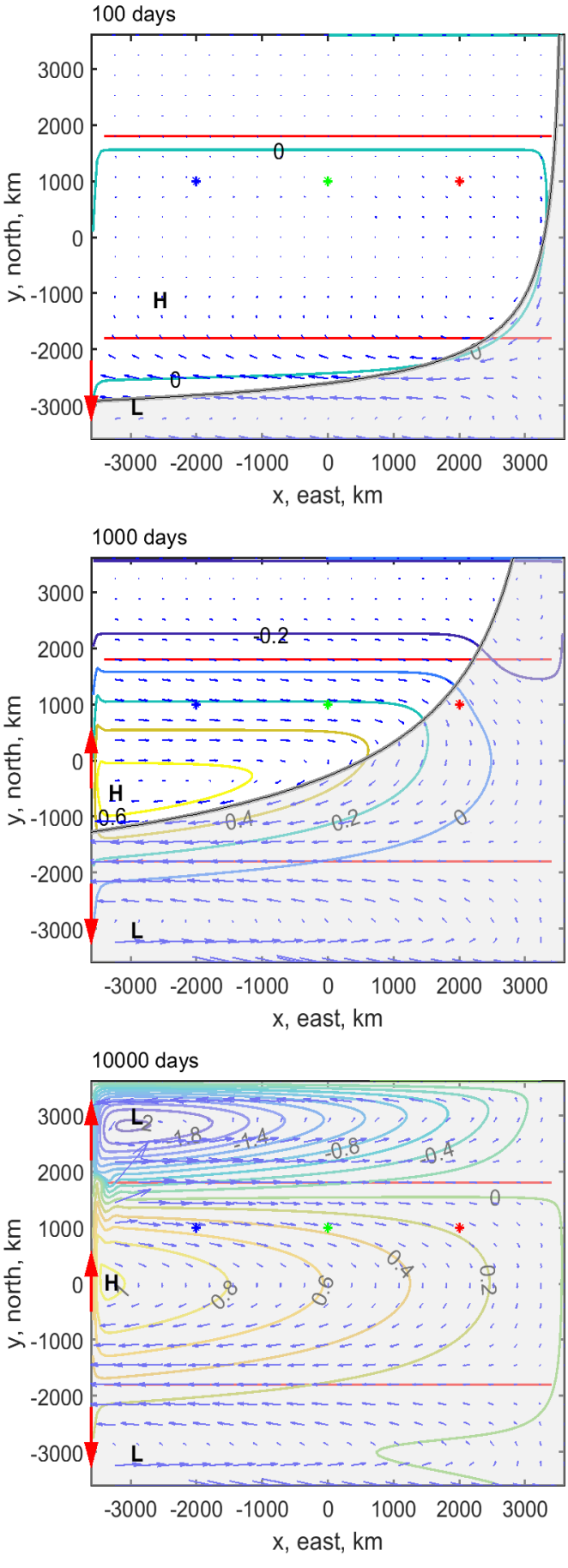

Figure 12: Three snapshots from the basic case, wind-driven experiment computed by the 1l-rg model and sampled at, from top to bottom, 100, 1000 and 10,000 days after the wind stress was switched on. The last time appears to be in a quasi-steady state throughout the interior of the basin. The thin red horizontal lines are the axis of the westerly and easterly wind stress (Fig. 6). The contours are of the inferred SSH anomaly in units of the Sverdrup geostrophic slope (Fig. 14) at basin center times the basin width, $2L$, about 0.4 m in this case. The field of small blue arrows are the current, though with the comparatively very large currents within the wbc omitted (shown in Sec. 3.3.2). The largest currents shown here are approx. 0.3 m sec^{-1}. The sense of the wbc is indicated by the red arrows on the west edge of the model domain. The blue, green and red dots along $y = 1000$ km mark the positions sampled in Fig. (15). The gray shading extends westward from the eastern boundary at the y-dependent speed of a long, baroclinic Rossby wave, $-\beta R_d^2$, and was sketched on top of the solution. Notice that the unshaded region to the north and west of the wave front (in the top two panels) shows mostly zonal currents, said to be the Stage 2 response. The shaded region to the south and east of the wave front is in Stage 3, and shows Sverdrup flow. An animation of these data is at www.whoi.edu/jpweb/threegyres.mp4

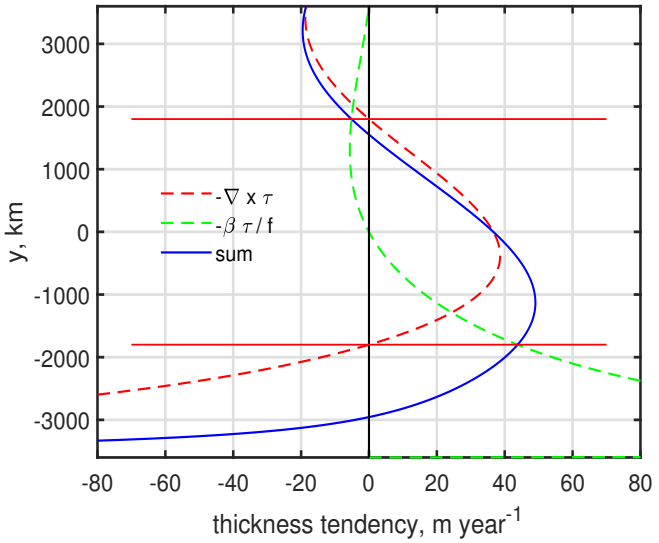

Figure 13: The divergence of the Ekman transport, Eqn. (58) (blue line), given the wind stress field Eqn. (37). Divergence of Ekman transport causes thickness tendency, which is a very significant aspect of the wind forcing on the ocean. At higher latitudes the divergence is due mainly to the curl of the wind stress (dashed red line). At lower latitudes, the beta-induced divergence of the Ekman transport (dashed green line) is appreciable.

At the site sampled in Fig. (9), $y = 1000$ km on the north side of the subtropical gyre, the rate of change in layer thickness is positive, and about 12 m year^{-1}. This is of no great importance for the Stage 1 response. At the same distance from the gyre center but to the south side, the thickness tendency is 45 m year^{-1} and also positive. If the interface is pushed downwards by the converging Ekman transport, this sign of thickness tendency is often called 'Ekman pumping'. When converted to SSH perturbation via the reduced gravity approximation, equivalent SSH change is about 0.1 m per 500 days, Fig. (14), at the gyre center. This raised SSH implies also a growing high pressure that characterizes the subtropical gyre. Over the tropical and subpolar regions, the sense of the Ekman divergence is positive and hence the layer thickness is decreased (interface is raised), sometimes called 'Ekman suction'. The resulting surface pressure anomaly is then a low, that will characterize the subpolar and tropical gyres.

Because the wind stress field is assumed here to vary with y only, the Ekman pumping also varies with y only (is independent of x) Fig. (14). Because the wind stress is constant once the wind stress is switched on, the Ekman pumping-induced thickness tendency given by Eqn. (58), is constant in time. The period during which the thickness rate of change is constant is said to be the Stage 2 of the transient response. Judging from Fig. (14), the duration of Stage 2 depends very much upon location: at $(x,\ y) = (0,\ 0)$ the thickness rate of change is constant for about 1000 days, and then becomes very small as Stage 3 Sverdrup flow begins to develop at that site (more on this in the next section). At the same y but closer to the eastern boundary, say $x = 2000$ km, Stage 2 goes on for only about 500 days.

In this experiment — conducted in a closed basin and with a wind stress field that is independent of x — it is very compelling that the duration of Stage 2 is greater with greater distance from the eastern

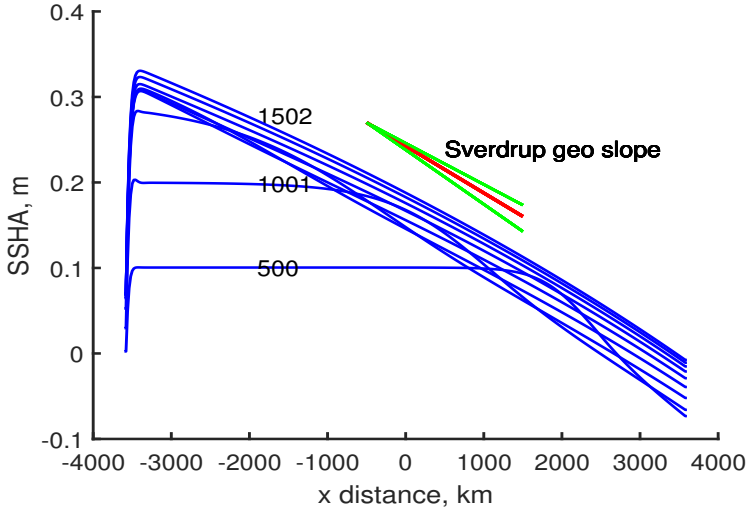

Figure 14: A sequence of sea surface height sections, $\eta(x)$, sampled at 500 day intervals up to 5000 days along $y = 0$, the center of the subtropical gyre. These were computed from the layer thickness via the reduced gravity approximation, Eqn. (46). The Stage 2 response is a steady rise of the sea surface, approx. 0.1 m per 500 days at this y, with no zonal tilt ($\eta(x)$ looks to be flat in this section). Stage 3 begins when the sea surface slopes down to the east and becomes quasi-steady; at $x = 2000$ km (eastern side of the basin) this starts at about 500 days, and at $x = -2000$ km (western side of the basin) the same thing starts much later, at about 1400 days. At this latitude, $\tau^x = 0$, and the meridional Ekman transport vanishes. Thus the quasi-steady meridional current over the interior region, $x \geq -3400$ km, is geostrophic and may be characterized by the zonal slope of the sea surface. The geostrophic slope expected from the Sverdrup relation Eqn. (1) for this y and given an average layer thickness, $h = 580$ m, is the red line that tilts down to the east. The flanking green lines are the sea surface slope for $h = 500$ and $h = 660$ m, which are found at the eastern and western ends of the section where the slope is slightly less and slightly greater than the average. This is a small but noticable finite amplitude effect.

boundary. However, this need not be the case if the important zonal length scale comes from the wind field rather than the basin geometry (an experiment considered in Sec. 5.3).

3.2.2 Zonal geostrophic currents accompany the changing stratification

The change in layer thickness causes a pressure anomaly in the surface layer that develops very slowly compared to f, and so is accompanied by slowly growing, nearly geostrophic zonal currents,

$$\frac{\partial u_{S2}}{\partial t} = -\frac{g'}{\rho_o f}\frac{\partial^2}{\partial y^2}\left(\frac{\tau^x}{f}\right), \tag{59}$$

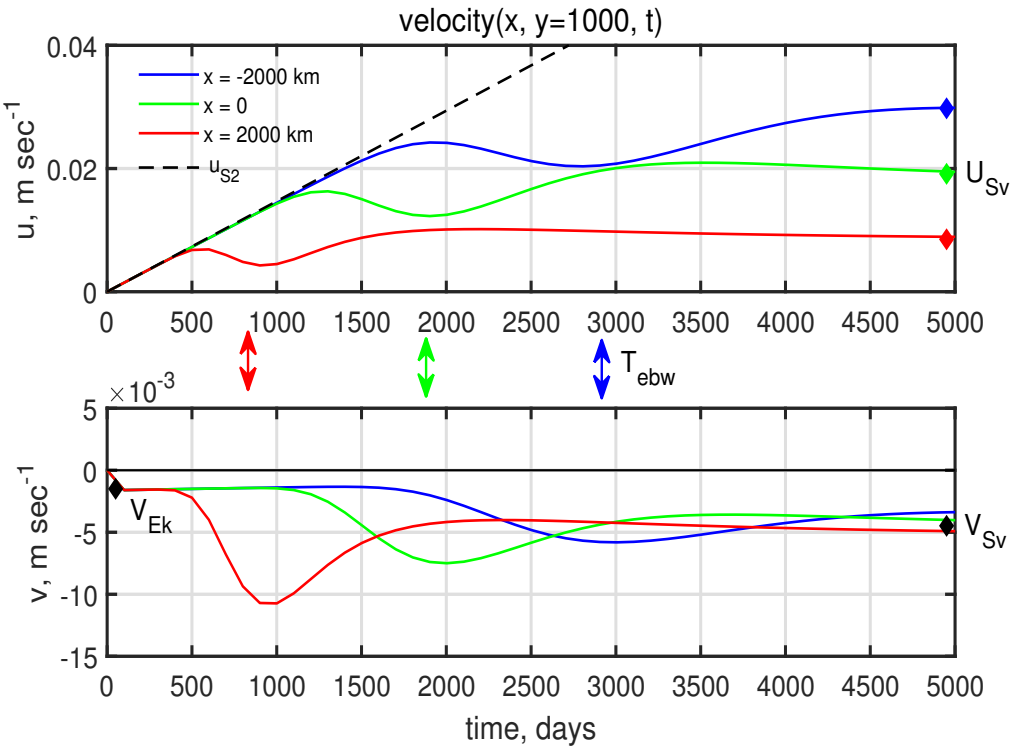

Figure 15: Zonal and meridional current components sampled in time along the northern side of the subtropical gyre, $y = 1000$ km, at three sites: $x = 2000$ km (red line), $x = 0$ (green line), and $x = -2000$ (blue line), which are nearest to farthest from the eastern boundary. The sampling time interval in this figure, 100 days, misses the inertial motions generated at start up (Sec. 3.1). **(upper)**. Zonal or east current component. The dashed black line is the estimate by Eqn. (60) of the zonal geostrophic current produced by Ekman pumping at this y and is the same at all x. The actual current follows this very closely for a few hundred or a few thousand days, depending upon distance from the eastern boundary. The red, green and blue double arrows denote the time, T_{ebw}, when a long Rossby wave starting on the eastern boundary at $t = 0$ is expected to arrive at the corresponding x. At around $t = T_{ebw}$, the zonal current shows a low frequency oscillation and then settles into a quasi-steady state consistent with the expected Sverdrup flow, marked by the colored diamonds on the right margin. Notice that the steady state zonal current increases approximately linearly with distance from the eastern boundary. **(lower)** Meridional or north current component. For short times, $t \leq T_{ebw}$, the meridional current is Ekman flow, Eq. (11), which is the same at these sites and noted by the black diamond near the left margin. The transition from Ekman flow to Sverdrup flow occurs around the time T_{ebw}. The expected Sverdrup flow at this y and for a nominal h is noted by the black diamond at right.

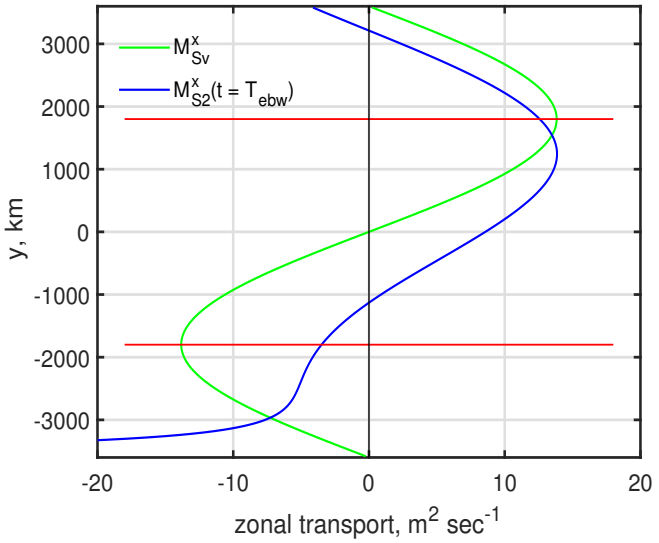

Figure 16: The zonal transport (per unit width) that accompanies the Sverdrup relation (green line that we will come to in Sec. 3.3) and the Stage 2 zonal current evaluated at $t = T_{ebw}$ (blue line) discussed in Sec. 3.1.3. At higher latitudes these currents are somewhat similar, but they are quite different at lower latitudes. The initial zonal currents in the interior closely match the Stage 2 profile (blue line) while the steady state zonal currents follow the Sverdrup profile (green line).

where the subscript $S2$ denotes that this is relevant to Stage 2 only. Because the stress is constant once switched on,

$$u_{S2}(y,t) \;=\; -\frac{g'}{\rho_o f}\frac{\partial^2}{\partial y^2}\left(\frac{\tau^x}{f}\right)t, \tag{60}$$

where t is the time elapsed since the start. In this experiment, the Stage 2 geostrophic current is purely zonal, since the Ekman pumping varies with y only, and it is independent of x, as is the wind stress. This is bound to fail on or very near the equator, where the Ekman balance is not appropriate, and also near a meridional (north-south runnning) boundary, which has far reaching effects discussed below.

The Stage 2 geostrophic zonal current (60) evaluated at $y = 1000$ km is sketched onto Fig. (15, upper) as a dashed black line. It gives a very good account of the actual zonal currents in the interior of the basin for a period of time — within the central subtropical gyre, (Fig. 15, the green line was sampled at $x = 0$) Eqn. (60) is valid for about 1000 days, just as noted before in the discussion of the Stage 2 layer thickness. The duration of Stage 2 depends upon both the latitude, being greater at higher latitudes, and greater also with increasing distance from the eastern boundary (the red, green and blue lines of Fig. (15) are at the same y, but increasing distance from the eastern boundary). An explicit estimate of the duration of Stage 2 will become apparent when we consider the onset of Stage 3 in the next section.

The Stage 2 zonal geostrophic current given by (60) is proportional to $1/f^2$, and, all else equal, is considerably larger at lower latitudes than at higher latitudes (Fig. 16). Most of this essay emphasizes the meridional Sverdrup flow and western boundary currents, since these transport sea water properties equatorward and poleward (subtropical gyre) and so are generally of greater significance for Earth's

climate. However, this locally wind-forced, zonal current is a robust signal in the transient response of this model, and is also prominent in the response of the tropical ocean to an annually-varying wind (O2 of Sec. 1.1.2 and Sec. 5.1).

3.3 Stage 3: Blocking at the boundaries and the onset of meridional Sverdrup flow

Because the present experiment is set within an enclosed, finite basin having impermeable meridional boundaries, the x-independence of the Stage 2 zonal geostrophic currents can not go on forever. The zonal flow that approaches a meridional boundary is blocked, and must turn either north or south. Meridional boundaries thus have the effect of breaking the zonal symmetry that characterizes the Stage 2 response. As this 'blocking effect' of meridional boundaries becomes important, the overall pattern of the layer thickness anomaly and geostrophic currents begins to resemble a closed, gyre-like circulation, e.g., within the eastern part of the subtropical gyre, $x > 2000$ km, this is evident by about 500 days (Fig. 40).[15]

The meridional flows can be described in two distinctly different regions: by far the greatest part of the basin develops a very slow Sverdrup flow, and there is a comparatively narrow western boundary region having a width of about 100 km.

The blocking effect of the eastern meridional boundary — a zonal tilt of SSH and thus a change from purely zonal to at least partly meridional flow — spreads westwards into the interior of the basin. At $y = 0$, equivalent to 30^o N, this spreading is at a slow but steady rate of about 3 km per day (Fig. 40), which is roughly the westward propagation speed of mesoscale eddies at that latitude (Part 3, and reviewed briefly in Sec. 1.1).

There are two fairly persuasive reasons to conclude that this westward 'spreading' of eastern boundary blocking is the same thing as the westward propagation of a long, divergent Rossby wave

[15] Imagine that the meridional boundaries are removed, and that the no-flow boundary condition on those boundaries is replaced by a symmetric or reentrant condition that $u(x = -L) = u(x = L)$, and the same for other variables. The domain would then be an east-west oriented channel, as more or less actually occurs in the Antarctic Circumpolar region. In a channel domain, the zonally-oriented thickness anomalies and geostrophic currents of the Stage 2 response would grow until the currents either became unstable and began to spread vertically and horizontally, or, drag on the current reached an equilibrium with the wind stress.

reviewed in Sec 1.1 (and more detail in Part 3, Sec. 2.5). First, the balance of potential vorticity is consistent with long Rossby wave motions. A β-effect (Sec. 1.5) begins immediately with the meridional component of the current. Because the horizontal scale of the currents is the scale of the wind stress and very much larger than the radius of deformation, the β-effect produces mainly a change in layer thickness rather than a change of relative vorticity (Part 3, Section 2.4). In fact, the relative vorticity remains very, very small, i.e., $\nabla\times\mathbf{u} \ll f$ (this is not true near the western boundary, however). Thus the potential vorticity balance in the vicinity of the spreading eastern boundary blocking is linear and divergent, Eqn. (2), in common with long (baroclinic) Rossby waves. The motion evolves very slowly and is very nearly geostrophic, and so the first order wave/advection equation (19) is expected to be valid and predicts westward propagation. Second, judging from Fig. (40), the westward spreading of eastern boundary blocking is markedly faster at lower latitudes. This invites a direct comparison to the long Rossby wave speed (Eqn. 18), which has been used to define a gray-shaded mask that extends westward from the eastern boundary by

$$X \;=\; C_{longRo}\, t \;=\; -\beta \frac{C^2}{f^2}\, t, \tag{61}$$

Fig. (40).[16] The long Rossby wave speed varies strongly with latitude; the gravity wave speed C is somewhat reduced at higher latitudes due to reduced stratification, but much more important at this early stage is the $1/f^2$ dependence, which implies much larger C_{longRo} at lower latitudes. Notice that the disruption of the Stage 2, zonal geostrophic flow is indeed closely coincident with the expectations of (61) at all latitudes (equator aside, Fig. 40). Given this line of evidence, the westward spreading of the boundary blocking effect will be referred to as an 'eastern boundary Rossby wave', or 'ebw', despite that the profile $h(x,t)$ looks nothing like an elementary wave (Fig. 14).

The end of the Stage 2 local response to Ekman pumping and the start of the Stage 3 non-local or basin scale response may then be estimated by

$$Stage\ 2 \;\rightarrow\; Stage\ 3: \quad t \;=\; T_{ebw}, \tag{62}$$

where

$$\boxed{T_{ebw} \;=\; -\frac{(L-x)}{C_{longRo}}} \tag{63}$$

with $(L-x)$ the distance from the eastern boundary. Thus T_{ebw} is $T_{ebw}(x,y)$ since C_{longRo} varies with y. Subsequent to T_{ebw}, the volume transport has a significant meridional component that approximates Sverdrup balance, Eqn. (29), Figs. (14) and (15), lower.

[16] The equatorial limit $f \rightarrow 0$ is handled by assuming that the westward wave speed can be no faster than the fastest, westward propagating equatorial Rossby wave, $-2C/3 \approx -2$ m sec^{-1}. See Part 3, Sec. 3 for a little more on equatorial wave dynamics.

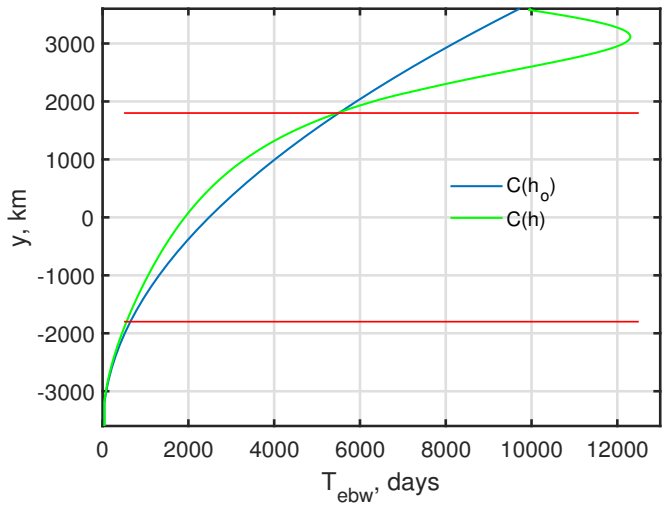

Figure 17: Transit time from the eastern boundary to the western boundary at the long Rossby wave speed. The blue line assumes the nominal layer thickness $ho = 500$ m for evaluating the baroclinic gravity wave speed, while the green line uses the actual, steady, zonal average thickness, which is somewhat different, especially in the western part of the subpolar gyre where $h \approx 100$ m. The expected transit times for the gyre centers are: tropical gyre, 350 days; subtropical gyre, 2500 (2000) days; subpolar gyre, 7500 (12000) days.

Judging from Fig. (15), the flow does not switch instantaneously from zonal to purely Sverdrup at $t = T_{ebw}$. Rather, the eastern boundary wave has a very gradual leading edge, Fig. (14), and a close Sverdrup balance requires as much as $2*T_{ebw}$, which can be another few hundred or even a thousand days, depending upon latitude and distance from the eastern boundary. The key point is that the time required for the eastern boundary (blocking) effect to reach a given point in the interior is proportional to T_{ebw}, and thus is strongly dependent upon latitude and distance from the eastern boundary. In this important respect, the meridional flow of low latitude oceans exhibits a comparatively fast response to changing wind stress. The latitudinal-dependence of the long Rossby wave speed Eqn. (18) is thus a very prominent, qualitative feature of the developing gyre circulation in this experiment, and often in the real ocean (Part 3, Sec. 2.6). (see Sec. 8.2, 5)

3.4 Western boundary currents

At the same time that the interior of the basin is developing very slow and broadly distributed currents, something quite different happens near the western boundary. The Stage 2 response includes zonal currents that impinge on the western boundary just as much as occurs on the eastern boundary. The result is necessarily meridional currents along the western boundary that are subject to a beta effect. Propagation of this western boundary blocking into the interior by wave propagation requires an *eastward* group velocity. You may recall from Part 3, Sec. 2.3, that short baroclinic Rossby waves have an eastward group velocity, but the maximum eastward group velocity of these waves is very, very slow, only a few hundred meters per day, which is just a few percent of the western group velocity of long

waves, C_{longRo}. Moreover, eastward group velocity obtains only for short waves, $kR_d \leq -1$ and $k \leq 0$. Such short waves are just barely resolved in the present numerical solution, and so it is not too surprising there is very little evidence of eastward spreading or propagation. Instead, the meridional currents along the western boundary appear to be effectively trapped to the boundary on a width of 50 - 100 km (Fig. 18), which is roughly the local radius of deformation (discussed below). The resulting western boundary current is comparatively very fast, up to 1 m sec^{-1}.

The volume transport of a wbc is estimated as

$$N_{wb} = \int_{-L}^{-L+L_{wb}} v\, h dx,$$

where L_{wb} = 150 km, by inspection (or several times R_d). The steady state wbc of the subtropical gyre has a volume transport about 28 Sv, and northward, which is opposite the Sverdrup volume transport of the interior. The western boundary currents of the tropical and subpolar gyres are southward, and opposite the Sverdrup transport in those regions.

The immediate cause of a western boundary current is zonal inflow: in the subtropical gyre, there is an inflow to the wbc at latitudes $0 > y > -L/4$, and an outflow at latitudes $L/4 > y > 0$. During the first one thousand days of the experiment, the zonal current near the wbc is mainly the Stage 2 geostrophic flow discussed in the previous subsection. As time runs, the inflow is better described as the Sverdrup zonal flow. From this we can infer that the time scale for development of a wbc is proportional to the time scale of U_{S2} and thus proportional to $1/f^2$, i.e., much faster at lower latitudes (Fig. 18, cf upper and lower panels). The subtropical wbc begins to appear within a few hundred days after the start of the wind stress, and reaches its full, steady state amplitude in about 2000 days. This is roughly the same time scale on which the subtropical gyre interior reaches steady state Sverdrup flow, and comparable to the transit time of the eastern boundary Rossby wave.[17] The same attends the volume transports of the wbc in the other gyres: — wbc steady state requires about 1000 days in the tropical gyre, and about 10,000 - 12,000 days in the subpolar gyre (Fig. 19), a factor of roughly ten.

[17]The arrival of an eastern boundary Rossby wave is not the dramatic event that the words seem to imply. And too, the coincidence in time does not imply that the eastern boundary Rossby wave is the cause of the western boundary current except in a very indirect way: the arrival of the eastern boundary wave implies that the interior region to the east and equatorward (subtropical gyre) is close to being in steady state with regards to meridional transport and the Sverdrup relation, and that is what really counts.

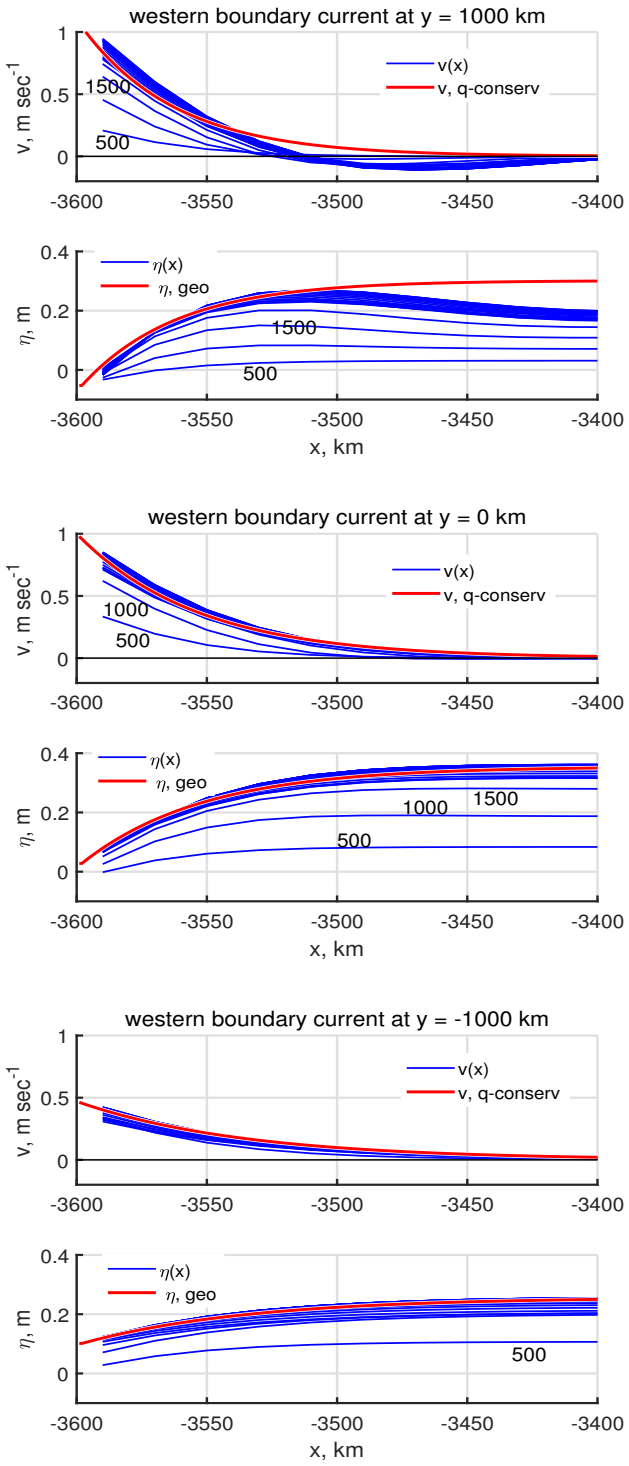

Figure 18: Zonal profiles of the north velocity and the SSH anomaly within 200 km of the western boundary at three sites within the developing subtropical gyre: **(upper)** $y = 1000$ km, on the north side of the subtropical gyre, **(middle)**, $y = 0$, the center of the subtropical gyre, and **(lower)** $y = -1000$ km, the south side of the subtropical gyre. Profiles are shown as the blue lines at 500 day intervals. The north velocity expected for a q-conserving inflow is shown as the red line, an exponential with the x scale being the radius of deformation, at $y = 1000$ km, $R_d = 36$ km; at $y = 0$, $R_d = 45$ km, and at $y = -1000$ km, $R_d = 64$ km (discussed in Sec. 3.2). The corresponding SSH anomaly profiles are computed from the respective q-conserving velocity using geostrophy (also plotted as a red line). Notice that currents and stratification at the more southerly site (lower panels) reach steady state in about 500 days, while the higher latitude site (upper panels) requires about 2000 days.

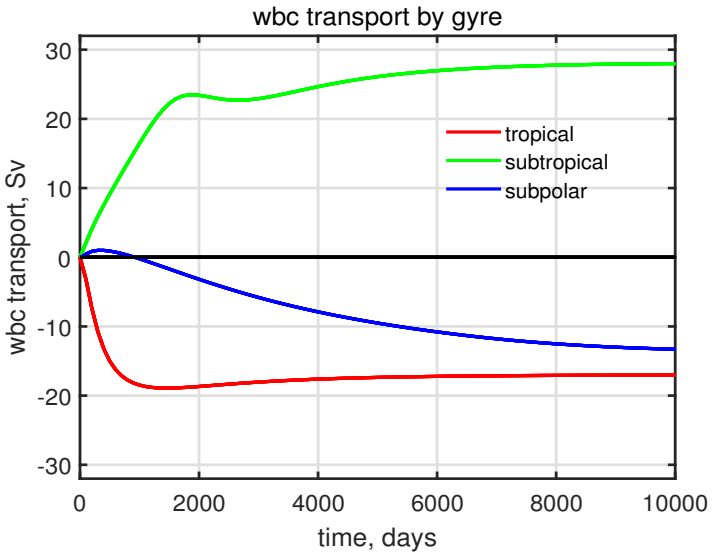

Figure 19: Meridional volume transport N_{wb} within the western boundary currents of the three gyres. These were sampled at the north-south center of the gyres. Notice that the wbc of the tropical gyre reaches a steady state within about 700 days after the start of the experiment, while the wbc of the subpolar gyre requires much longer, roughly 12,000 days.

3.4.1 Changing mass field

There is a very strong hint in the discussion above that a wbc is just a mirror (compensates)of the Sverdrup flow of the interior. To test this in detail, we can evaluate the mass balance over a control volume that we are free to choose: for this case, the entire southern half of the basin, the light green shading of Fig. (20) having an area A. The areally integrated continuity equation appropriate to this control volume is

$$A\frac{dh_{avg}}{dt} = \oint h\mathbf{V}\cdot\mathbf{n}ds$$

since our shallow water model has no source term, i.e., no mechanism to convert upper layer water to abyssal water, for example. Thus the areal-average thickness of the layer within the control volume can change only if there is a net volume flux across the horizontal sides of the control volume. In practice we can break up the line integral into pieces that represent the flow across specific sides of the control volume, e.g., in this case

$$N_{int} = \int_{-L+L_{wb}}^{L} vh\,dx,$$

is the volume transport across $y = 0$ in the interior of the basin (no need to identify this as Sverdrup flow), and the volume flux of the comparatively very narrow and intense northward flowing western boundary current (Fig. 18) is N_{wb}, already noted. The integrated mass balance (continuity equation) then reads

$$A\frac{dh_{avg}}{dt} = N_{int} + N_{wb}.$$

Either of the volume flux terms is considerably larger than the storage term, but they do not sum to zero: during the first several thousand days of the experiment there is a small but significant net meridional

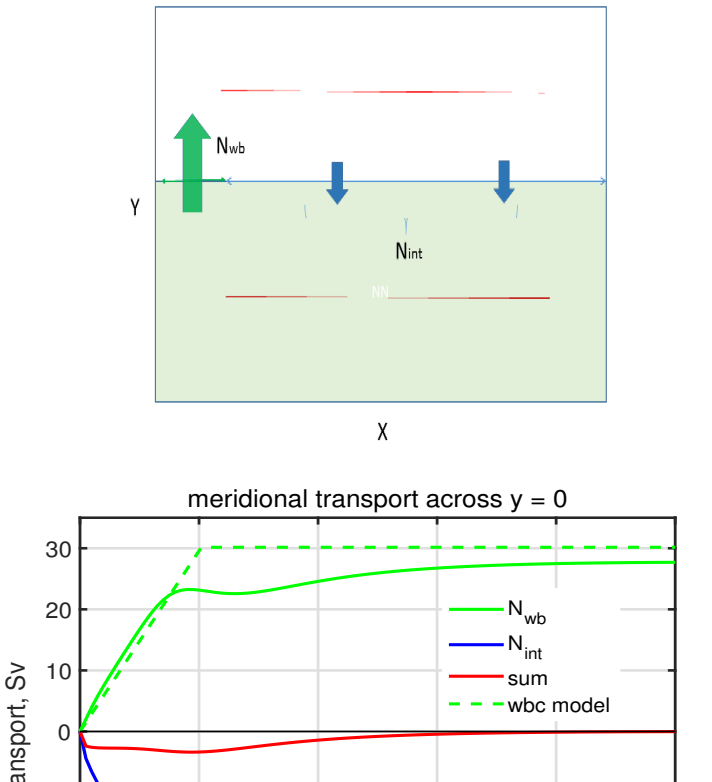

Figure 20: **(upper)** A control volume (light green area A) defined over the southern half of the basin. The volume transport through $y = 0$ is evaluated over a western boundary, N_{wb}, and an interior, N_{Sv}. **(middle)** The volume transports through $y = 0$ (green and blue lines) and their sum (red line). The dashed green line is a model of wbc transport, Eqns. (64) and (65). **(lower)** The time-integrated net volume flux into the control volume (blue line) and the observed thickness change over the control volume (red line), about 40 m. Given the adiabatic continuity equation (41), these should be exactly equal.

transport across $y = 0$, $N_{Sv} + N_{wb}$, (the red line of Fig. 20, middle). The subtropical gyre is a region of increased layer thickness, about 40 m on areal average, and thus elevated SSH and higher pressure. Indeed, the subtropical gyre is characterized mainly by this high pressure. The volume of fluid required to thicken the layer in the region south of $y = 0$ is provided by (must be provided by) the basin-wide meridional volume flux across $y = 0$ (Fig. 20, lower). As the region to the south of $y = 0$ reaches a steady state and $\partial h/\partial t = 0$, which requires a little more than 5000 days, the net volume flux across $y = 0$ also vanishes. Note that this is considerably longer than the time required to reach a steady state within the subtropical gyre alone.

3.4.2 A simple model of transport in a time-dependent wbc*

We can construct a very simple estimate of the time-dependent western boundary transport on the assumption that the transport will be opposite and equal to the meridional Sverdrup transport to the east of the eastern boundary Rossby wave, i.e., as if

$$N_{int} \; + \; N_{wb} \; = \; 0.$$

and now $N_{int} = N_{Sv}$. While the eastern boundary wave is in transit across the basin,

$$0 \; < \; t \; < \; T_{ebw}(x = -L, y); \quad N_{wb} \; = \; -\frac{\nabla \times \tau}{\rho_o \beta} \, C_{longRo} \, t \; = \; -N_{Sv} \tag{64}$$

The wind stress curl and the long Rossby wave speed are evaluated at the y of the wbc observation, in Fig. (19), the center of the subtropical gyre, $y = 0$. After the wave arrives on the western boundary, the western boundary transport is assumed to exactly compensate the steady state Sverdrup transport across the basin interior and so for longer times,

$$t \; > T_{ebw}; \quad N_{wb} \; = \; constant \; = \; -\frac{\nabla \times \tau}{\rho_o \beta} \, 2L. \tag{65}$$

This estimate (64) and (65) is shown as the green dotted line of Fig. (20) middle, and is a plausible first description of the actual (numerical) boundary current transport, though far from perfect. There are two ways we know that this model and this estimate are inconsistent in detail with the numerical solution: the transition from Stage 2 purely zonal, local flow to Stage 3 Sverdrup flow is not instantaneous as Eqn. (64) assumes, and, the northward wbc transport does not return all of the southward Sverdrup transport during the first several thousand days of the experiment when some fluid is stored at the rate of several Sv within the thickening layer south of $y = 0$. Those fairly significant details aside, what is most striking and very robust is that a wbc develops much faster in the tropical gyre, within very roughly 1000 days, than in the subpolar gyre, where the time scale is closer to 10,000 days (Fig. 19). This very large difference in the rise time of the wbc in these gyres is a consequence of the $1/f^2$ dependence of the Stage 2, locally wind-forced geostrophic current, Eqn. (60), and of the long Rossby wave transit time, Eqn. (63).

3.4.3 Western boundary current width*

The water that makes up the western boundary current of the subtropcial gyre flows into the boundary current from the eastern side. This inflow begins with the start of the Stage 2 zonal current, and continues into the steady state. Assuming that the inflowing water conserves its potential vorticity and that the across stream momentum balance is geostrophic, we can make an estimate of the boundary current profile and width. (See Stommel (1966) [4], Ch. 8, who has an interesting discussion of this applied to the actual Gulf Stream.) The relative vorticity is approximated well by the x variation of the north component of the current, and hence the potential vorticity inside and just outside of the western boundary current are

$$\frac{f+\frac{\partial v}{\partial x}}{h} \;=\; \frac{f}{h_0}, \tag{66}$$

where h_0 is the thickness just outside the boundary current. If we evaluate this at $y = 0$, $h_0 \approx 600$ m. The momentum balance is very nearly geostrophic,

$$fv \;=\; g'\frac{\partial h}{\partial x},$$

which may be combined with (66) to form a single equation for the boundary current velocity,

$$\frac{\partial^2 v}{\partial x^2} \;= \frac{f^2}{g'h_0}v. \tag{67}$$

This has exponential solutions

$$v(x) \;=\; V_0 \exp\left(\pm((x+L)/R_d\right), \tag{68}$$

where $R_d \;=\; \sqrt{g'h}/f$ is the familiar radius of deformation. Suitable boundary conditions are that $v \to 0$ as $x+L$ becomes large, which selects the minus sign in the exponential, and then we are free to choose the amplitude, V_0. For the central latitude of the subtropical gyre, $y = 0$ of Fig. (20), $V_0 = 1.0$ m sec^{-1}. The solution for $v(x)$ is then complete, and the corresponding geostrophic thickness, represented here by the SSH anomaly η, may then be easily computed as well (Fig. 20, red lines). These make quite good representations of the actual velocity and thickness (or η), and hence we can conclude that the width of the western boundary current is approximated well by the radius of deformation, the natural length scale of the shallow water model. That is a neat and satisfying result that we will cite repeatedly in the description of the circulation. However, closer inspection and thought suggests that there may be more to this than the simple, local inflow model takes account of. First, this simple model doesn't work so well along the northern side of the subtropical gyre, $y = 1000$ km (upper panel of Fig. 18) where the boundary layer current appears to have a reversal offshore that is not captured by the monotonic profile (68). In one respect that is not all bad, since that region is characterized by *outlfow* from the wbc into the interior, not an inflow. So, there is evidently more to the wbc dynamics than just (67). Second, the water that makes

up the wbc at $y = 0$, say, came mostly from lower latitudes, not from a local inflow. If the wbc current was q conserving along stream, then the q at that latitude should be lower than the local q. Later we will see that frictional effects are expected to be significant in the western boundary current, and friction acts to increase q along the path of the current. Friction implies a length scale that, for the r used here, is the same order as R_d (Sec. 4.2.2). It appears that while Eqn. (67) works very well in a numerical sense, local inflow and q conservation are not a complete explanation.

3.5 Stage 4: Inter-gyre exchange, and basin-wide steady state

The three gyres come into steady state at quite different times, as described above, and clearly the laggard is the subpolar gyre. Even after 10 years, most of the subpolar region is still in Stage 2 and continuing to lose volume from the upper ocean since $\nabla \times \tau > 0$ (Ekman suction). The decrease of layer thickness within the subpolar gyre is quite pronounced, with h eventually reaching a minimum of about 100 m just offshore of the western boundary current (Fig. 40, bottom). The basin-wide volume of the layer is conserved and so the fluid that is expelled from the subpolar gyre is absorbed into the subtropics and tropics where the layers continue to slowly thicken more or less uniformly over the basin, long after the Sverdrup flow has reached a near steady state. A literal steady state of the subtropics, i.e., constant h and constant $\mathbf{v}$, here dubbed Stage 4, requires that the entire basin, subpolar region included, must be swept by an eastern boundary Rossby wave. Thus a basin-wide steady state requires an elapsed time

$$Stage\ 4: \quad t \ = \ max(T_{ebw}) \ = \ \frac{2L(f_o + \beta L)^2}{\beta C^2},$$

where *max* is evaluated over the basin as a whole. If we use a nominal value of the gravity wave speed, $C \ = \ 3$ m sec^{-1}, then we find $max(T_{ebw}) \approx 9200$ days. In fact, the numerical solution indicates a somewhat longer time, closer to 12,000 days, mainly because the gravity wave speed is significantly reduced within the subpolar gyre (Fig. 17) due to the greatly reduced layer thickness in especially the western part of the gyre (Fig. 40, lower panel). (see Sec. 8.2, 4) This is one of several finite amplitude effects associated with large thickness changes away from the (arbitrary and unrealistic) initial condition of uniform upper ocean thickness.

The currents and stratification in the interior of the basin eventually reach an instantaneous steady state, $\partial(\ )/\partial t \ = \ 0$. However, there is one region where the flow never becomes even approximately steady, the confluence of the western boundary currents of the subtropical and subpolar gyres at around $y = 1800$ km. There the colliding western boundary currents meander and produce intense, mesoscale eddies of both signs. The eddies remain close to the western boundary, and do not appear to affect the

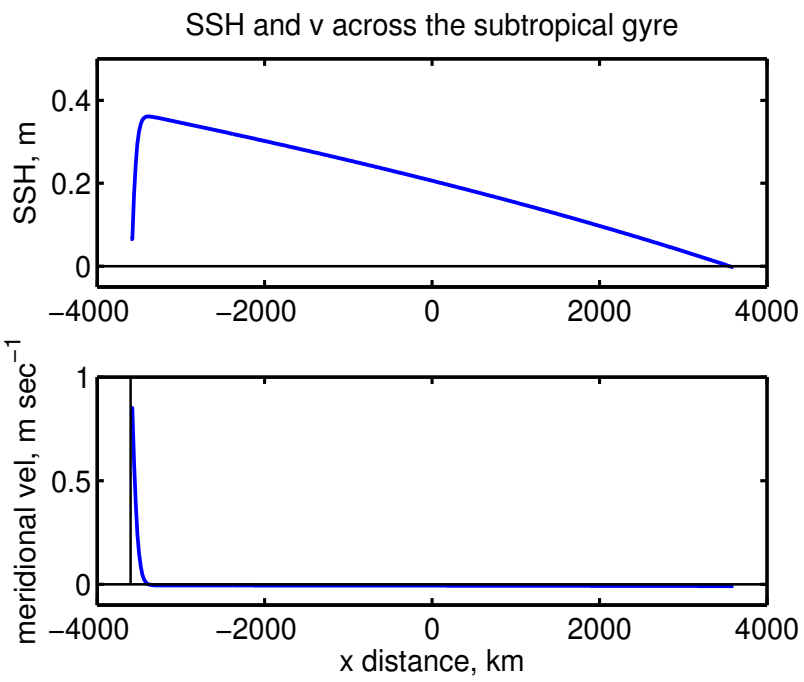

Figure 21: **(upper)** A zonal section of SSH across the center of the subtropical gyre, $y = 0$, computed from layer thickness anomaly via the reduced gravity approximation. The basin-scale variation of SSH is much like that seen in the North Atlantic (Fig. 1); a very narrow western boundary current and a broad interior with almost uniform slope down to the east. Notice, though, that the amplitude of the SSH high in this model solution is considerably less than is observed in the real North Atlantic subpolar gyre (about which more in Sec. 7). **(lower)** The meridional velocity along the section above. The velocity is very nearly geostrophic and is northward and very fast in a thin western boundary current, up to about 1 m sec^{-1}. The interior, meridional velocity is southward and very slow, a little less than 0.01 m sec^{-1}.

interior region. The confluence region does become steady in the statistical sense that the eddy amplitude, size and frequency are no longer changing after about 10,000 days. So, whenever we say 'steady' in reference to the basin-wide circulation, read that as a shorthand for steady excepting the wbc confluence region.

One straightforward way to characterize the basin-wide, steady circulation is to simply make a cut of SSH anomaly and northward velocity through the center of the subtropical gyre Fig. (21), which may be compared to Fig. (1). There is a comparatively very narrow western boundary region, e-folding on the radius of deformation and so the full width is O(100 km), within which SSH slopes up to the east and the current is northward and fast, up to 1 m sec^{-1}. Over the much broader interior region — the rest of the basin — there is a quasi-linear decrease of SSH all the way to the eastern boundary (Fig. 21). Given the zonally uniform wind stress curl of the model winds, this nearly constant slope of SSH would be expected for a linear Sverdrup interior for which $\delta h \ll H_o$. This is the shallow water model-equivalent of the east-west asymmetry of the observed wind-driven ocean circulation noted as O1 in Sec. 1.1.

4 The (almost) steady circulation

4.1 A streamfunction depiction of the circulation

A second and very useful way to characterize the basin-wide steady circulation is to construct a map of the streamfunction. When the solution is in steady state, $\partial h/\partial t = 0$, the volume transport, $\mathbf{M} = H\mathbf{V}$, is nondivergent, $\nabla\cdot\mathbf{M} = 0$. In that case the vector field $\mathbf{M}(x,y)$ may be represented by a scalar field, the streamfunction, $\Psi(x,y)$, without loss of information. The streamfunction is related to the east and north components of $\mathbf{M}$ by

$$\frac{\partial \Psi}{\partial y} = HU \quad \text{and} \quad \frac{\partial \Psi}{\partial x} = -HV, \tag{69}$$

or in a vector form,

$$\mathbf{M} = -\mathbf{k}\times\nabla\Psi$$

where the upper case H and U,V are the steady state thickness and velocity components. The sign convention of (69) is arbitrary, and may be reversed in some applications. The streamfunction may be computed from the vector field by integrating either of (69). Here we integrate the HV term westward, starting from the eastern boundary,

$$\Psi(x,y) = \Psi(L,y) \; - \; \int_L^x H(x,y)V(x,y)dx. \tag{70}$$

The dimensions (units) of this streamfunction is volume transport, $\mathrm{m}^3\ \mathrm{sec}^{-1}$. The volume transport of major ocean currents is in the range 1 - 150 $\times 10^6\ \mathrm{m}^3\ \mathrm{sec}^{-1}$ and often reported in a non-SI but widely used and accepted unit, 'Sverdrups', with 1 Sv = $10^6\ \mathrm{m}^3\ \mathrm{sec}^{-1}$. The normal component of the velocity vanishes on all of the side walls, and hence $\Psi(L,y) = constant$, that may as well be taken to be zero. It would be equally valid to perform an integration of HU in the y direction. The resulting streamfunction lines (Fig. 22, left) are everywhere parallel to $\mathbf{M}$, and hence the streamfunction makes a very clear presentation of the direction of the underlying vector field. With this choice of sign, lower values of Ψ are to the right of the vectors (which is opposite the geostrophic relationship for SSH). The density of streamfunction lines is proportional to the magnitude of $\mathbf{M}$ and notice that $\partial\Psi/\partial x$ is very large in thin western boundary regions where the wbc current is correspondingly very large compared to the currents in the interior of the basin.

Sverdrup transport may also be represented by a streamfunction (Fig. 22, right), here computed from Eqns. (29) and (70) and integrating westward from the eastern boundary,

$$\Psi_{Sv}(x,y) = \Psi_{Sv}(L,y) \; + \; \frac{1}{\rho_o \beta}\int_L^x \nabla\times\tau(x,y)dx. \tag{71}$$

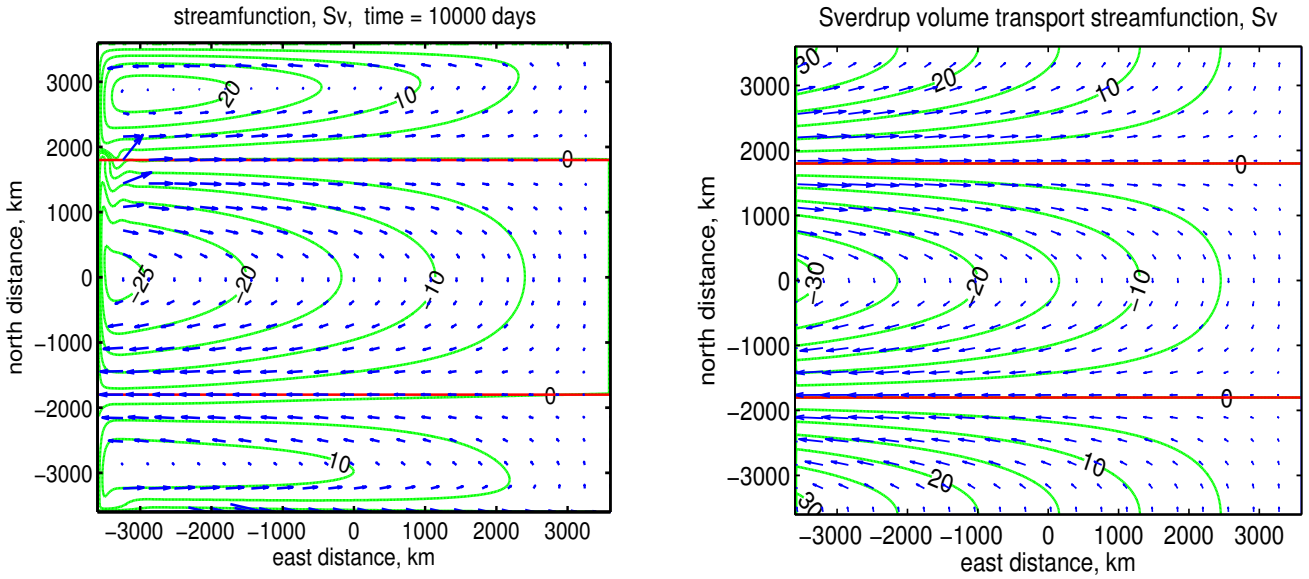

Figure 22: **(left)** The volume transport streamfunction (green lines) computed from the steady state numerical solution by integrating Eqn. (70) starting from the eastern boundary. Labeled in Sverdrups, 10^6 m^3 sec^{-1}. The blue vectors are the volume transport per unit width, **M**, and are parallel to lines of constant streamfunction. The very large **M** vectors in the western boundary regions are omitted here but shown in a later Fig. 14. The red horizontal lines are the axes of the westerly and easterly winds, and also approximate gyre boundaries. **(right)** The Sverdrup volume transport streamfunction (green lines) computed from the wind stress of the numerical experiment (Fig. 6) and Eqn. (71) and starting from the eastern boundary. In the numerical model-computed streamfunction field at left, $\Psi = 0$ is found on all of the boundaries, indicating no normal flow through the boundaries, as should hold exactly. The Sverdrup streamfunction at right can not satisfy a zero normal flow condition on more than one boundary, here chosen to be the eastern boundary.

The starting value is taken to be $\Psi_{Sv}(L,y) = 0$ for all y, which ensures that there is no normal flow through the eastern boundary. Since only one integration is needed to compute Ψ_{Sv}, no other boundary data may be applied and so the Sverdrup streamfunction can not satisfy a no normal flow condition through any of the other boundaries. In this case the stress curl $\nabla \times \tau(x,y) = -\partial \tau^x / \partial y$ and independent of x and hence the streamfunction is

$$\Psi_{Sv}(x,y) = -\frac{(L-x)}{\rho_o \beta} \frac{\partial \tau^x}{\partial y}. \tag{72}$$

The zonal component of mass transport is then

$$HU = \frac{\partial}{\partial y} \Psi_{Sv}(x,y) = -\frac{(L-x)}{\rho_o \beta} \frac{\partial^2 \tau^x}{\partial y^2}, \tag{73}$$

and the meridional component is Sverdrup transport,

$$HV = -\frac{\partial}{\partial x}\Psi_{Sv}(x,y) = -\frac{1}{\rho_o \beta}\frac{\partial \tau^x}{\partial y}, \tag{74}$$

as expected.

A comparison of the two streamfunction fields (Fig. 22) is one way to see where Sverdrup balance is valid in the numerical solution. The steady circulation in this experiment consist of three gyres within which the meridional flow has the sign of the wind stress curl, e.g., equatorward in the subtropical gyre where $\nabla \times \tau < 0$, and so qualitatively consistent with the Sverdrup relation Eqn. (29). Each of these gyres is very strongly compressed onto the western side of the basin in the sense that the largest SSH and thus the largest pressure anomaly is found about a hundred kilometers offshore of the western boundary. (see Sec. 8.2, 6)

Another and more quantitative way is to evaluate the interior meridional transport for all y, Fig (23). The Sverdrup relation gives a fairly accurate account of the meridional transport over the interior of most of the subtropical gyre, and to a much lesser degree, the subpolar and tropical gyres. The Sverdrup relation is clearly not valid within about 100 km of a western boundary as discussed in Sec. 3.3, nor is it valid within roughly 500 - 1000 km of the northern and southern zonal boundary regions. In the zonal boundary regions the Sverdrup relation indicates significant meridional flow which does not happen in the numerical model solution. What is perhaps surprising is how broad the affected zonal boundary regions are (more on this in Sec. 4.3). One consequence of such broad zonal boundary regions is that the transport of the western boundary currents of the tropical and the subpolar gyres is somewhat less than is the transport of the subtropical gyre, which is not similarly affected by a zonal boundary (Fig. 19).

4.2 Dynamics of the steady circulation: the balance of potential vorticity

The dynamics of the circulation may be described most fruitfully in terms of the balance of potential vorticity, Eqn. (44), here expanded and multiplied by H,

$$\begin{aligned} \beta VH &= \frac{1}{\rho_o}\nabla\times\tau - rh_o\nabla\times\mathbf{V} + HOT, \\ beta &= curl\ tau + curl\ drag + higher\ order\ terms. \end{aligned} \tag{75}$$

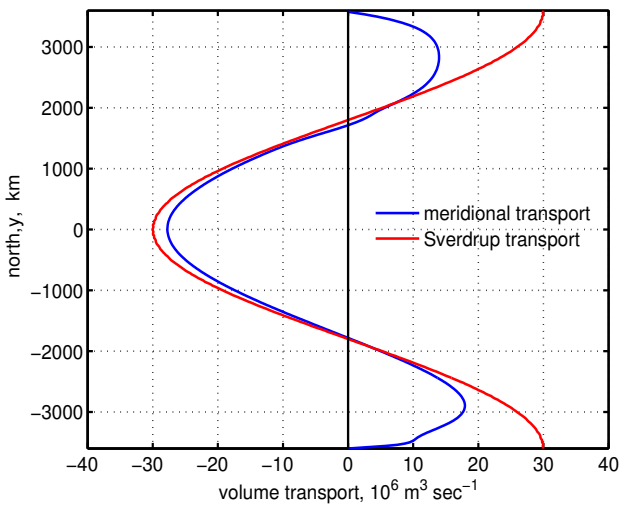

Figure 23: The north-south variation of the zonally-integrated meridional transport computed from the steady model solution (blue line) and computed via the ideal Sverdrup transport relation, Eqn. (29) (red line). The integration extends from the eastern boundary to just outside of the western boundary current. Notice that the actual (numerical) meridional transport vanishes on the zonal boundaries at $y = \pm 3600$ km due to a no normal flow boundary condition. This is something that the Sverdrup relation (red line) can take no account of. The north-south extent of the affected zonal boundary region is 500 - 1000 km, which is a significant part of the tropical and subpolar gyres.

The higher order terms are the collected nonlinear terms involving the advection of potential vorticity and the gradient of layer thickness;

$$HOT = -H\mathbf{V}\cdot\nabla\xi \; + \; h_o H Q \mathbf{V}\cdot\nabla H \; - \; \frac{1}{\rho_o h}\tau\times\nabla H \; + \; \frac{r h_o}{H}\mathbf{V}\times\nabla H.$$

In general, the steady potential vorticity balance includes a contribution from all of these terms, including the HOT. However, in this solution the nonlinear HOT terms are important only in special places (marked with red dots in Fig. 24) where large currents are combined with large horizontal gradients, e.g., the confluence of the subtropical and subpolar western boundary currents near $(x,y) = (-L, L/2) = (-3600, 1800)$ km.

4.2.1 Sverdrup interior

Aside from these important but spatially limited regions, the steady potential vorticity balance can be characterized by the regional distribution of two term balances or modes among the linear terms of Eqn. (75), Fig. (24). One of these, the Sverdrup mode,

$$\begin{aligned} \beta V H &= \frac{\nabla\times\tau}{\rho_o}, \\ beta &= curltau, \end{aligned} \qquad (76)$$

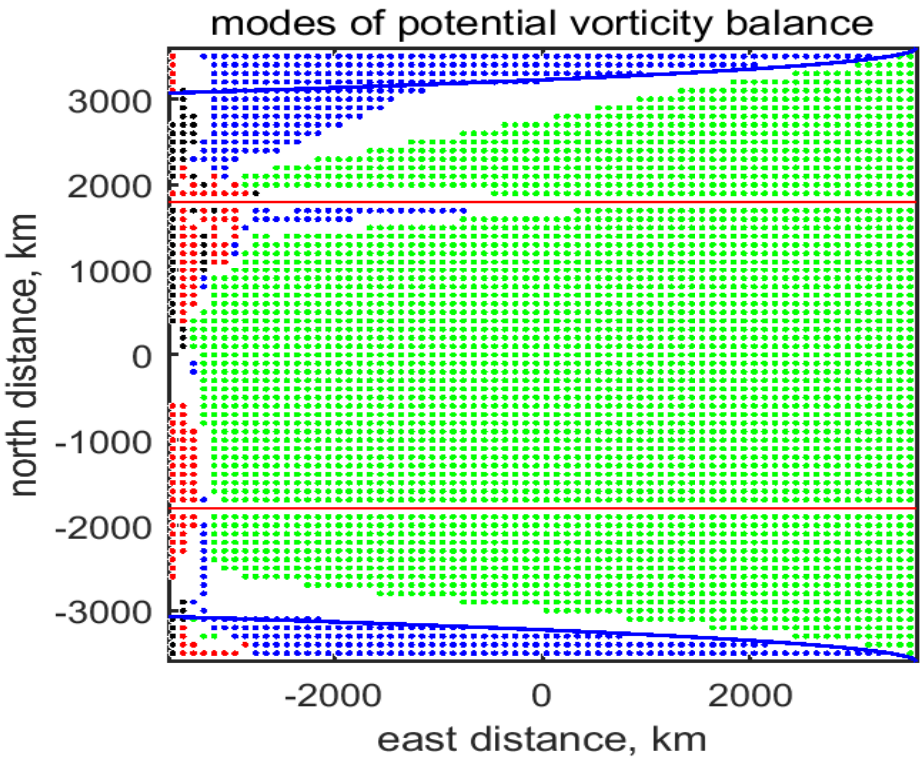

Figure 24: The steady potential vorticity balance characterized by the distribution of the modes (approximate two term balances) of Eqn. (75). Horizontal red lines are the gyre (wind stress curl) boundaries as before. A **green dot** indicates that the Sverdrup mode, $beta = curltau$, accounts for more than 90% of the variance of the steady potential vorticity balance at that point. This (approximate) Sverdrup balance holds over about 75% of the basin. A **black dot**, shows where $beta = drag$ is the dominant mode, mainly near the western boundary. A **blue dot** indicates the mode $0 = curltau + drag$ found near the northern and southern zonal boundaries . A **red dot** indicates that the HOT, the collection of nonlinear terms, was larger than two of the linear terms. If there is **no colored dot**, then there is no dominant mode, and the balance of potential vorticity is shared among at least three of the terms of Eqn. (75). The blue lines near the northern and southern zonal boundaries are a simple, linear estimate of zonal boundary region width that is discussed in Sec. 4.2.3.

accounts for at least 90% of the variance of the potential vorticity balance over most of the interior region of the basin (the green dots of Fig. 24), especially within the subtropical gyre, and which is often and appropriately called the Sverdrup interior.

Eqn. (44) describes the potential vorticity balance at a fixed point. Consider a site in the subtropical gyre interior where the wind stress curl is negative, which by itself would cause Q to decrease with time. A steady state will occur if the meridional flow advects higher Q water from the north at the same rate (opposite sign) of the stress curl. Since the potential vorticity in the interior is approximated well by the

planetary vorticity, $Q \approx f/h_o$ (with h_o a constant), then this occurs by the advection of planetary vorticity, $V\partial f/\partial y$, as if f was a fluid property. For this steady, Sverdrup balance to exist throughout the interior of the basin, there must be some mechanism that serves to recharge the higher latitudes (within the subtropical gyre) with high Q water, or specifically, with water having $Q \approx f/h_o$. What is the source of this high Q water? The western boundary current, described next. (see Sec. 8.2, 7)

4.2.2 Western boundary currents

The Sverdrup balance certainly does not hold within the western boundary currents (Figs. 21 and 22), where the meridional current is counter to the Sverdrup flow. The beta effect on a fast-flowing wbc current is in any case far larger than can be balanced by the curl of the wind stress (as occurs in the Sverdrup interior), and so in this model the steady vorticity balance within a wbc is mainly between the beta effect and the curl of the friction, 'drag',

$$\begin{array}{ccc} \beta VH & \approx & -\ rh_o \nabla\times\mathbf{V}, \\ beta & & drag. \end{array} \tag{77}$$

For example, the western boundary current of the subtropical gyre has very large negative relative vorticity (Fig. 18) , and a correspondingly large, positive, curl of the friction, or 'drag'. This drag largely balances the negative vorticity tendency of the beta effect, allowing a steady state within the subtropical wbc. Regions where this frictional balance holds in the sense described above are denoted by the black dots in Fig. (24), and are very near the western boundary in all three gyres.

To characterize this balance we can define an Ekman number equivalent for the vorticity balance,

$$E_Q \ = \ \frac{drag}{beta} \ = \ \frac{r\nabla\times\mathbf{V}}{\beta V}, \tag{78}$$

ignoring signs and taking $H = h_o$. The usual Ekman number is the ratio of frictional force to Coriolis force, but in this case we have curl of the friction divided by (compared to) the beta effect (see Problem 11, Sec. 8.2). To evaluate E_Q it is helpful to use a streamfunction representation of the velocity and its curl. Thus

$$V \ \approx \ \frac{\Psi}{L_{wb}},$$

where L_{wb} is the east-west width of the wbc, which for now we will treat as an unknown. Within the narrow western boundary current, the horizontal scale in the x direction (normal to the boundary) is much

less than the scale in the y direction and hence the curl of the velocity (the Laplacian of the streamfunction) is approximately

$$\nabla \times \mathbf{V} \;=\; \nabla^2 \Psi \;\approx\; \frac{\partial^2 \Psi}{\partial x^2} \;\approx\; \frac{\Psi}{L_{wb}^2}.$$

Using these estimates in (78) gives

$$E_Q \;=\; \frac{r}{\beta L_{wb}}. \tag{79}$$

If the balance is indeed Eqn. (77), then we can assert $E_Q \approx 1$ and readily solve for the purely frictional wbc width, $L_{wb} \;=\; L_{fric}$ and find

$$L_{fric} \;=\; \frac{r}{\beta}. \tag{80}$$

For the present values of r and β, $L_{fric} \approx 50$ km, which is numerically about the same as the (subtropical) radius of deformation (Sec. 3.3.2). Said a little differently, for the present r, the Q balance of a wbc having a width equal to the radius of deformation is significantly frictional. Recall (Sec. 2.3) that in this experiment, the value $r \;=\;$ 1/15 days, was chosen in an *ad hoc* manner, the minimum r (least viscous) that permitted a near steady state solution. This is a partial rationalization of this choice. However, there is no independent means for identifying an appropriate value of r (that I know of), and so we have to be cautious about interpreting the present model solution as if it were a fully realistic model of a real wbc.

To understand the shallow water model solution, at a minimum we need to know what happens when r is changed; say that r is doubled to 1/7.5 days, which makes the solution more viscous. The pattern of the Sverdrup interior is unaffected, but the amplitude of the Sverdrup transport is reduced slightly, a few percent. The Sverdrup interior is thus not much affected by the choice of r. The wbc becomes somewhat thicker, as (80) indicates it should. Since the wbc transport is reduced and the wbc width increased, the wbc speed is reduced considerably, by about 30%. In that event the flow is steady throughout the model domain. More interesting is that r is reduced to half the present value, to $r = 1/30$ days. The volume transport in the interior is then a few percent greater and so is a better match to the ideal Sverdrup transport. But again the overall pattern of the interior circulation is indistinguishable from the nominal experiment. The width of the subtropical wbc is slightly narrower, though not nearly as much as the purely frictional boundary layer width (80) suggests, and so it appears that $L_{wb} = R_d$ is a lower limit that obtains for smallish friction. The wbc current speed is slightly greater, by about 10%, and so the inertia of the wbc is also greater. The nonlinear terms of the q balance are enhanced, and the colliding western boundary currents at the subpolar/subtropical gyre confluence (on the western boundary at about $y = 1800$ km; the largest red dot region of Fig. 24) are considerably more vigorous than in the nominal experiment (Fig. 40, lower). This kind of unstable, eddying flow is an important and

interesting characteristic of nearly all strong ocean currents that are not constrained by topography. However, this aspect of boundary current dynamics is sensitively dependent upon details of the ocean bottom topography and the vertical structure of currents, among others, and so is outside the scope of a shallow water model and of this essay. (see Sec. 8.2, 9, 11)

4.2.3 Zonal boundary regions

There are extensive regions adjacent to the zonal boundaries (northern and southern boundaries) where the ideal Sverdrup balance does not hold, as evident in the qualitative mismatch of Sverdrup transport with the actual transport within about 500 to 1000 km of the zonal boundaries (Figs. 22 and 23). As noted at the outset, the Sverdrup balance *per se* is unable to satisfy the boundary condition that the meridional current must vanish on the zonal boundaries, and so if there is wind stress curl on these boundaries (as there is here, Fig. 6) then the Sverdrup balance will necessarily fail; something else must happen. Very near the zonal boundaries there is no meridional velocity and thus no β effect. The steady, linear potential vorticity balance in this model must reduce to the steady, linear, forced, damped mode,

$$\begin{aligned} 0 &= \frac{1}{\rho_o}\nabla\times\tau - rh_o\nabla\times\mathbf{V} \\ &= curltau + drag, \end{aligned} \tag{81}$$

indicated by blue dots in Fig. (24).

Like the wbc, this boundary region is also anisotropic, but in this case the meridional, north-south scale is much less than the zonal, east-west scale and hence $\nabla^2\Psi \approx \frac{\partial^2\Psi}{\partial y^2}$. The balance (81) may then be written via the streamfunction as

$$0 \approx \frac{1}{\rho_o}\nabla\times\tau + r\frac{\partial^2\Psi}{\partial y^2}.$$

The curl of the drag has to be large enough to balance the wind stress curl in the zonal boundary region, and the question is what zonal boundary layer width, L_{zb}, is required to achieve this? Estimating $\partial(\,)/\partial y \approx 1/L_{zb}$ and $\partial^2(\,)/\partial y^2 \approx 1/L_{zb}^2$, then

$$0 = \frac{1}{\rho_o}\nabla\times\tau - \frac{r\,\Psi}{L_{zb}^2}.$$

It is not obvious what Ψ should be, but as a first guess, let's try the Sverdrup streamfunction, Eqn. (71), even though we know for sure that the Sverdrup Ψ can not be correct right on the boundary. We can be a little bit bold with this, since we can check the result against the numerical solution. Given a tentative

estimate $\Psi = (L-x)\nabla\times\tau/\rho_o\beta$, where $L-x$ is the distance from the eastern boundary (positive), the boundary layer width is easily found to be

$$L_{zb} = \sqrt{\frac{r\,(L-x)}{\beta}}. \tag{82}$$

This is sketched onto Fig. (24 as blue lines near the southern and northern zonal boundaries. At the midpoint of a zonal boundary, $x = 0$, $L_{zb} \approx 400$ km, which is a reasonable estimate of the half-width of the zonal boundary region evident in Figs. (24) and (23). Notice that the region significantly affected by the zonal boundary dynamics (the no dot transition region between the blue and green dot regions) is about twice this width.

The width of this boundary layer estimate decreases toward the east, which is qualitatively consistent with the distribution of modal balances, i.e., a narrower blue region toward the east. An eastward decrease of L_{zb} arises because, while the vorticity needed to achieve the balance $0 = curltau + drag$ on the zonal boundary is uniform along the boundary (recall that *curltau* is here taken to be uniform in x, which is generally not true over the real oceans, Fig. 3) and hence the zonal current, which is qualitatively the zonal component implicit in the Sverdrup relation, decreases eastward. As a consequence, the north-south horizontal scale over which the current varies must also decrease eastward in order to have the necessary relative vorticity and thus curl of the friction sufficient to balance the curl of the wind stress.

Like the western boundary layer, the width of the zonal boundary regions is expected to be independent of f and thus should be the same along the southern and northern zonal boundaries since the imposed wind stress is the same on those boundaries (Sec. 4.2). However, judging from the east-west distribution of q-balance modes found in the numerical model solution (Fig. 24), the zonal boundary layer is in fact markedly wider in the western-most third of the sub-polar zonal boundary region. The reason for this discrepancy is mainly that the subpolar gyre of this numerical experiment has a significantly reduced layer thickness compared to the initial thickness, h is as little as 100 m in the western subpolar gyre, and hence there is considerably greater drag than is accounted for by the linear equation (81) that presumed $H = h_o = 500$ m. A straightforward experimental test of this hypothesis follows from setting the imposed wind stress small enough — $\tau_o = 0.01$ N m^{-2} suffices — that the dynamics are linear in the respect that $H \approx h_o$ throughout the model domain. In that case the comparison between the numerical and the estimated boundary layer width (82) is quite good throughout. Thus the linear estimate of zonal boundary layer width (82) is valid for a linear problem, and it is straightforward to understand the sense and the approximate magnitude of the finite amplitude effects that occur when there are large spatial variations in layer thickness, as do occur in this numerical solution.

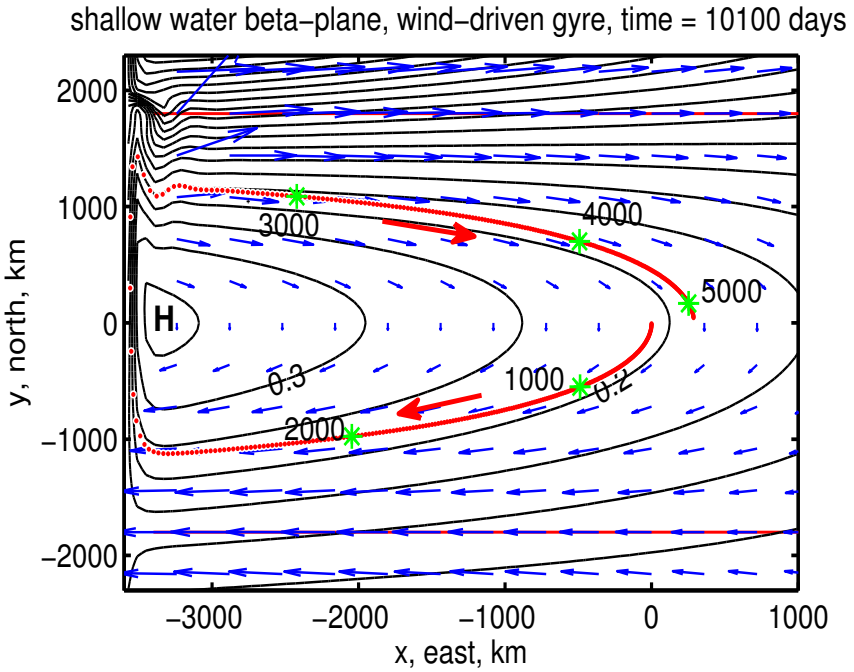

Figure 25: The (almost) steady subtropical gyre, shown by contours of SSH anomaly and a field of velocity vectors. A parcel trajectory that was started at $(x,\ y) = (0,\ 0)$ and followed for 5,500 days is the red line. The green asterisks along the trajectory are at 1000 day intervals. The parcel entered the western boundary current at about 2,600 days after starting, and it exited the western boundary current about 200 days later. The parcel returned close to its starting position. Notice that the trajectory is almost parallel to isolines of SSH, but not exactly so.

4.3 A trip around the subtropical gyre

In the previous section, our analysis considered the currents, vorticity, etc., as observed at fixed locations, a point of view often dubbed 'Eulerian'. This is the natural starting point, since the shallow water equations and their numerical implementation are Eulerian. However, our intuition for classical mechanics has roots in a parcel-following, or 'Lagrangian' description, since the m and the a of $F = ma$ are the mass and acceleration of a specific chunk of material, and not the fluid properties observed at a point in space (the Eulerian view). In this section we will take this kind of parcel-following view on a complete trip around the gyre. Besides connecting a little better with our intuition for mechanics, this also gives a holistic view of the circulation in that it shows how the western boundary current is an essential component of a steady circulation.

To construct a Lagrangian description we have to solve for parcel trajectories,

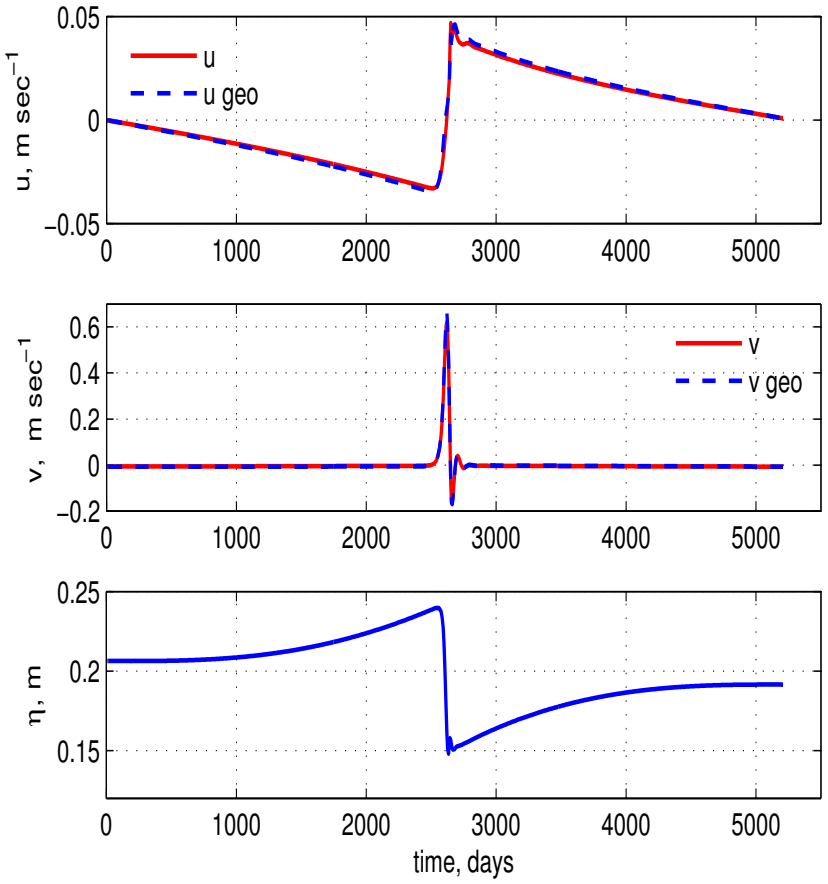

Figure 26: Velocity components along the trajectory of Fig. (25). **(upper)** East velocity (red line) and the geostrophic velocity estimated from the layer thickness (dashed blue line). **(middle)** North component of velocity. Note the very large change in the scale compared to the east component above. The actual velocity and the geostrophic velocity are close enough that the lines are difficult to distinguish. **(lower)** The SSH anomaly along the trajectory. While within the interior region, the parcel slowly climbs the SSH high of the subtropical gyre. While in the wbc, it descends comparatively very rapidly.

$X(t;(X_o,Y_o)), Y(t;(X_o,Y_o))$ by integrating the velocity along the path of a specific parcel,

$$X(t) = \int_0^t U(x,y)dt + X_o, \qquad \text{and,} \qquad Y(t) = \int_0^t V(x,y)dt + Y_o, \tag{83}$$

where (X_o,Y_o) is the initial position and the $t = 0$ here is the time this integration starts (not the starting time of the numerical integration as in Sec. 3). The key thing is that the (x,y) dependence of the velocity field is continually updated as the integration proceeds, i.e., the $(x,\ y)$ in the integrand is set $= (X,\ Y)$ at each time step. Since the velocity field is available only at the 20 km resolution of the numerical model, the evaluation of velocity at an arbitrary parcel position requires an interpolation of the discrete model data, which is bound to incur some error, much like the finite difference evaluation of a derivative.

The initial position may be chosen anywhere in the model domain; the trajectory shown in red in Fig. (25) was started in the center, $(X_o,\ Y_o) = (0,\ 0)$. The initial position is, in effect, the tag on the parcel that happened to be there at the time t_o. Not surprisingly, different initial positions result in different

trajectories. In this circulation, small initial position differences yield only rather small trajectory differences (some examples to follow). A flow having this property may be described as 'laminar'.[18]

A complete trip around the subtropical gyre from this starting position $(X_o,\ Y_o) = (0,\ 0)$ requires a little more than 5000 days and extends over about 11,000 km. If the circulation was exactly steady (it isn't quite), and if the integration method used to construct the trajectory was without error (it can not be), then the parcel would return to it's starting point. Notice that this parcel didn't quite make it (Fig. 25). However, the interesting changes in parcel properties along the track are considerably larger than the starting point/ending point mismatch, and so the semi-quantitative inferences that we can make from this trajectory are reliable.

Assuming that the fluid is not at rest, then there is no Lagrangian steady state comparable to the steady state of an Eulerian frame. Rather, fluid parcels continuously change position and generally all other properties with time. To find say the potential vorticity of the parcel, we can either evaluate the (presumably known) $q(x, y)$ field at the parcel position, or, integrate the q conservation equation along the trajectory.

4.3.1 Momentum balance and energy exchanges

The relationship of parcel motion to the local slope of the SSH anomaly (the pressure or geopotential anomaly) is closely analogous to the motion of a dense parcel on a slope studied in Part 1. Differences in detail include that the slope changes quite a lot along the trajectory, especially near the western boundary, and, there is an additional external force, the wind stress, which is essential for compensating the slow but inexorable effects of friction.

During the first several hundred days, the parcel moved very slowly toward the south, which is consistent with the meridional Sverdrup flow at the starting latitude. Eventually, the parcel turned toward the southwest (Fig. 26) and began to pick up some speed. The trajectory was roughly parallel to the SSH lines with higher SSH to the right. Thus the parcel motion was, to a first approximation, geostrophic.

An important departure from strict geostrophy is that the parcel had a rather small but sytematic component of motion across the SSH lines. While the parcel was in the interior, it slowly climbed up the

[18] If instead the sensitivity to initial position was large, then the flow would be characterized as chaotic or turbulent. Most large scale fluid flows, and including the real ocean circulation, are turbulent in this sense.

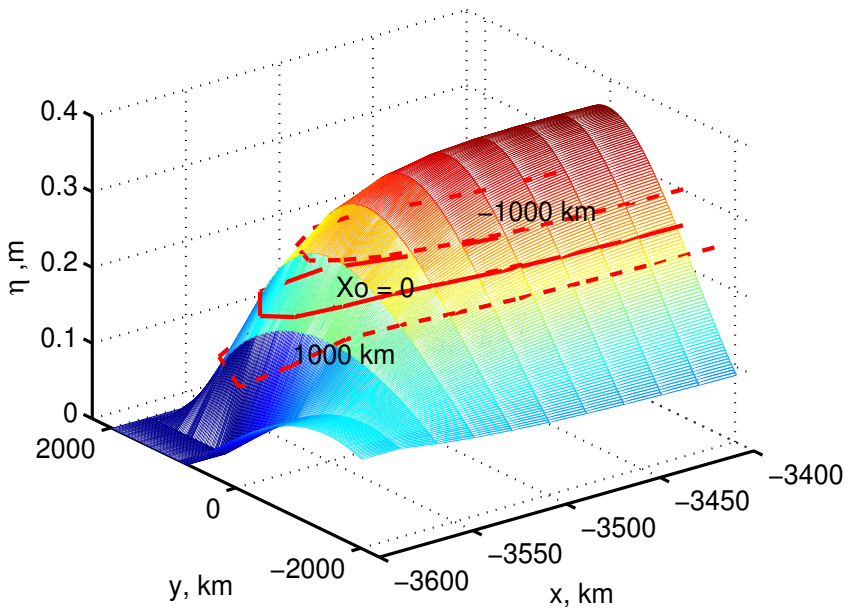

Figure 27: Three trajectories superimposed on the SSH anomaly, η, of the western side of the subtropical gyre. The trajectories differ in their starting points, X_o, that is noted. The solid red trajectory has $X_o = 0$ and is shown also in Fig. (25). Notice that the x scale is greatly expanded compared to the y scale so that the very large zonal slope of SSH within the wbc and its relationship to these trajectories is apparent.

SSH high of the subtropical gyre. The damping effect of friction causes the parcel to descend the local SSH slope, though at a very small angle consistent with the small Ekman number, E is O(0.01). We can therefore infer that the small component of motion toward higher SSH is a consequence of the wind stress. From an energy perspective, the positive wind work that occured while the parcel was in the interior was stored as potential energy.

After several thousand days, the parcel began to approach the western boundary, where the SSH topography was by comparison, very steep, about two orders of magnitude greater than in the interior. As the parcel neared the western boundary it accelerated to the north, reaching speeds of O(1 m sec^{-1}), or about two orders of magnitude greater than the speeds that characterize the slow, Sverdrup flow of the interior. The parcel motion never showed any significant inertial motion, and the momentum balance remained almost geostrophic (Fig. 26, middle). This implies that the acceleration associated with the steep wbc topography was slowly-varying compared to the rotation time, $1/f$. The kinetic energy associated with the rapid northward flow came from the potential energy that was released as the parcel descended about 0.1 m while within the western boundary current (Fig. 26, lower). There was also some energy loss to friction. After about 200 days, the parcel left the western boundary current and entered the slow eastward flow along the north side of the subtropical gyre. While moving eastward, it slowly climbed back up the high SSH of the subtropical gyre and returned close to its starting value of SSH anomaly.

4.3.2 Potential vorticity balance

Potential vorticity conservation provides another way to think of the Sverdrup relation. Given that the field of q is presumed to be steady at fixed locations, $\partial q/\partial t = 0$, then the q of the moving parcel is just the q at it's present position (this sounds both profound and trivial at the same, but be sure to understand this before going on) . Moreover, the spatial variation of Q is due mainly to the spatial variation of f, at least in the subtropical gyre interior, where the circulation is very slow. The parcel was subject to the overlying wind stress, whose curl was negative, and thus would tend to reduce the q of the parcel (Fig. 28, upper). Since the q of the parcel had to be consistent with the q of the presumed steady field, the parcel must move southward toward lower q, assuming that the q field is dominated by the meridional variation of f. Said a little differently, the southward motion of the parcel must be just sufficient to keep the q of the parcel consistent with the steady field of potential vorticity, $(\nabla \times v + f)/h$. In the subtropical gyre, the spatial variation of q is due mainly to the latitudinal variation of f, and hence we are led to the Sverdrup relation. This is a rigorous argument for the Sverdrup relation, given the assumptions of a steady, linear q balance. However, it feels awfully thin as an explanation for existence of the circulation in the first place. And of course, so does the usual (Eulerian) Sverdrup relation.

It is a fair surmise that a parcel can not be subject solely to a negative wind stress curl, or else the basin-wide average of q would surely decrease with time, which is not consistent with the steady state of the Eulerian circulation. It must be the case that parcels occasionally experience a process that increases q — a (relatively) quick pass through the western boundary current where there is a very strong, positive curl of the drag. This positive drag curl resets the parcel's q to a value that is consistent with the interior q (Fig. 28) where it reenters the Sverdrup interior. Thus the western boundary current is a crucial part of the gyre-scale circulation with respect to potential vorticity.

4.3.3 Depth dependence*

The shallow water form of the Sverdrup relation implies that the wind stress acts upon the entire layer of thickness h that participates in the Sverdrup transport. That is indeed exactly what happens in a shallow water model, but not within the real ocean. Instead, the Sverdrup transport occurs within an Ekman layer of thickness d_{Ek} that is typically O(100 m) that absorbs all of the direct wind stress, i.e., $\tau(z < -d_{Ek}) = 0$, and a geostrophic layer that is much thicker, O(1000 m). If the wind stress penetrates no deeper than 100 m, say, then how is the much thicker geostrophic layer affected by the wind? The answer is vortex stretching contained within the z-dependent vorticity equation, (30), but not in the integrated Sverdrup relation. Just to be specific, consider the subtropical gyre where the wind stress curl is negative, and so

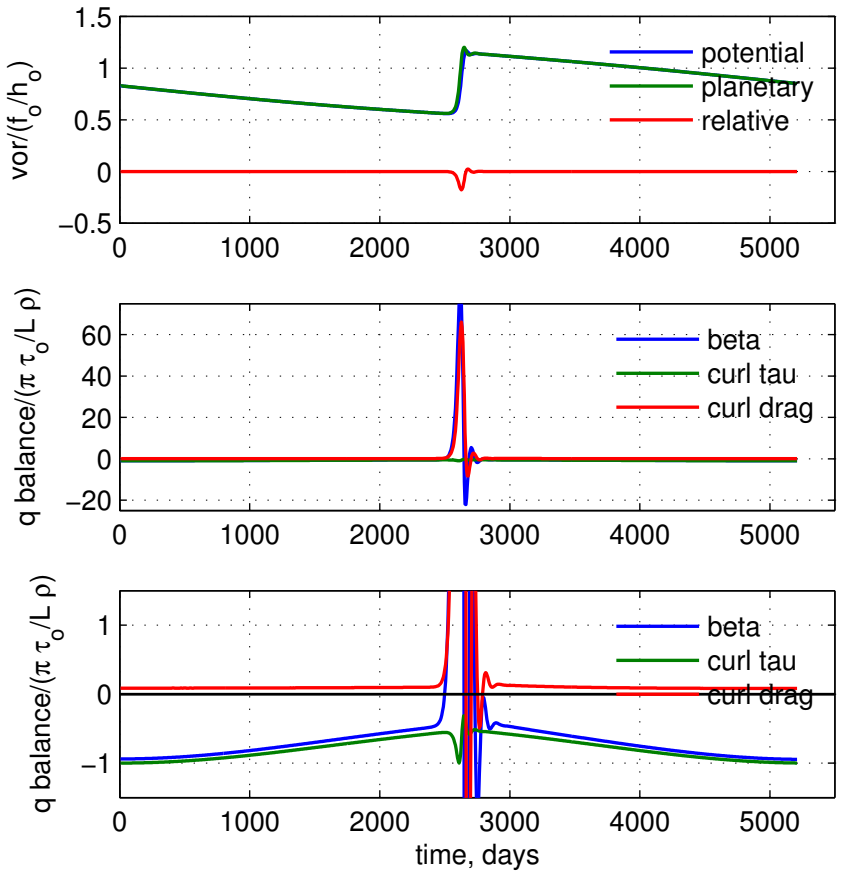

Figure 28: Potential vorticity along the trajectory of Fig. (25). **(upper)** The full potential vorticity (blue line), the planetary vorticity (green line) and the relative vorticity (red line). These are normalized by f_o/h_o. Notice that the relative vorticity is very small except when the parcel is within the western boundary current where it has a maximum magnitude of -1/4 (normalized). **(middle)** Leading terms in the potential vorticity balance, Eqn. (75). These data are normalized by a nominal wind stress curl, 8×10^{-8} m sec^{-2}. When plotted at this scale, about all that can be told is that the beta term is approximately balanced by the drag curl term while the parcel is within the western boundary current. **(lower)** Same data as above, but with a clipped ordinate that reveals the interior balance between the beta term and wind stress curl.

that the Ekman layer transport is convergent. The vertical velocity at the base of the Ekman layer due to wind stress curl alone is just $\frac{1}{f}\nabla\times\tau$ and the beta effect acting upon the meridional component of Ekman transport contributes another $\frac{\beta}{f}\tau^x$. The net vertical velocity is then

$$W(-d_{Ek}) \;=\; \frac{1}{\rho_o}\nabla\times(\frac{\tau}{f}).$$

Only the stress at the sea surface appears here, and letting $d_{Ek}\to 0$ does not alter the Ekman transport or its divergence. Thus, while it is unphysical, it is not incorrect to imagine that this vertical velocity is present at the sea surface (though in practice it is largest at the base of the Ekman layer). This Ekman-induced vortex stretching is expected to accompany a meridional, geostrophic transport,

$$\beta\int_{-d}^{0} V_{geo}dz \;=\; fW(-d_{Ek}) \;=\; \frac{f}{\rho_o}\nabla\times(\frac{\tau}{f}), \tag{84}$$

which is the same as Eqn. (34).

There is an important distinction between the shallow water version of Sverdrup transport and the vortex stretching induced transport described above insofar as in the former, all of the water in the Sverdrup layer follows a forced q balance, $dq/dt = \nabla\times\tau/\rho_o$. In that event, all of the water that participates in the Sverdrup transport must go through the western boundary current in order to reset q (this is a Lagrangian description so we use q vs. Q). In the vortex-stretching case, the water that makes up the geostrophic Sverdrup transport follows the linearized q conservation, i.e., $dq/dt = 0$, or in the z-dependent case, $\beta v = f\partial w/\partial z$. In that event, the water that circulates within the gyre need not go through the western boundary current to reset q to larger values, since q is not changed by the wind stress. The real ocean is somewhere between these two extremes: some fraction of the water that participates in the Sverdrup transport is directly wind-forced, but not all, or even most.[19]

4.4 Another way to view the Sverdrup relation

The Sverdrup relation implies or requires a steady state not only of potential vorticity but also of momentum, energy, and of the stratification (layer thickness). Consideration of this latter yields what I believe is the most insightful view of the Sverdrup relation.

The east-west tilt of SSH over the subtropical gyre interior implies a meridional geostrophic current that is equatorward and that is divergent (thinning) on account of the beta effect (Sec. 1.3),

$$\frac{\partial h_{geo}}{\partial t} = \frac{\beta h}{f} V_{geo} < 0.$$

Thus a meridional geostrophic current on a beta plane can not, by itself, be steady. Something more must be present, and of course we know that that could be a wind stress and an associated, convergent Ekman transport,

$$\frac{\partial h_{Ek}}{\partial t} = -(\frac{\partial hU_{Ek}}{\partial x} + \frac{\partial hV_{Ek}}{\partial y}) = \nabla\times(\frac{\tau_o}{\rho_o f(y)}) > 0.$$

Assuming that the current is the sum of geostrophic and Ekman currents only, then

$$\frac{\partial h}{\partial t} = \frac{\partial h_{geo}}{\partial t} + \frac{\partial h_{Ek}}{\partial t}$$

[19] To follow up on this requires a depth-dependent model and some means to specify the depth of the Ekman layer, d_{Ek}. These are outside the present scope, but note that a landmark advance on the theory of wind-driven circulation was developed along this line by Jim Luyten, Joe Pedlosky and Hank Stommel, 'The ventilated thermocline', J. Phys. Oceanogr., Feb. 1983, https://doi.org/10.1175/1520-0485(1983)013¡0292:TVT¿2.0.CO;2.

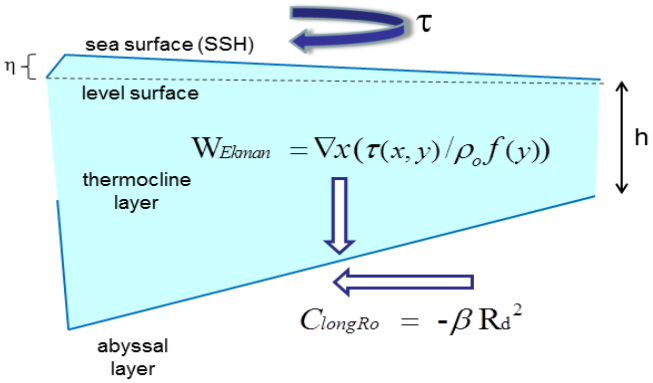

Figure 29: A schematic cross section of the North Atlantic subtropical thermocline, sliced east-west and viewed looking toward the north as in Fig. (1). The wind stress over the subtropical gyre produces an Ekman transport that is convergent and that would tend to thicken the thermocline layer. The Sverdrup relation may be viewed as a steady balance between this positive thickness tendency and the negative thickness tendency associated with the beta effect acting upon the equatorward geostrophic flow.

and a little rearranging gives

$$\frac{\partial h}{\partial t} = \frac{\beta h}{f}(V_{geo} + V_{Ek}) - \frac{1}{\rho_o f}\nabla \times \tau.$$

This is the wind-forced version of the first order wave equation (19) that contains both the Rossby wave propagation mechanism, a balance of the left side and the first term on the right side, and the Sverdrup relation, if the layer thickness is steady.

The large scale thickness field of the subtropical gyre interior may thus be viewed as an arrested, long Rossby wave. The westward translation expected from the β-effect and the first order wave equation is balanced by a wind stress-induced convergence of the Ekman transport. Wind-driven gyres and mesoscale eddies are closely related in as much as they have the same β-effect acting upon meridional flows (this seems obviously true), the difference is that wind stress does not vary appreciably on the horizontal scale of a mesoscale eddy and hence the westward propagation.

5 Experiments with other wind fields and basin configurations

The idealized, steady, zonal wind field considered up to here is, of course, just one possibility. In this section we will consider briefly some other, equally idealized wind fields and basin configurations that help reveal several important aspects of the wind-driven circulation.

5.1 Annually-varying winds and circulation

The model experiments of Sections 3, 4 and 5 assumed that the wind field was steady, once switched on. That is a reasonable starting point for a study of the wind-driven circulation. However, almost everyone with experience living in a coastal region will attest that the wind over the ocean varies with the seasons, and in some regions it varies quite a lot. For example, the annual variation of the westerlies over the northern North Atlantic is very roughly $\pm 50\%$ of the annual mean, with the highest winds during winter. The annual variation of easterly wind magnitude is somewhat less, though the annual migration of the Inter-Tropical Convergence Zone (furthest north in summer) produces a large annual variation in the local wind stress curl.[3,11] Meridional winds (not included in this study) show an especially marked annual variation that also contributes significantly to the annual variation of stress curl. Given this large amplitude annual variation, and the day-to-day variation of winds with weather, one might argue that the time-mean wind scarcely exists, outside of our climatologies. This raises an obvious question — what have we missed by considering only the long-term average winds?

Given what we have learned about the response time of the western boundary current, we might guess that an annually varying wind will not have a large effect on at least the western boundary current of the subtropical gyre. But to find out more, let's calculate the solution for an idealized, annually-varying wind stress,

$$\tau^x(x,y,t) = (0.1 + 0.05 \sin(2\pi\, t/365)) \sin(\pi y/L),$$

where t is the time in days. Note that this wind stress amplitude varies quite a lot, between 0.05 and 0.15 Pa. This annually-varying wind was applied from the start of an integration that was continued past 10,000 days. The solution never comes to a steady state, but the annual cycle in the ocean circulation becomes stationary in the sense that it repeats from one year to the next and so the startup transient has been minimized by 10,000 days.

Snapshots of the resulting circulation at times that are near the minimum and maximum response in the tropical gyre are in Fig. (30), and a series of slices through the center of the gyres shows the (inferred) η (Fig. 31). The $\eta(x)$ from the steady wind experiment (red dashed line) runs through the center of the envelope of the time-varying $\eta(x,t)$, indicating that the dynamics are effectively linear, i.e., the time-mean of the solution computed with an oscillating wind stress is very nearly the same as the solution computed with the time-mean of the wind stress. The first result of this experiment is that if the steady or long time-mean of the ocean circulation was the only thing of interest, then we would not have to be concerned with resolving explicitly the annual variation of the wind; the long term (yearly or more) time-mean of the wind stress would evidently suffice, at least for this model.

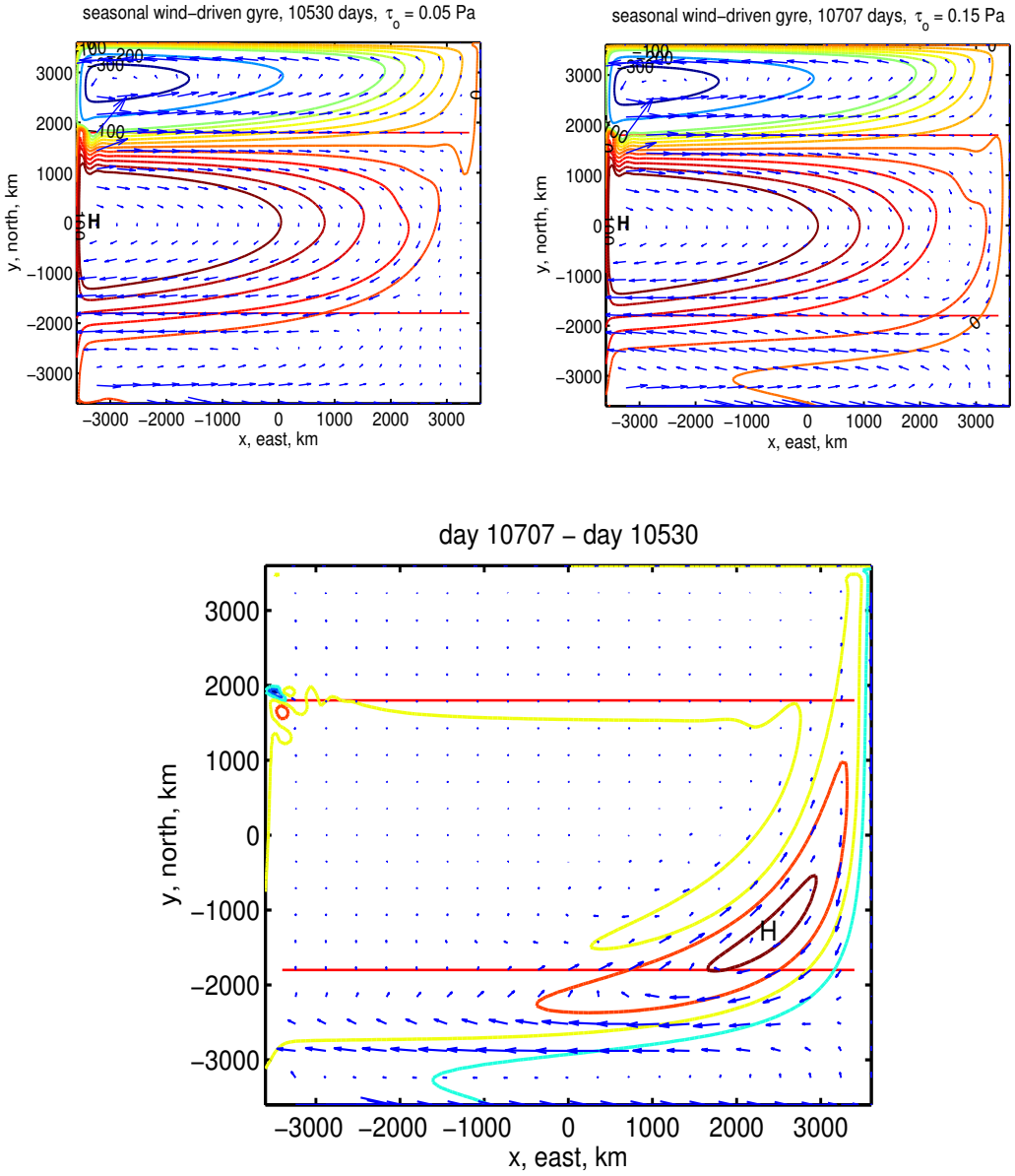

Figure 30: **(upper)** Two snapshots of the circulation taken 180 days apart and near a minimum (left) and maximum (right) of the tropical circulation. The latter occurs about one month after the maximum of the annually-varying wind stress amplitude. An animation of these data is available from www.whoi.edu/jpweb/seasonal-gyres.mp4 **(lower)** The difference of the two snapshots, showing the pattern of the annual cycle. Notice the small, intense eddies near the western boundary at about $y = 1800$ km, the confluence of the subpolar and subtropical western boundary currents. This kind of time-dependent eddy variability is present even with a steady wind stress.

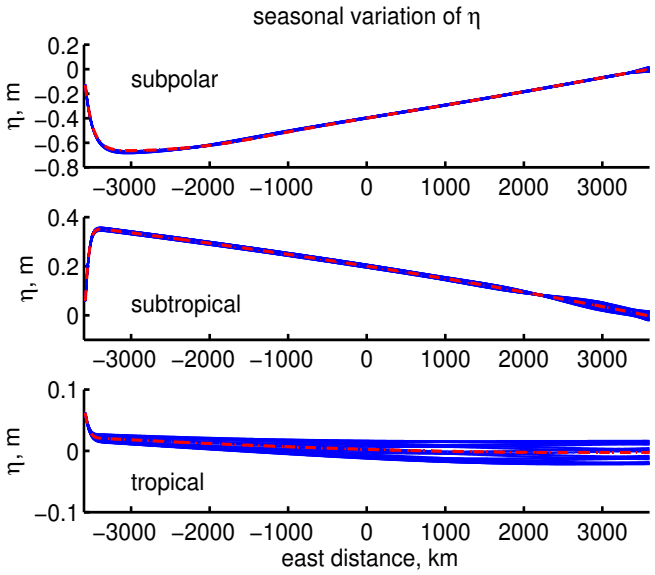

Figure 31: Zonal profiles of SSH, $\eta(x)$, from the annually-varying winds experiment. These profiles were taken through the centers of the three gyres noted. The blue lines were taken at 40 day intervals after time = 10,000 days when the solution appeared to be in a statistically steady state. The single red dashed line is a slice through the base case solution having steady winds, and notice that it goes through the center of the envelope of blue lines. Notice too that the η scale differs considerably between the three panels, consistent with the considerably larger η in the subpolar gyre.

A second important result of this experiment is that the amplitude of the annual variation in the ocean varies greatly with latitude. Specifically, the tropical gyre responds much more vigorously to the annually-changing wind than does either the subtropical or especially the subpolar gyre. This is what we should have expected from the start up experiment, which showed a much faster rise of the tropical gyre vs. the subpolar gyre. The amplitude of the annual variation in the ocean depends very much upon the variable of interest. For example, the zonal current sampled on the north side of the middle of the tropical gyre (Fig. 32, solid red line) varies by $\pm 50\%$ in this experiment, or the same as the wind stress. The explanation for this vigorous low-latitude response appears to be as simple and direct as the $\propto 1/f^2$ dependence of the local, wind-induced (Stage 2) geostrophic current, Eqn. (60). The observed annual variation of zonal currents in the tropics is likely of this sort.[3] There is also an annual period eastern boundary wave that has an appreciable amplitude in the lower subtropics. This wave penetrates only about one wavelength into the interior.

Wbc transport is one measure of the gyre circulation (Rossby et al., 2010, footnote 2): in the subpolar gyre, the wbc transport varies by about ± 0.3 Sv, in the subtropical gyre by about ± 0.7 Sv, and in the tropical gyre, by about ± 1.2 Sv or only about $\pm 8\%$ (Fig. 33). The latter is much less than the response of zonal current just noted. The western boundary current transport is a bulk property of a gyre, and responds on the time scale of the basin-wide meridional (Sverdrup) flow, $2L/C_{longRo}$, Eqn. (63). The long Rossby wave speed is $\propto 1/f^2$ and much faster within the tropical gyre, but nevertheless, the rise time of the wbc transport of the tropical gyre is many hundreds of days (Fig. 19) and fairly long compared to the time scale of the annually-varying wind, a few months. The response time of the subtropical and subpolar gyres is much longer still, a thousand to many thousands of days, and hence the

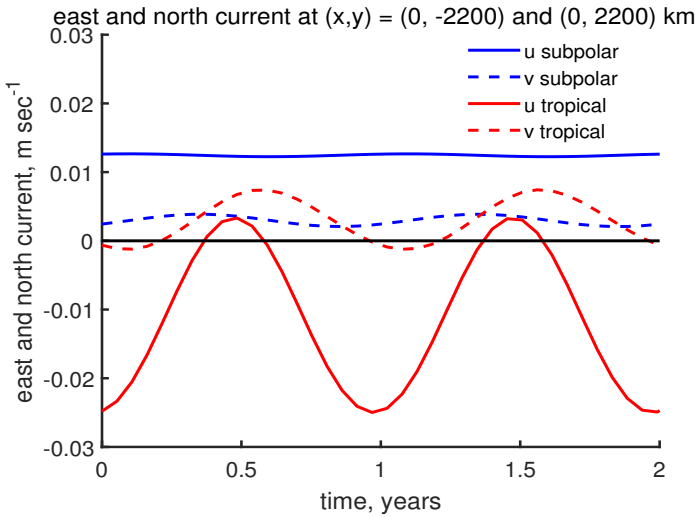

Figure 32: East and north component of the current from the annually-varying wind experiment. The current was sampled at two sites, on the south side of the subpolar gyre (blue lines) and the north side of the tropical gyre (red lines). The current at the high latitude site is almost constant in time despite the annually-varying wind stress. The current at the low latitude site oscillates by about $\pm 50\%$ around a mean which is very close to the steady state current found in the steady wind stress experiment of Sec. 3.

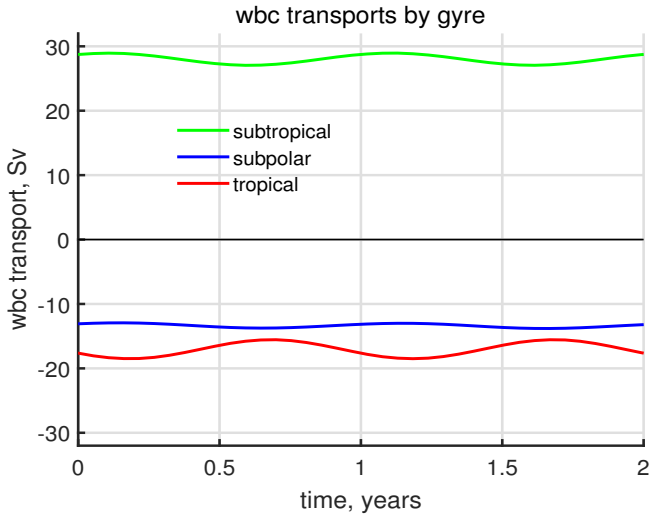

Figure 33: Transports of the western boundary current in each of the gyres from the annually-varying wind experiment. Colors are as in Fig. (19). Notice that the annual variation of the wbc transport in the tropical gyre (red line) is modest when compared to the very large annual variation of especially the zonal current in the interior of that gyre, cf. the red, solid line of Fig. (32).

wbc transport of higher latitude gyres varies even less in response to annually-varying wind.

5.2 A stress field with no curl*

The discussion of wind stress has emphasized importance of the curl of the wind stress curl, rather than the stress itself. And yet, the Ekman transport depends only upon the stress, and the Stage 2 response

includes a term proportional to the β-induced divergence of the Ekman transport, and thus the stress. This raises the question, can there be a steady circulation driven by wind stress alone, that is, by a stress field with no curl?

To find out we can conduct an experiment in which a spatially uniform stress is imposed over the ocean basin. To avoid troublesome instances of vanishing layer thickness near boundaries, the stress is made very small, 0.01 N m^{-2}. The amplitude of the resulting currents and layer thickness are also very small, but our interest will be the structure of the response, rather than it's amplitude.

If the spatially uniform stress is eastward, say, then the Ekman transport is southward throughout the basin, and divergent, Eqn. (58). For short times, $t \leq 1000$ days, this produces a thinning of the active layer (low pressure) that is most pronounced at lower latitudes, while also causing a pileup of water near the equatorial boundary where there is a growing high pressure. The resulting zonal current near the equatorial boundary is thus eastward, and there is a weaker, more distributed westward flow at higher latitudes, evident at $y >$ -2000 km in Fig. (34) (upper and middle).

Just as we have seen before, these zonal currents are necessarily turned into the meridional direction along the eastern boundary, and the result is to initiate a long Rossby wave-like front that propagates westward across the basin. This eastern boundary Rossby wave signals the adjustment toward a steady state, and not too long after the Rossby wave passage the stratification (layer thickness) and flow are indeed quasi-steady. The steady state sea surface (inferred from the layer thickness) slopes up toward the east so that a zonal pressure gradient opposes the wind stress. Most notably, the current in the adjusted steady state vanishes. Absent a curl of the wind stress, there is a vanishing meridional flow in the interior, which comes as no surprise if we have already accepted the Sverdrup relation. Since this applies within a closed basin, neither can there be a steady zonal flow. (see Sec. 8.2, 12)

5.3 Meridional winds over a basin without sidewalls (a channel)*

One last experiment: consider a basin with dimensions as before, but now replace the no normal flow boundary condition on the eastern and western boundaries with a reentrant boundary condition, i.e., for the zonal velocity,

$$u(x = -L) \; = \; u(x = L),$$

as if the basin was a channel that wrapped all the way around a cylinder. Similar boundary conditions are applied to h and v. We have had occasion to think about a zonal wind stress acting on a channel of this

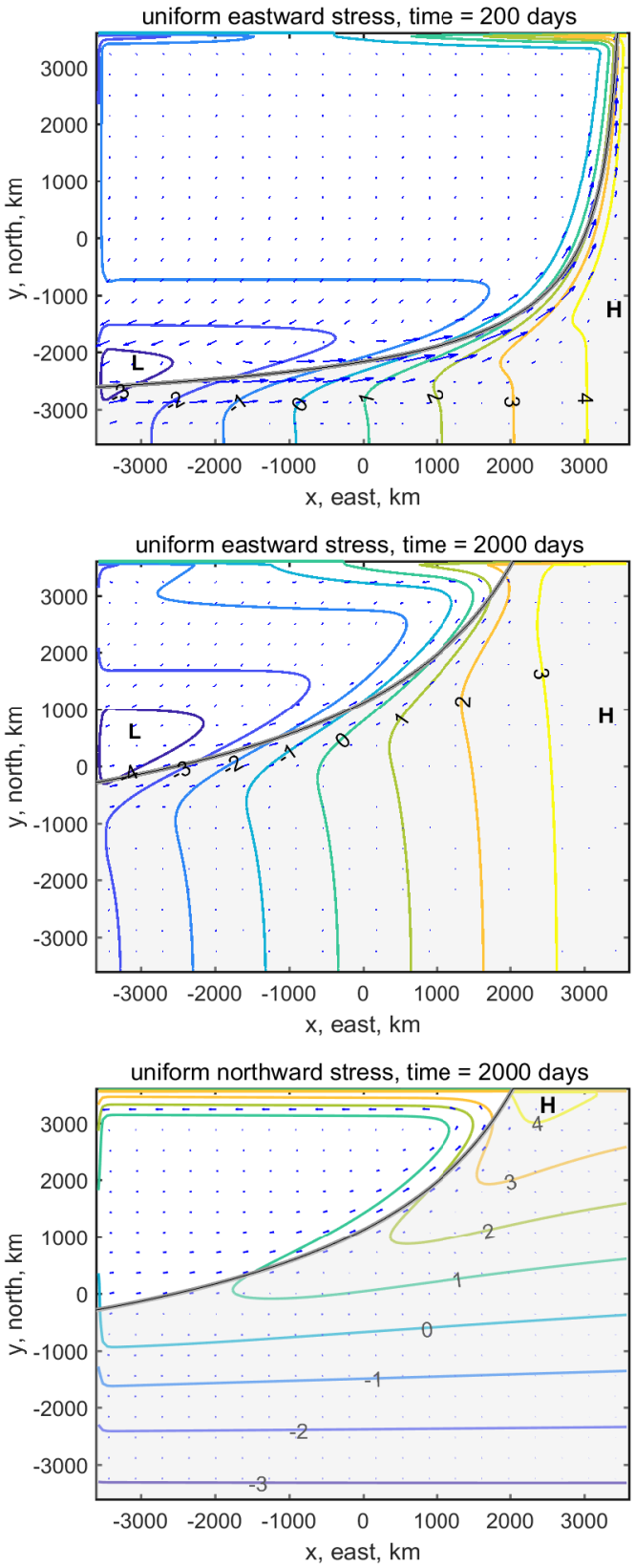

Figure 34: **(upper)** and **(middle)**Two snapshots from a wind-driven experiment in which the wind stress was spatially uniform and eastward at a very small value, 0.01 N m^{-2}. The times were 200 and 2000 days after the stress was switched on. The contours are of the anomaly of layer thickness, in meters. The blue arrows are the current, though with the comparatively very large currents within boundary currents omitted. The gray shading extends westward from the eastern boundary at the y-dependent speed of a long Rossby wave. **(lower)** A snapshot at 2000 days from an experiment in which the wind stress was spatially uniform and northward.

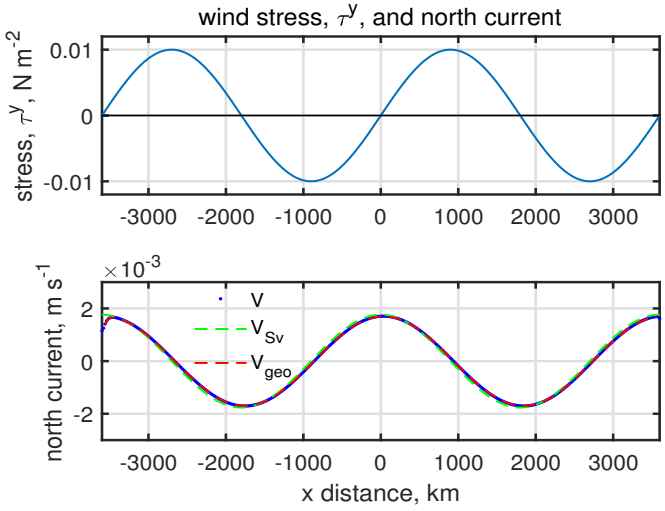

Figure 35: **(upper)** The x profile of the northward wind stress field applied in the channel experiment. The stress was independent of y. **(lower)** The north component of current across $y = 0$ at time = 10,000 days (blue dotted line) along with the expected Sverdrup current (green dashed line) and the meridional, geostrophic current estimated from the thickness field (red dashed line). These are almost identical, and hence the steady meridional flow in this experiment is both geostrophic and Sverdrup, there being no meridional Ekman flow.

sort (Sec. 3.3) and so for this experiment the wind stress is presumed to be in the *meridional* direction. To be consistent with the channel configuration and the reentrant boundary conditions,

$$\tau^y(x) \;=\; \tau_0 \sin(2\pi x/L), \tag{85}$$

(Fig. 35, upper) so that $\tau^y(-L) \;=\; \tau^y(L)$ and independent of y. The stress amplitude is made very small, $\tau_o = 0.01$ N m^{-2}, to avoid vanishing layer thickness in boundary currents. Meridional winds certainly do occur over the oceans, especially near boundaries, but a basin-wide, meridional wind stress field of this sort is not realistic of any wind stress field observed in nature. Regardless, it does help to make an important point regarding the role of an eastern boundary vis-á-vis the Sverdrup relation. Given the boundary condition (85) the zonal length scale of the stress field will be written

$$L^x_\tau \;= 2\pi/L,$$

to distinguish from the distance to the eastern boundary that plays such a prominent role in the closed basin cases considered to now.

The Ekman transport that accompanies this meridional wind stress is zonal, and is divergent. The resulting Stage 2 thickness anomaly grows linearly with time as

$$h_{S2} \;=\; \frac{\tau_o}{\rho_o f L^x_\tau} \cos(2\pi x/L)\, t,$$

and forms alternate highs and lows, Fig. (36). The Stage 2 meridional geostrophic current is

$$v_{S2} \;=\; \frac{\tau_o g'}{\rho_o f^2 L^{x2}_\tau} \sin(2\pi x/L)\, t$$

where f is $f(y)$, and so v_{S2} is much bigger at lower latitudes (smaller y) as we have seen before. Like the Stage 2 response of the closed basin cases, this steadily accelerating current persists for only a finite time, hundreds or thousands of days depending upon y, after which it is supplanted by a steady or nearly steady Sverdrup balance,

$$v_{Sv} = \frac{\tau_o}{\rho_o L_\tau^x \beta H} \cos(2\pi x/L).$$

In this experiment, where there is no eastern boundary, the near-steady Sverdrup balance develops first at low latitude, and then spreads northward. At a given y, the adjustment occurs in the time required for a long Rossby wave to propagate westward over the distance L_τ^x, the length scale of the wind stress. The northward extent of the adjusted region is then estimated by

$$L_\tau^x = \frac{\beta C^2}{f^2}\, t, \tag{86}$$

where f is $f(y)$. Using the beta-plane representation of $f(y)$ and solving for the northward extent of the adjusted region, Y, gives

$$Y = \sqrt{\frac{C^2}{\beta L_\tau^x}}\; t^{1/2}, \tag{87}$$

which is used to define the gray shading of Fig. (36). This makes a plausible estimate of the y that separates the Stage 2 response to the north from the quasi-steady Sverdrup regime to the south. Of course, L_τ^x is propoprtional the basin scale, and so this one case is not completely convincing. The test is that when the east-west scale of the wind stress is made smaller, say $L_\tau^x = L/4\pi$ and thus $\tau^y(x) \propto \sin(4\pi x/L)$, while holding the basin width L constant, the adjustment to Sverdrup balance at a given y occurs in half the time seen in this case. Thus the relevant east-west scale for adjustment to Sverdrup balance is the zonal scale that is imposed on the meridional flow. In the case of a closed basin with zonal winds that are independent of x, that scale is the distance to the eastern boundary; in the present experiment, this zonal scale comes directly from the wind field itself.

6 Barotropic and baroclinic circulation of the three layer, free surface model, 3l-fs

The reduced gravity model is contained within the new three layer model - let $h_2 \to 0$, and $h_3 \to \infty$. Thus the phenomena of the reduced gravity model are a part of the new model, though with somewhat different

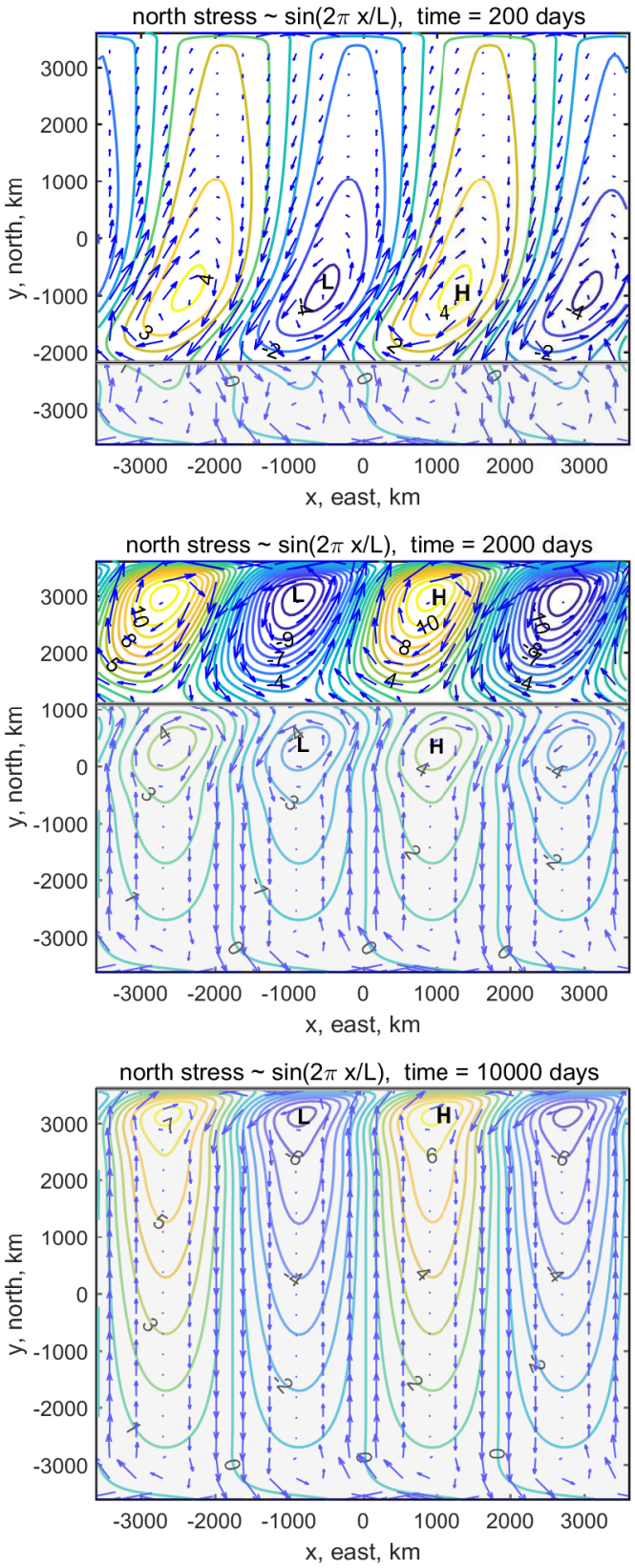

Figure 36: Snapshots from a wind-driven experiment in which the basin is a channel, and the wind stress was northward and x-dependent (Fig. 35, upper). The stress was set to a very small value, 0.01 N m^{-2}. Times were 200, 1000 and 10000 days (upper, middle, lower) after the stress was switched on. The contours are the anomaly of layer thickness in meters and the blue arrows are the current, though with boundary currents omitted. The gray shading extends northward from the southern boundary to a distance Y determined by the time, the y-dependent long Rossby wave speed and the zonal scale of the wind, L_τ, via Eqn. (87). Poleward of Y the flow is in Stage 2. Notice that there is clear evidence of westward propagation in especially the southern part of this region. Equatorward of Y the flow is adjusted to a near steady state Sverdrup balance (Fig. 35, lower). At a given y, the progression from Stage 2 to Sverdrup flow occurs at the same time across the entire channel (independent of x).

amplitudes. The important thing to note is that everything we learned from the reduced gravity model makes a useful contribution towards understanding the more comprehensive model results described next.

The solution of the multi-layer model contains additional phenomenon, and especially barotropic phenomena, and in general the new solution is more complex since $u = u(x,y,z,t)$ in place of $u = u(x,y,t)$. Though the z dimensionality is strongly truncated by a three layer representation, it is nevertheless challenging to display the full solution in a manuscript. We have to make choices. To start, we are going to emphasize one 'latitude', $y = -1000$ km, which is on the south side of the subtropical gyre. At this latitude there is both an appreciable wind stress, $\tau^x = -0.075$ Pa toward the west, and a significant stress curl, $\nabla \times \tau = -5.8 \times 10^{-8}$ Pa m^{-1}, which implies clockwise turning. The data from this latitude are shown in three forms. 1) At the basin center 'longitude', $(x,y) = (0,-1000)$ km, the current east and north components for each layer are shown for the first 30 days in Fig. (37). 2) The meridional component of the transport at the same site but for short and long times is in Fig. (38). 3) The meridional volume transport across the interior of the basin is in Fig. (39).

6.1 Inertial motion and Ekman transport in the surface layer

For short times, a few tens of days, the surface layer current and transport is familiar from the reduced gravity model, or for that matter, a purely local model, viz., near-inertial currents in both components, and Ekman transport in the meridional component, (the surface layer is represented by the red lines of Figs. (37) - (39). At the site sampled in these figures, $y = -1000$ km, the wind stress is westward, hence the Ekman transport is positive (northward) and has the magnitude expected for the wind stress at this site. This Ekman transport occurs throughout the model domain, though of course with varying amplitude and sign depending upon the local wind stress (Sec. 3.2).

6.2 Transient, barotropic flows

Over the region of negative stress curl that becomes the subtropical gyre, the Ekman transport is convergent. If that was all that was relevant, this Ekman convergence would thicken the surface layer at a rate of about 3 cm per day. In the context of a reduced gravity model, this produces a slowly growing baroclinic pressure gradient, and consequently a slowly increasing baroclinic, geostrophic current. By slowly we mean that it takes hundreds of days for this purely baroclinic process to produce an appreciable response. The presence of an active (or free) sea surface and an active abyssal layer in the

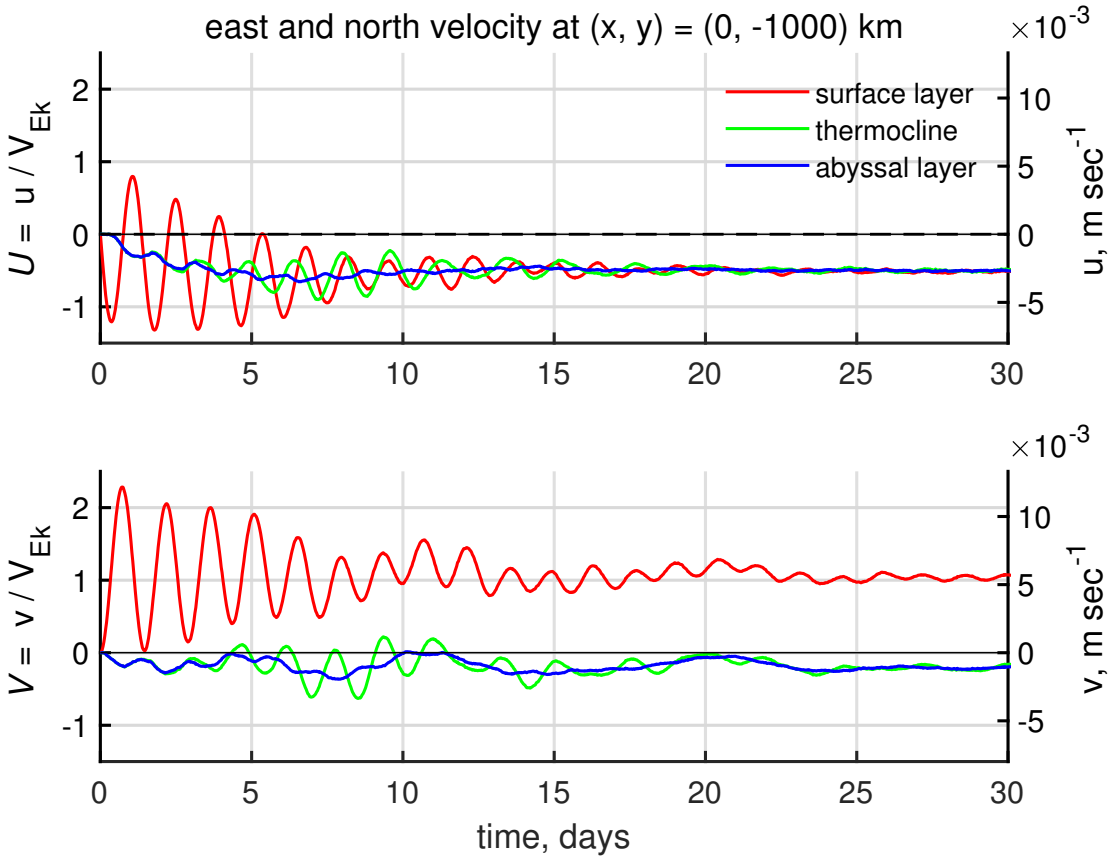

Figure 37: The short time evolution of the east and north components of the current computed by the three-layer model and sampled on the southern side of the subtropical gyre, $(x,y) = (0,-1000)$ km. Currents are normalized by the Ekman velocity scale, Eqn. (55), evaluated at this location, $V_{Ek} = 5 \times 10^{-3}$ m sec^{-1}. **(upper)** East currents in each of the the three layers; surface layer currents are in red, etc. The high frequency oscillations seen here are near-inertial motion. The time-mean of u is associated with barotropic Sverdrup flow discussed in the main text of the Appendix. **(lower)** North currents. The time mean dimensional current is about 5×10^{-3} m sec^{-1} and the non-dimensional value is about 1. This is as expected if the surface layer current is mainly Ekman flow. Layers 2 and 3 are unaffected by the direct wind stress, but nevertheless evidence a small, southerly barotropic Sverdrup flow that is modulated by barotropic Rossby waves having a period of about five days. The barotropic (depth independent) motions are much more prominent in the transport, bext figure.

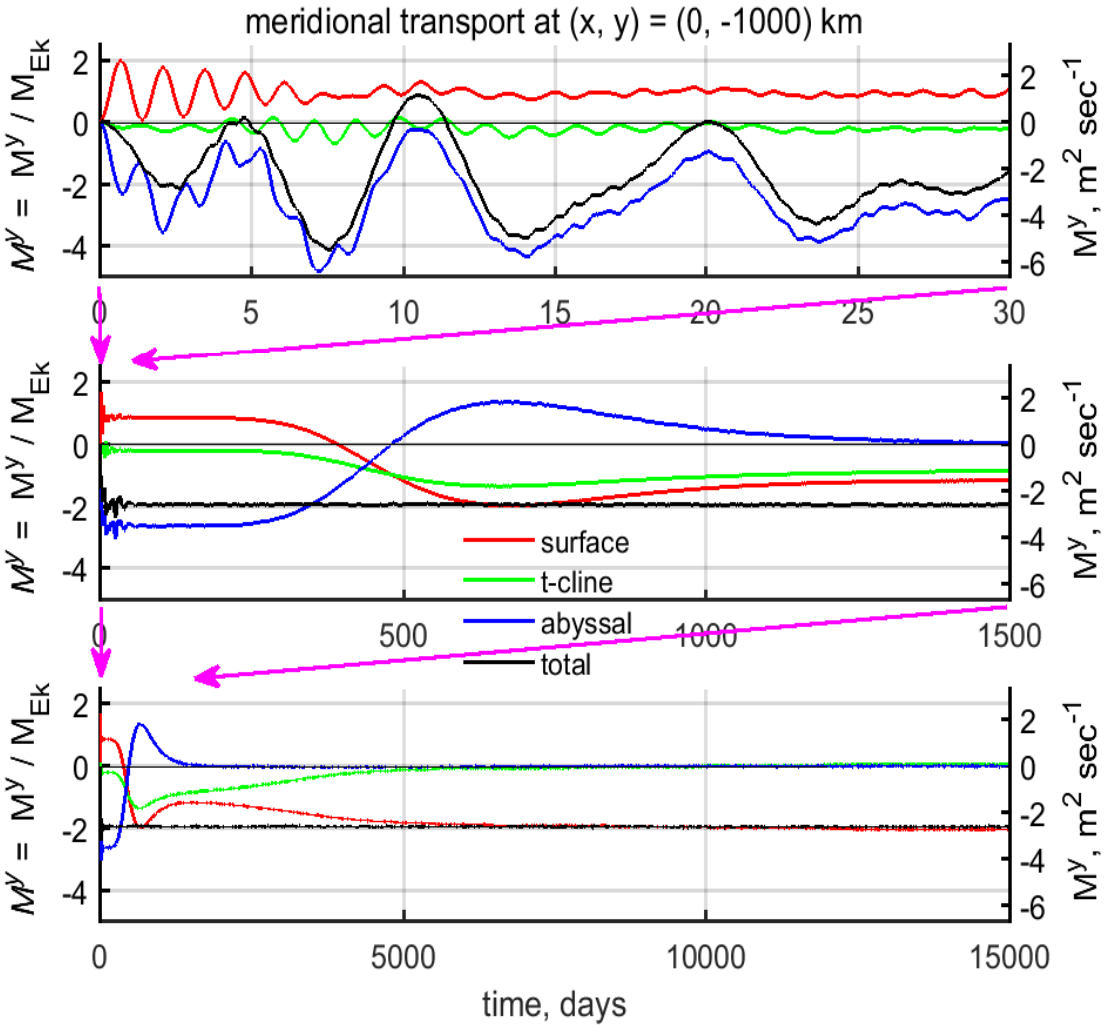

Figure 38: The meridional component of the transport at $(x, y) = (0, -1000)$ km. The data are shown on three time scales, **(upper)** 0 - 30 days, **(middle)** 0 - 1500 days, and **(lower)** 0 - 15000 days. Dimensional scale is shown at right, and nondimensional scale is at left. In this figure the transport is normalized with the expected Ekman transport magnitude at this y, $M_{Ek} \approx 1$ m^2 sec^{-1}. The surface layer transport (red line) is mainly Ekman transport and is northward. The total transport (all three layers) is the black line, which notice, has a very large contribution from the abyssal layer at short times, and is southward.

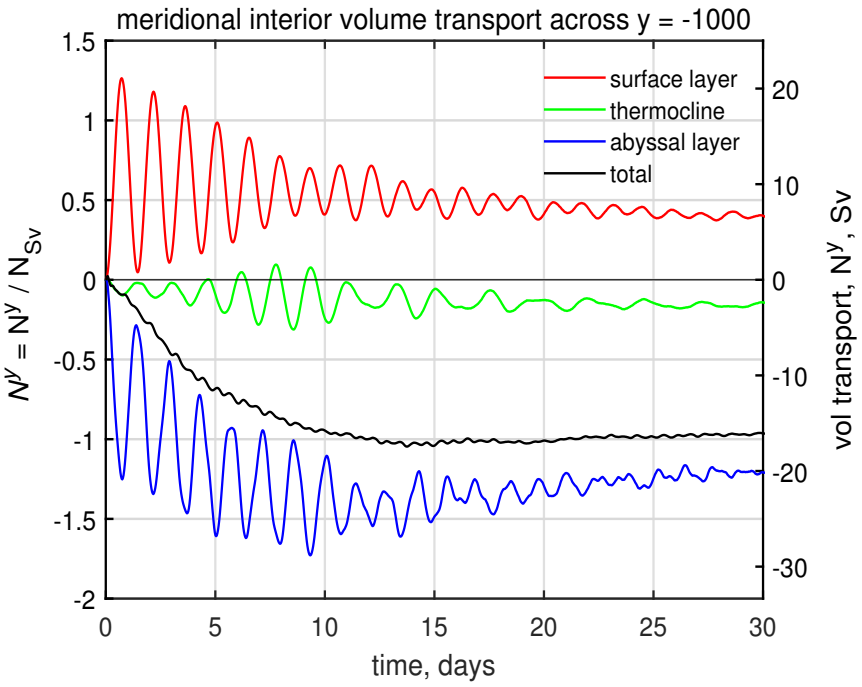

Figure 39: Meridional volume transport in the basin interior across y = -1000 km. The transport has been integrated from the eastern boundary to within 200 km of the western boundary. The volume transport within the surface layer (red line) is mainly Ekman transport and is northward as in the previous figure. The volume transport in the thermocline and abyssal layers is shown by green and blue lines; the sum over the three layers (the full water column) is the total volume transport shown as the black line. The dimensional scale is at right, and a nondimensional scale based upon the expected Sverdrup transport magnitude at this y, $N_{Sv} = 17$ Sv, is at left. Notice that the total transport appears to be quasi-steady from day 10 onward, and is -1 in these nondimensional units. Hence, the total transport is consistent with Sverdrup transport at this y.

present model gives a much quicker barotropic response. A thickening of the surface layer by a few centimeters will tend to cause a positive displacement of the sea surface by a few centimeters/2. A displacement of the Layer 2 interface by this amount is hardly noticable, but a displacement of the sea surface by a few centimeters is significant insofar as it produces a significant pressure gradient and thus flow within the thick abyssal layer. The resulting abyssal and thermocline layer currents are small amplitude, but the associated transport (current times thickness) is significant since the abyssal layer is very thick, (Fig. 38). For short times, a few weeks or even just a few days (Fig. (39, upper) the meridional transport at the observation site $(x, y) = (0, -1000)$ km shows a time mean to the south, and a pronounced oscillation having a period of about five days. These oscillations are associated with short, barotropic Rossby waves, which like higher frequency inertial oscillations, are an unintended byproduct of the impulsive start of the wind stress.

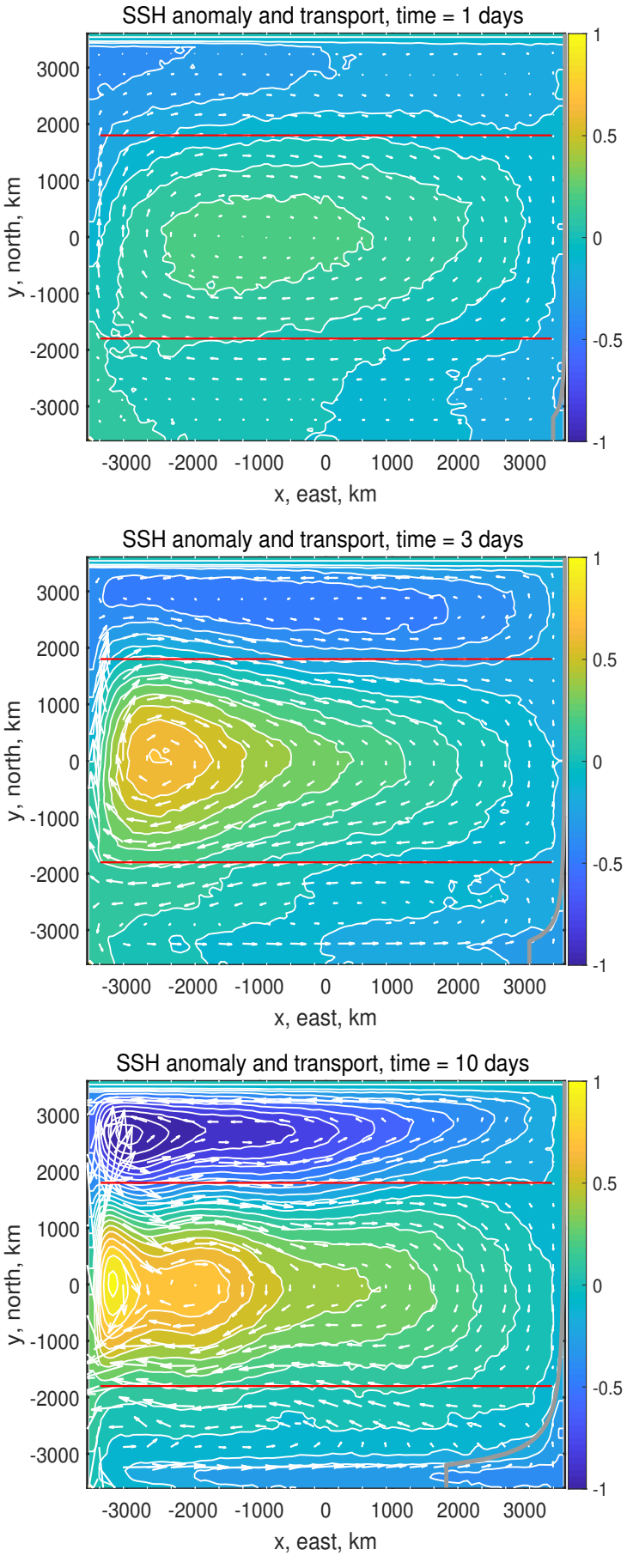

Figure 40: Three snapshots of SSH anomaly from a wind-driven, three-layer experiment at 1 day, 3 days and 10 days (top to bottom) after wind stress was switched on. The thin red horizontal lines are the axis of the westerly and easterly wind stress (Fig. 6). The small white arrows are the transport, though with the comparatively very large transports within the wbc omitted. The contours and colors are the SSH anomaly normalized with the barotropic Sverdrup SSH scale, Eqn. (89), evaluated at 30^o N $\eta_{Sv-btr} = 0.06m$. The largest positive SSH anomaly at day 10 is (dimensional units) $\eta \approx 0.06$ m in the western central subtropical gyre, and the greatest negative value is ≈ -0.09 m in the western subpolar gyre. The basin scale pattern evident here, *viz*, three highly asymmetric gyres, persists with minor changes for hundreds of days. An animation of these data is at www.whoi.edu/jpweb/BaroSver.mp4

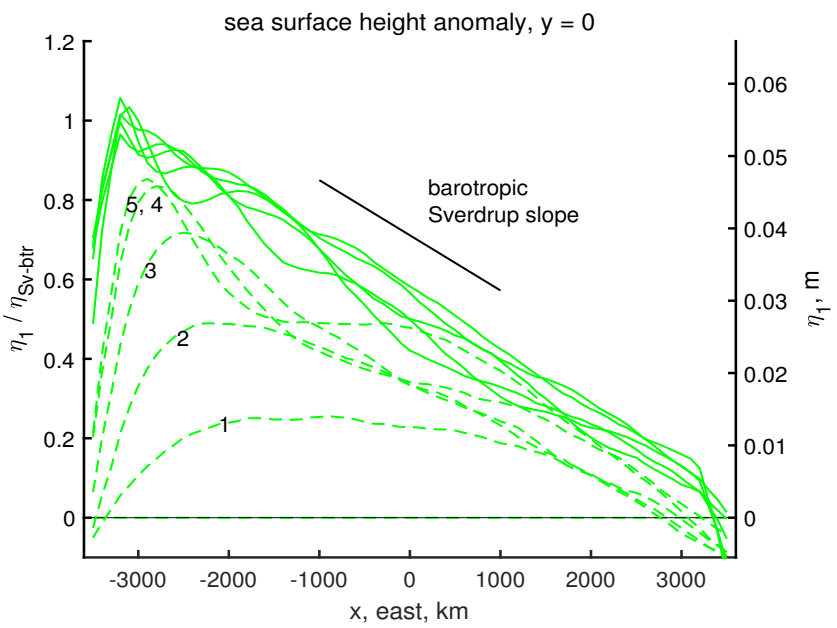

Figure 41: Successive across-basin profiles of SSH anomaly along $y = 0$. The first five days are the dashed green lines at 1 day intervals, and the next 25 days are solid green lines at 5 day intervals. The amplitude is scaled with the barotropic scale, Eqn. (88) which, for the parameters of this experiment, $\eta_{Sv-btr} = 0.05$ m. Note that on day 1 the SSH was a fairly symmetric mound. By day 3 this mound had shifted noticeably to the west, implying very rapid westward propagation, O(1000 km day^{-1}). After only about a week, the SSH slope over the interior region was close to the slope expected for a barotropic Sverdrup flow in geostrophic balance.

6.3 Basin scale circulation; barotropic Sverdrup flow

The convergence of Ekman transport in the middle of the model domain leads to a small positive SSH anomaly and thus a high pressure, Figs. (40) and (41). On day 1, SSH was a fairly symmetric mound with an amplitude of about 1 cm, centered in the model domain, and accompanied by geostrophic currents that flowed clockwise around the high pressure. These currents were subject to the beta-effect, divergence where the flow was southerly and convergent where it was northerly. The result is that the growing SSH anomaly had a tendency for a beta-induced westward translation, just like we have seen for a mesoscale eddy. A key difference is the rate, O(1000 km day^{-1}), which is much, much faster than westward translation of baroclinic mesoscale eddies and baroclinic Rossby waves. This speed is in the range of long, barotropic Rossby waves. By day 3, the positive η_1 was compressed up against the western boundary, and by day 10 the slope over the interior of the subtropics was an almost uniform tilt down from west to east. The plan view of the SSH shows cyclonic gyres in the tropics and subpolar regions and an anti-cyclonic gyre that fills the subtropics. Thus within the first ten days of the experiment, the ocean circulation develops as three gyres that in many respects — save for their depth-independence and small amplitude — are a foretelling of the baroclinic circulation that will follow in the next several years of this integration, and that was the major topic of the main essay.

If the barotropic flow in the interior is consistent with the Sverdrup relation, then the barotropic

meridional velocity is

$$V_{Sv-btr} = \frac{1}{\rho_o H \beta} \nabla \times \tau.$$

Along $y = 0$, the center of the subtropical gyre, the expected Sverdrup flow has a dimensional amplitude $V_{Sv-btr} = 1.0 \times 10^{-3}$ m sec^{-1}. In the gyre center $y = 0$, the wind stress and Ekman flow vanish, and so this V_{Sv-btr} is nearly geostrophic. The sea surface slope is thus expected to be

$$\frac{\partial \eta_{Sv-btr}}{\partial x} = \frac{f}{g} V_{Sv-btr} = \frac{f}{\rho_o g H \beta} \nabla \times \tau. \tag{88}$$

If this holds across the entire basin, then the SSH amplitude across the basin is just

$$\eta_{Sv-btr} = 2L \frac{\partial \eta_{Sv-btr}}{\partial x} = \frac{2fL}{\rho_o g H \beta} \nabla \times \tau. \tag{89}$$

For the present experiment at $y = 0$, $\eta_{Sv-btr} \approx 0.06$ m. These estimates are very close to the slope and SSH amplitude found in the numerical experiment, Fig. (41), but are much, much less than the amplitude found in the western subtropical North Atlantic, which is about 1 m east-to-west, Fig. 1. At this time the volume transport within the subtropics was very close to that expected from the Sverdrup relation (Fig. 42, left), and of the expected sense in the tropics and subpolar regions. As we saw before with the reduced gravity model, there is a rather wide region adjacent to the northern and southern boundaries within which the meridional transport goes to zero as it must to satisfy the no normal flow condition on the solid boundaries. At this short time, the Sverdrup transport occurred throughout the water column, and in fact was mainly in the abyssal layer, Fig. (42, right).

6.4 Baroclinic adjustment to a surface intensified, steady state

After the first week, the SSH slope over the interior appeared to be quasi-steady. However, there was also evidence that SSH was continuing to evolve, albeit slowly. Sea level was rising very slowly over the entire subtropics, and, there was a region of much steeper SSH slope developing close to the eastern boundary and spreading slowly westward. This was the start of a baroclinic adjustment toward a surface-intensified, steady state.

The currents at $(x, y) = (0, -1000)$ km continued to evolve, albeit very slowly compared to the very rapid onset of the barotropic state. The abyssal layer transport, which early on made up most of the total Sverdrup transport, began to weaken at about 400 days, and then oscillated once and settled to nearly zero at about 1400 days, Fig. (38, middle). The total transport remained consistent with Sverdrup

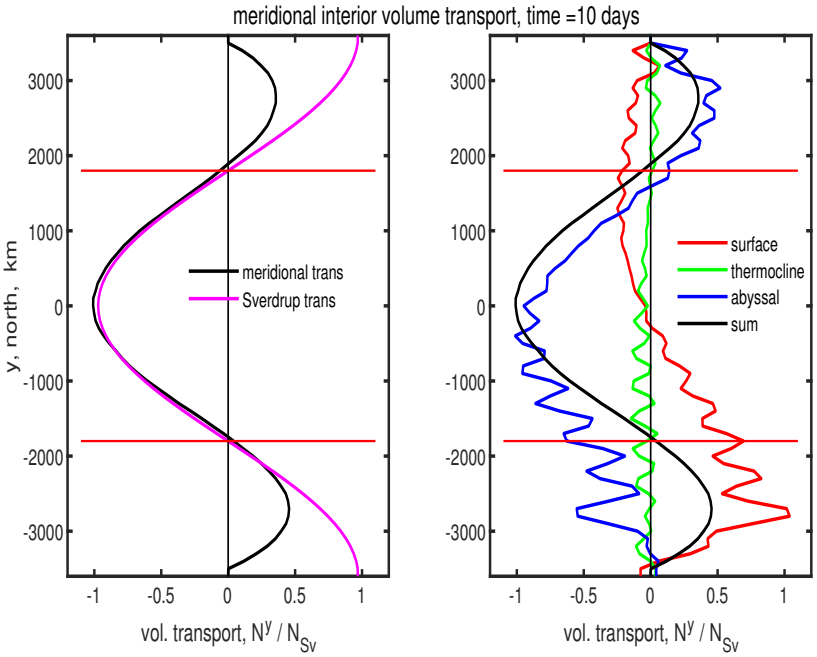

Figure 42: Meridional volume transport across the interior portion of the basin for all y and at time = 10 days. **(left)** Total transport (black line) and the expected Sverdrup transport (magenta). These are very similar over the subtropical gyre, but differ considerably near the northern and southern boundaries where the actual meridional transport must vanish. **(right)** Meridional transport in each of the layers of the three layer model, and summed to give the total transport, the black line, which is the same as at left.

transport, but thereafter, the Sverdrup transport was contained within the thermocline and surface layers. At about 1500 days, the thermocline layer transport started a slow decrease and then nearly vanished by about 7000 days, Fig. (38, lower). Thereafter, the Sverdrup transport was contained almost entirely within the surface layer. These times, very roughly 1000 days and 5000 days, are very broadly consistent with the expected transit time of the first and second baroclinic modes from the eastern boundary to the basin center, about 700 days and 2700 days for the first and second baroclinic modes at this y which is equivalent to about latitude = 22^o . Consistent with this, and perhaps more convincing of a modal description is that the change of the current profile over time looks a lot like the first and second baroclinic modes (Fig. 44), e.g., from 1500 days to 7000 days the change in the current is consistent with the arrival of a second mode (the abyssal layer remains at rest, while the thermocline and surface layers accelerate in opposite directions). If you look closely you can see that the change in the current profile is not exactly like a second mode in that the decrease of the thermocline layer is greater in amplitude than the is the evident increase of the surface layer. The size of the change is inversely proportional to the layer thicknesses, which at this time had changed quite a lot from the initial values; the surface layer was considerably thicker and the thermocline significantly thinner than in the initial state, Fig. (45).

The total transport — Sverdrup transport — is unchanged as these baroclinic waves pass by, but the distribution of the transport becomes increasingly surface intensified. In the final, steady state, the Sverdrup transport occurs entirely within the surface layer. At one level this is not surprising, as the surface layer absorbs all of the wind stress and stress curl. Thus, only the surface layer can sustain a

steady meridional flow in the presence of a beta effect. The deeper layers can be set into motion during the transient stage of the response, since they are subject to pressure gradients, and hence can sustain geostrophic motion. They are also subject to being compressed and stretched, Fig. (46), and so can display some of the consequences of potential vorticity conservation, i.e., there can be a q-conserving flow in the deep and thermocline layers so long as they are being stretched. However, this can not continue into a steady state in which stretching (time changing thickness) vanishes.

7 Summary and closing remarks

7.1 O1: East-west asymmetry of the subtropical and subpolar gyres

Sverdrup flow over most of the interior of a basin. The basin-scale, horizontal structure of the wind-driven ocean circulation, including western intensification and several of the qualitative differences between tropical, subtropical and subpolar gyres, have a plausible analog in solutions of the shallow water model. Over the subtropical North Atlantic, where the wind stress curl is negative, the interior meridional flow is southward as expected from the Sverdrup relation. Over the tropical and subpolar regions, the stress curl is positive and the meridional flow is northward, also as expected from the Sverdrup relation. This general result — that the Sverdrup relation provides a plausible and useful explanation of the major wind-driven gyres — has been accepted since at least the 1940s, and has been tested and validated quantitatively in modern, field data-based studies[5].

The Sverdrup relation is expected to be valid provided that the dominant processes of the potential vorticity balance are just two: the beta effect acting upon a very gentle and thus linear meridional current balanced by the curl (torque) of the wind stress. In practice, this holds in the majority of interior regions that are well away from zonal or meridional boundaries.

Departures from Sverdrup flow in zonal and meridional boundary regions. In a steady circulation, the meridional Sverdrup transport across every zonal, cross-basin section must be returned in the opposite direction by some other process. In the shallow water model and in the real ocean, this return flow occurs in a comparatively narrow and thus very intense western boundary current (wbc). The wbc is northward in the subtropical gyre where the Sverdrup transport is southward, and reversed in the subpolar and tropical gyres. The width of the western boundary region is observed to be very narrow, O(100 km). In the present shallow water model, the width of the wbc is the baroclinic radius of

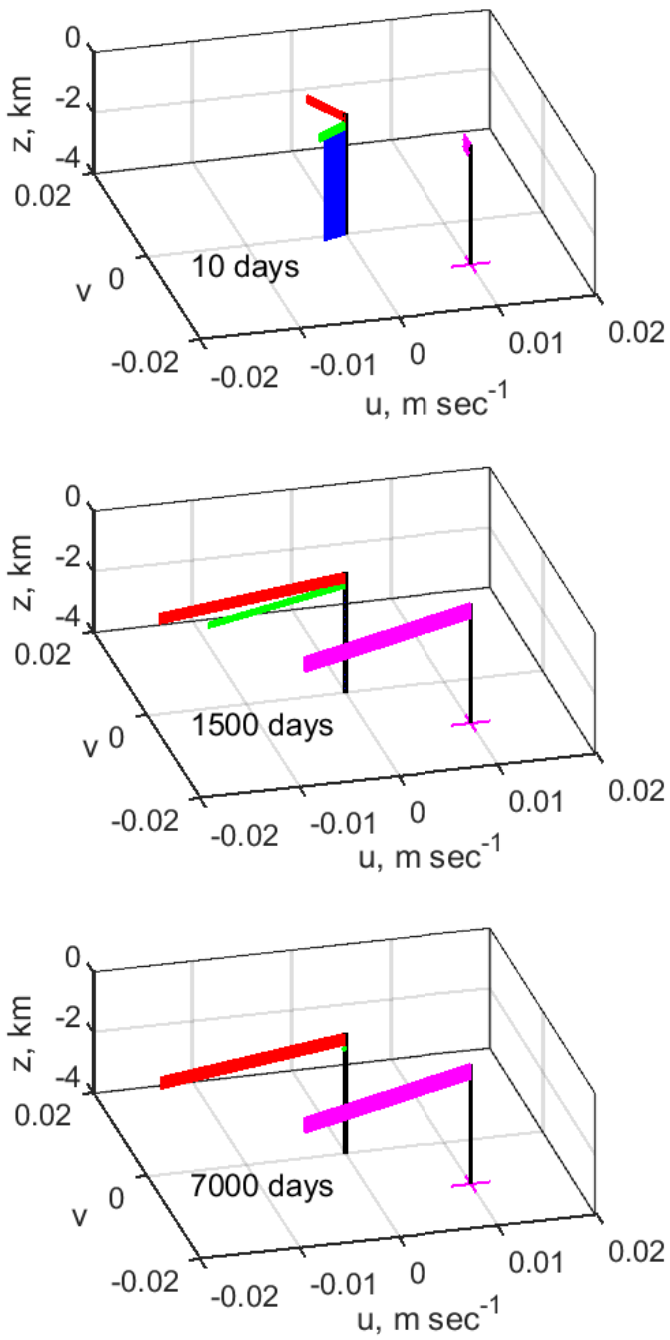

Figure 43: Current profiles from the site $(x,y) = (0,-1000)$ km, shown at three times, **(top)** to **(bottom)**, 10 days, 1500 days and 7000 days. Red, green and blue are the surface layer, thermocline and abyssal layers, respectively. An abyssal layer flow is appreciable only in the top panel. The view is towards the north-northeast. Notice that the profile goes from being barotropic with a small Ekman flow in the surface layer at 10 days, to entirely surface trapped at 7000 days. At this site the flow in the steady Sverdrup regime at 7000 days is somewhat stronger in the zonal direction than in the meridional direction, cf. Fig. (47). The magenta vectors are from the reduced gravity model, and offset by $(u,v) = (0.01-0.01)$ m sec^{-1}. They are very similar to the three layer model currents except at very short time.

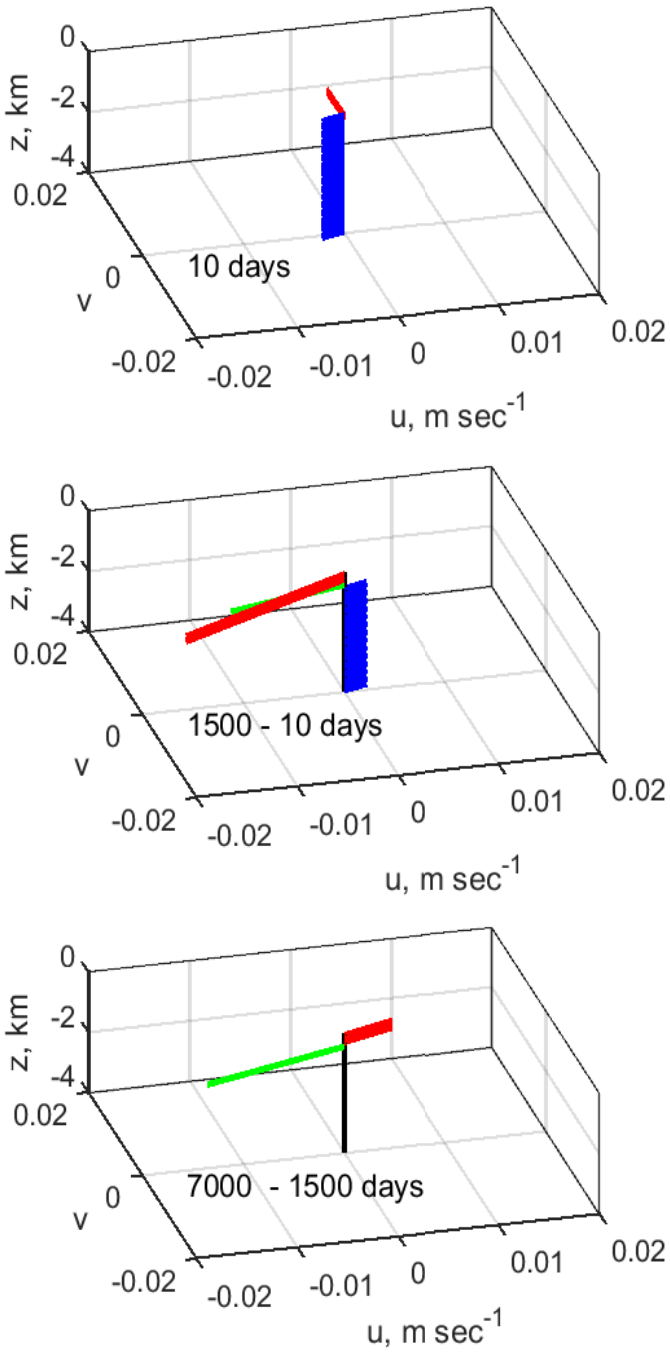

Figure 44: Current difference profiles from the site $(x,y) = (0,-1000)$ km, shown at three times, **(top)** to **(bottom)**, 10 days, 1500 days and 7000 days. In the top panel, the red arrows are the Ekman flow, and blue vectors are the depth independent barotopic flow at 10 days. The middle panel is the velocity difference, $u(t = 1500) - u(10 \text{ days})$. Red, green and blue are for the surface, thermocline and abyssal layers as in the previous figure. Notice that velocity difference at this time is qualitatively much like the first baroclinic mode (Fig. 8). The bottom panel is the velocity difference $u(t = 7500) - u(1500 \text{ days})$. There is essentially no signal from the abyssal layer, while the surface and thermocline layers are in approximately opposite directions. This shape is much like the second baroclinic mode.

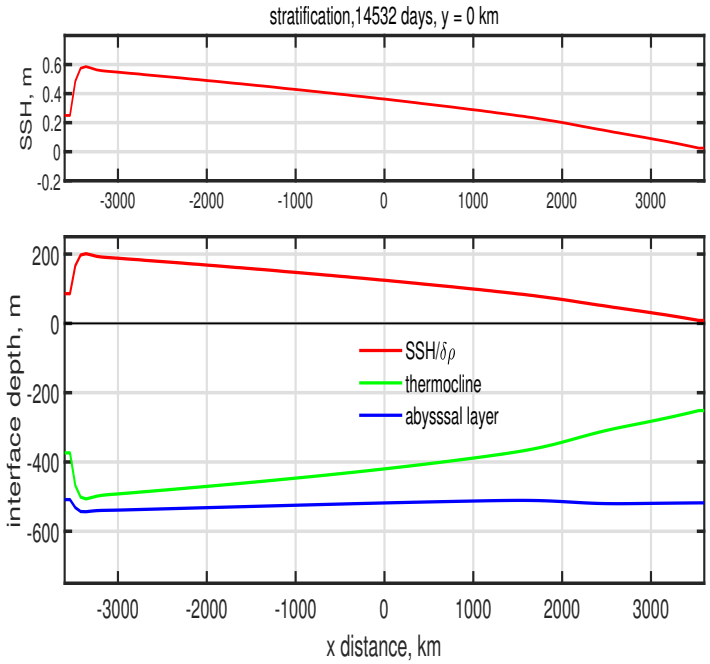

Figure 45: The SSH (upper panel, red line) and the interface between layers across the basin at y = -1000 km (red, green and blue; lower panel). Notice that the interface between the abyssal and thermocline layers (blue line) is essentially flat; there is almost no flow in the abyssal layer or the thermocline at this time. Also, note that the surface layer thickens markedly to the west and is generally much thicker than it was in the initial condition (250 m). The thermocline is generally much thinner.

deformation, the natural length scale of a shallow water model. The inviscid, linear Sverdrup interior fills the rest of the basin, 7000 km, and hence the westward intensification (east-west asymmetry) of the major ocean gyres is very pronounced, about 7000/100 in a North Atlantic-size basin.

The meridional flow must vanish on zonal boundaries. In the present model, the zonal boundary dynamics includes a significant contribution from linear friction, which is dubious as a model of dissipation in the real ocean. The width (north-south extent) of the affected zonal boundary region is rather wide, O(1000 km) and thus the meridional flow in the northern half of the subpolar region is somewhat less than would be expected from a Sverdrup balance.

7.2 O2: Time scales of the wind-driven circulation

Startup time of the baroclinic circulation. A wind-driven, start-up experiment in the 1l-rg (one layer, reduced gravity) model shows that the baroclinic circulation at a given point in the interior reaches an approximate, steady, Sverdrup flow some time after the passage of what amounts to a long, baroclinic Rossby wave starting from the eastern boundary. The long Rossby wave speed, $\beta C^2/f^2$, which has a strong dependence upon latitude, is thus a crucial parameter in the time-dependent response of a

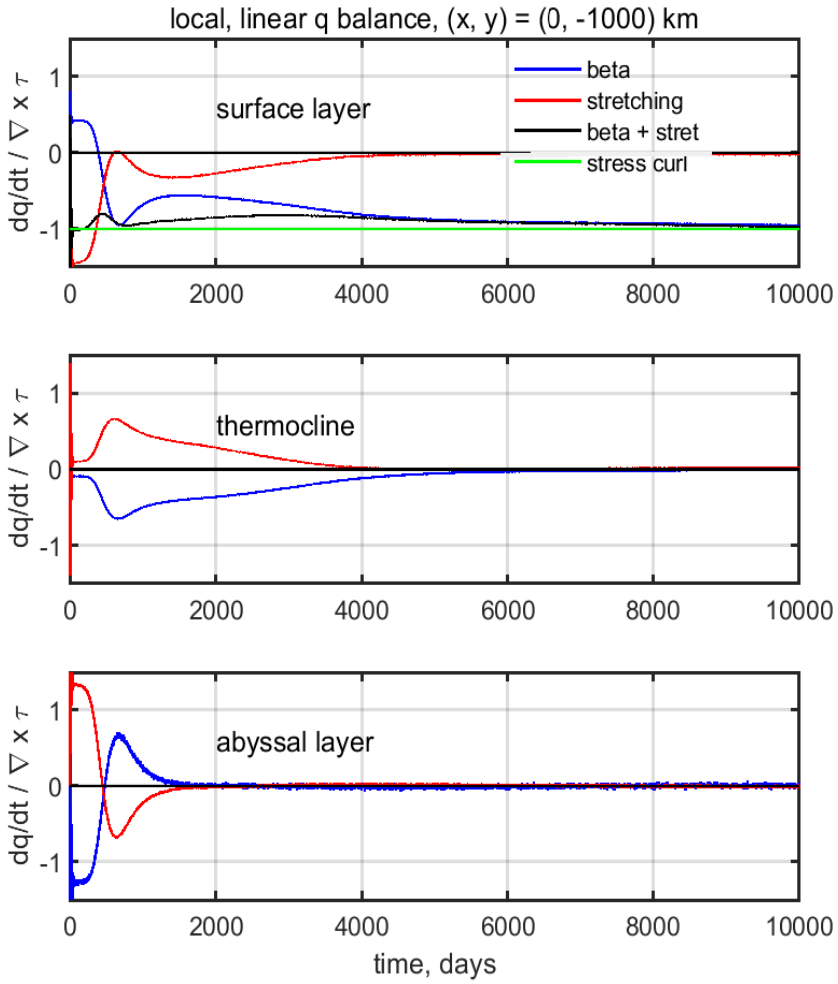

Figure 46: The linear balance of potential vorticity in, top to bottom, the surface layer, the thermocline and the abyssal layer.

wind-driven gyre. For a North Atlantic-sized basin, the elapsed time required to reach full steady state is about thirty years at a subpolar latitude, about five years in the subtropics, and much less, about a year, in the tropics.

Annually-varying winds. This marked latitudinal variation in the rise time of the baroclinic wind-driven circulation is relevant to understanding the observed response to an annually-varying wind stress. Model experiments that assumed a $\pm 50\%$ annual period variation of the wind stress find that the subpolar circulation varies almost not at all, the subtropical gyre varies only a little, while some aspects of the tropical circulation vary quite a lot. The transport of the tropical wbc varies by only about $\pm 10\%$, but the zonal flow in the eastern half of the tropical gyre varies by $\pm 50\%$. This latter variation is mainly a local a response to the annually-varying stress curl, and partly a Sverdrup flow. Thus a seasonally varying

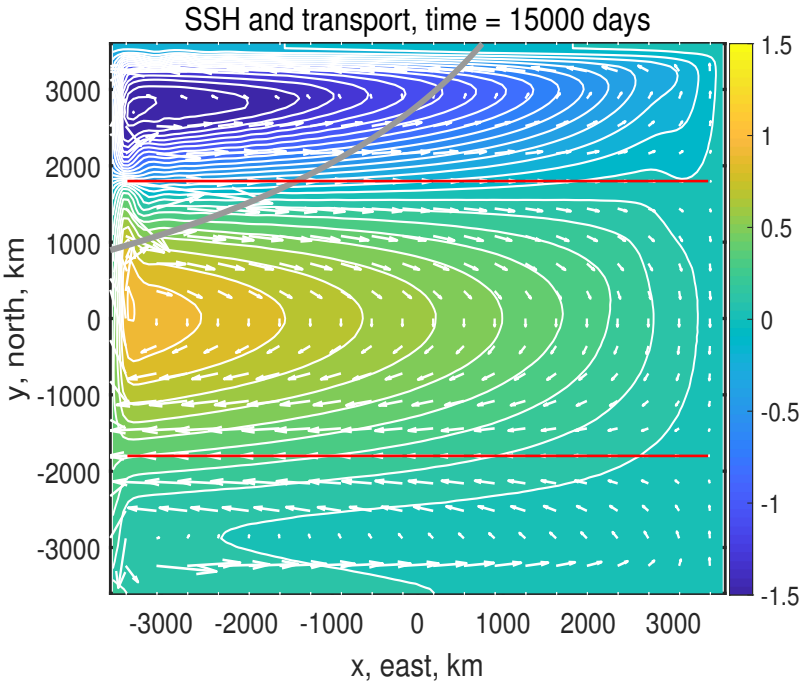

Figure 47: SSH anomaly from the three layer model experiment at time 15000 days. The thin red horizontal lines are the axis of the westerly and easterly wind stress (Fig. 6). The small white arrows are the transport, though with the comparatively very large transports within the wbc omitted. The SSH anomaly is nondimensionalized by the baroclinic scale, $\eta = 0.9$ m. The parabola at upper left is the second baroclinic eastern boundary wave, which notice, has still not swept the entire basin.

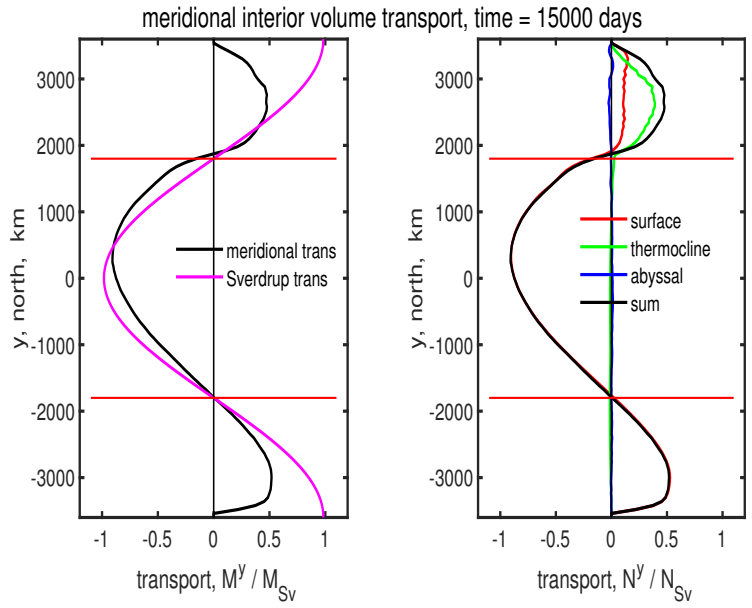

Figure 48: Meridional volume transport across the interior portion of the basin for all y and at time = 15000 days. **(left)** Total transport (black line) and the expected Sverdrup transport (magenta). These are similar over the subtropical gyre, but differ considerably near the northern and southern boundaries where the actual meridional transport must vanish. **(right)** Meridional transport in each of the layers of the three layer model, and summed to give the total transport, the black line, which is the same as at left. Notice that the total transport is mainly in the surface layer except in the subpolar gyre where there is still considerable transport in the thermocline, cf. Fig. (47).

wind stress that will have almost no effect on the subpolar or subtropical circulation (interior or wbc) and yet will produce a fairly pronounced response of especially the zonal, open ocean SSH and currents within the eastern tropical ocean.

Barotropic circulation. This essay emphasizes the baroclinic circulation because that is what we can see in the kinds of observations that are most widely available — SSH from satellites and upper ocean density from a variety of *in situ* methods, e.g., Figs. (1) and (2). As well, baroclinic circulation contributes the majority of meridional heat transport by the oceans. However, we shouldn't dismiss out of hand the possibility and importance of a barotropic circulation (which is inaccessible to the 1l-rg model). To get a sense of the barotropic circulation requires a model with a free (moving) sea surface and that supports very fast barotropic waves (here, 3l-fs). Now let's ask the question — how long does it take to establish a quasi-steady Sverdrup regime after the onset of a wind field? The answer is about one week, if we acknowledge the barotropic response. The currents associated with the barotropic response are distributed throughout the water column, and hence the upper ocean current is very small. Similarly, the SSH signature is about 10% of that observed.

7.3 What's gone missing?

This essay has emphasized the basin-scale horizontal structure and the time scales of the wind-driven circulation in no small part because that is what the shallow water model can do without misleading us. What does the shallow water model miss?

Amplitude and vertical structure. The amplitude of the circulation is very important too, of course, and here the assessment of the Sverdrup relation in the present idealized solutions is problematic. The SSH anomaly in the numerical subtropical gyre (Fig. 14) is about 0.4 m, while the SSH anomaly of the North Atlantic subtropical gyre Fig. (1) is considerably greater, more like 1.1 m. The underestimate made by the shallow water model is likely contributed by several sources. In the first place, the shallow water model gives the meridional volume transport and not SSH *per se*. The gradient of SSH is diagnostic of the surface geostrophic velocity, not the water column integral that is volume transport. The transport in the numerical model is not sensitive to the stratification. Thus if the model's layer thickness is made smaller, say $h_o = 250$ m, then the current speed is roughly doubled, as is the predicted SSH anomaly and slope. The comparatively large initial value of h_o used here, 500 m, was necessitated by the numerical (non-physical) requirement that h could not be allowed to vanish anywhere in the model domain. This is especially at issue for the subpolar gyre where the change in layer thickness was very large. This need for a large h_o is a kluge that betrays a physical deficiency of the present shallow water

model: a more complete and realistic model physics should include multiple layers in the vertical, as well as a vertical mixing process that would serve to keep the directly wind-driven surface layer of the ocean finite and realistic no matter what the upwelling might be.

The overturning circulation and eddy variability. The discrepancy in SSH amplitude involves much more than just a detail of the vertical structure. There is known to be considerably larger transport in the observed Gulf Stream than is predicted by the Sverdrup relation in numerical ocean models that have much better vertical resolution and fully realistic wind fields.[4] The larger-than-Sverdrup western boundary current transport in the North Atlantic likely arises from two very different sources. We have already had occasion to note that a global scale, meridional overturning circulation contributes about 20 Sv to the poleward-going, upper ocean transport at the latitude of the subtropical gyre. Deep, cold currents, well below the thermocline, provide mass balance across zonal sections. These are completely missing from the present shallow water model. As well, the vigorous eddying of the Gulf Stream (subtropical western boundary current) is known to produce an intense, and nearly depth-independent recirculating gyre which also adds significantly to the poleward transport of the western boundary current and so contributes to the large positive SSH anomaly of the observed subtropical gyre. The Sverdrup relation applied to the North Atlantic basin certainly isn't wrong, but neither is it the complete story of the ocean circulation.

7.4 Acknowledgements

Thanks to Iam-Fei Pun of WHOI for careful comments on a previous draft of this essay, and to Jiayan Yang of WHOI for encouraging the inclusion of barotropic dynamics.

8 Supplemental material

8.1 Links to models and updated manuscripts

The code used to solve the wind-drive circulation problems discussed here is very similar to that used in the Parts 2 and 3 treatments of geostrophic adjustment and eddy propagation. However, the data required to specify the configuration of the wind-driven experiments is sufficiently different that a dedicated

program was written:

gyre.for is a Fortran code that solves the shallow water equations for the wind-driven circulation in an enclosed ocean basin. A variety of wind stress forms and time histories may be specified. The numerical methods are not highly sophisticated or complex, and the code should be fairly amenable to modification. The longest integrations shown here will run in a few hours on a fairly capable, PC workstation. Output goes to a Matlab.mat file which may be read by a Matlab script,

gyre_plot.m makes several kinds of diagnostic plots from the data generated above.

This model and the most up to date version of these essays may be downloaded from the author's web page, https://www2.whoi.edu/staff/jprice/

8.2 Homework problems

1. At 30^o N, $f = \Omega$, and the inertial period is $2\pi/\Omega = 23$ hrs, 56 min, or less than a day by $\approx 1/365$ days. Can you explain where this small difference with a day comes from?

2. Starting with Eqns. (5) and (9), eliminate v to derive the corresponding governing equation for h. Is it significant that this wave equation is first order vs. the more common second order equation, e.g., shallow water gravity waves? What is the consequence of the beta effect in the case that the zonal gradient of thickness is positive? Is it relevant that the momentum balance Eqn. (5) is geostrophic?

3.

4. The steady solution Fig. (40) includes three gyres, tropical, subtropical and subpolar. Contrast the model-computed tropical and subpolar gyres with respect to the magnitude of their currents, layer thickness anomaly, and transports. Compare the solution Fig. (40, lower) with the observed SSH of Fig. (2). Why does the tropical gyre (or region) have a comparatively small SSH anomaly? The subpolar and tropical gyres have roughly comparable anti-clockwise circulations, and yet the wind over the subpolar gyres is westerly, and the wind over the tropical gyre is easterly. But haven't we been saying all along that these gyres are wind-driven?

5. Explain the signs and the comparative magnitudes of the current components of Fig. (15). Notice that the Sverdrup meridional flow at the three sites is not identical. Why is there a small but systematic difference?

6. The overall pattern of SSH (Fig. 6, lower) and of the transport streamfunction (Fig. 11, left) are similar but not identical. Why is there a difference?

7. The potential vorticity derivation of the Sverdrup relation in Sec. 5.1 omitted some important details. 1) Can you show that the drag term in the q-balance equation for the interior is proportional to the Ekman number times L_{Earth}/L_{tau}, where L_{tau} is the horizontal scale of the wind stress field. 2) Given speed and space scales of the interior (Sverdrup) flow, show that the relative vorticity of the Sverdrup flow is indeed very, very small compared to planetary vorticity, f, and so to an excellent approximation the potential vorticity in the interior is given by $q \approx f/h$. 3) The advective term of Eqn.(44) may be approximated as Eqn. (19) because the geostrophic flow does not advect layer thickness. What evidence can you find in the steady solution, Fig. (40), that supports this (highly plausible) assertion?

8. The real ocean thermocline is continuously stratified in the vertical, and so the best one layer baroclinic model representation of the thermocline will likely have to compromise on something. The values used here, H =500 m, and $\delta\rho = 2$ kg m^{-3} are round numbers that give an appropriate gravity wave speed. What thickness slope is consistent with the Rossby wave view of the subtropical gyre developed in Sec. 4.4, and where is that slope found in the water column of Fig. (1)?

9. Assuming that the boundary current will have a maximum current adjacent to the boundary (and so a single sign of relative vorticity), show that the mode $beta = drag$ can obtain also for the case of an equatorward western boundary current as occurs in the tropical and subpolar gyres. Can you envision this balance for an eastern boundary current of either sign?

10. In the discussion of the Stage 3 transient response we noted that the change in the current from Stage 2 zonal flow to meridional Sverdrup flow occurs at a time that is proportional to the transit time of a long Rossby wave starting from the eastern boundary. This suggests an interesting derivation of the Sverdrup relation (albeit for a slightly special wind field) that makes especially clear the crucial role of the eastern boundary in a problem in which there is no other imposed zonal scale. Assume that the wind stress is purely zonal, and is switched on at $t = 0$ and then held constant, as in the base case. The Stage 2 zonal flow u_{S2} then grows linearly with time until the arrival of the eastern boundary wave. How does the then extant zonal flow compare with Sverdrup zonal flow? In general, the $u_{S2}(x,y)$ current is not the same as the steady state Sverdrup zonal flow, since the former depends upon $\partial^2(\tau/f)/\partial y^2$ and not $f^{-1}\partial^2\tau/\partial y^2$ as does the Sverdrup zonal current (and see Figs. 13 and 16). To remedy this, suppose that the y scale of the wind stress field is much less than R_E. This will result from setting $n = 6$ in the wind stress Eqn. (37), and thus $\tau^x(y) \propto \sin(6\pi y/L)$. Can you show that the zonal transport at $t = T_{ebw}$ is then approximated well

by

$$hu_{S2}(t = T_{ebw}) \;\approx\; -\frac{(L-x)}{\rho_o \beta}\frac{\partial^2 \tau^x}{\partial y^2} \;=\; \frac{\partial \Psi_{Sv}}{\partial y},$$

where the last step used Eqn. (73). Why does the zonal transport increases in magnitude in proportion to distance from the eastern boundary, $L-x$?

11. Can you show that the vorticity balance form of the Ekman number appropriate to a western boundary current, Eqn. (78), is related to the usual, momentum balance form $E = r/f$, by

$$E_Q \;=\; E\frac{L_\tau}{R_d}.$$

12. Assume a steady, wind-driven circulation. What would you expect to follow if the wind stress suddenly vanished? Check your intuition against www.whoi.edu/jpweb/wind-off.mp4 Now Imagine an experiment in which the wind stress is spatially uniform over the entire basin, and northward. What would you expect for Stage 2 and Stage 3? (Major hint: consider the stress curl.) What is the steady response? Once you have formed your answer, take a look at the circulation computed from such an experiment shown in Fig. (34, lower).

Index